UNIVERSITY OF SOUTHAMPTON

FACULTY OF NATURAL AND ENVIRONMENTAL SCIENCES

School of Ocean and Earth Science

The Oligocene-Miocene Transition: New Insights from the Newfoundland Margin

by

Richard Edward Smith

Thesis for the degree of Doctor of Philosophy

December 2017

ABSTRACT

UNIVERSITY OF SOUTHAMPTON

FACULTY OF NATURAL AND ENVIRONMENTAL SCIENCES

School of Ocean and Earth Science

Thesis for the degree of Doctor of Philosophy

THE OLIGOCENE-MIOCENE TRANSITION: NEW INSIGHTS FROM THE NEWFOUNDLAND MARGIN

by Richard Edward Smith

As a major site of deep water formation, the North Atlantic plays a critical role in global climate. To understand better how Earth's climate system works it should therefore be a priority for geologists to study the record of past climate change encoded in the sedimentary archives that accumulate in the deep Atlantic. Here, sediment drilled in several cores on the Newfoundland Margin by International Ocean Discovery Program (IODP) Expedition 342 is utilized to provide fresh insights into palaeoclimate history, focusing on one of the more enigmatic events of the Cenozoic: the Oligocene-Miocene Transition (OMT), 23 million years ago. This is a time interval that Expedition 342 sediments have recorded in an continuous and expanded fashion unparalleled in previous records. This thesis aims to shed new light on North Atlantic OMT climate variability on both orbital and millennial-centennial timescales, and to increase the fidelity of foraminiferal proxies in this time interval. In Chapter 3, late Oligocene climate is shown to change cyclically on sub-orbital timescales. Centennial-millennial timescale variability is a key feature of Plio- Pleistocene climate; the record presented here is the first such record from earlier in the Cenozoic. These results show that Atlantic meridional overturning circulation is variable on sub-orbital timescales over a wider range of climate states than previously recognized. In Chapter 4, orbital- resolution planktic stable isotope records spanning the OMT are presented. These results – the first orbital-timescale record of sea surface conditions over the OMT – reveal that temperature changes in North Atlantic surface waters precede Antarctic glaciation/deglaciation and bottom water cooling/warming by tens of kyrs. In Chapter 5, the excellent preservation quality of foraminifera recovered by IODP Expedition 342 is exploited in a rigorous assessment of the taxonomy of several planktic foraminiferal species often used to generate palaeoclimate records over the OMT, with a focus on *Globigerina bulloides*. This quantitative, statistical approach enables non- subjective delineation of morphological variability into morphospecies, and highlights subtle morphological features that are critical to distinguish when picking foraminifera for stable isotope analyses. Together, the results of this thesis reveal that Earth's climate system in the late Oligocene to early Miocene was much more dynamic and complex than previously recognized.

Table of Contents

Table of Figures

Table of Supplementary Figures

Academic Thesis: Declaration of Authorship

I, Richard Edward Smith, declare that this thesis ("The Oligocene-Miocene Transition: New Insights from the Newfoundland Margin") and the work presented in it are my own and have been generated by me as the result of my own original research.

I confirm that:

1. This work was done wholly or mainly while in candidature for a research degree at this University;
2. Where any part of this thesis has previously been submitted for a degree or any other qualification at this University or any other institution, this has been clearly stated;
3. Where I have consulted the published work of others, this is always clearly attributed;
4. Where I have quoted from the work of others, the source is always given. With the exception of such quotations, this thesis is entirely my own work;
5. I have acknowledged all main sources of help;
6. Where the thesis is based on work done by myself jointly with others, I have made clear exactly what was done by others and what I have contributed myself;
7. None of this work has been published before submission.

Signed: Date:

27/04/2018

Acknowledgements

I am incredibly grateful that my time in Southampton has given me the opportunity to work with and befriend so many inspirational people. It's not possible to name everyone in a single page, but I would like to take this opportunity to extend particular thanks to several individuals.

Firstly, thank you to my supervisors, Paul Wilson and Steve Bohaty. The expertise and guidance you provided over the course of my PhD were invaluable, as were many of the skills I have learned from you that will stay with me for life. Thanks to Paul for having an open mind about the directions my PhD has taken over the years, and for ensuring those directions were the right ones. Thank you also for staying open minded and supportive in our discussions about my career path post-PhD. Thanks to Steve for expanding the horizons of my scientific thinking on all the occasions you imparted some of your encyclopaedic knowledge of palaeoclimate to me. Thanks also to Tom Ezard and Paul Pearson for invaluable discussions about statistics and foraminiferal taxonomy.

Thank you to my examiners Ian Harding and Ian Bailey for taking the time to read this thesis, and to my panel chair John Marshall, who, despite me asking (somewhat naively) in our first meeting whether he knew what a foram was, helped keep my PhD on track.

I have had the privilege of working with several academics from outside Southampton. I would like to thank Ursula Rohl and Thomas Westerhold for hosting me in the XRF lab in Bremen. I would've been lost in Bremen without Walter Hale, Vera Lukies and Anna Joy Drury. Thanks also to Brad Opdyke and Aleksey Sadekov for their assistance with preliminary trace metal analyses.

Thank you to everyone in the lab in Southampton, both for your help and your company over those many, many hours of lab work. Particular thanks to Megan Spencer – from my first day in the lab you've always been happy to help, and I enjoyed our diverse range of conversations over the years. Thank you to Bastian, for putting up with my never-ending questions about the Kiel mass spectrometer; to Richard Pearce, for your help with the SEM; and to everyone I have shared the lab with over the years, particularly Vicki Taylor, Yuxi Jin, Emmeline Gray and Lizzie Mullinger.

Thank you also to the rest of the Palaeo group. Over the years you have been an excellent source of wisdom and guidance, both academic and otherwise. I couldn't have asked for better officemates than Anieke Brombacher, James Spray and Wendy Kordesch, or for better mentors than Diederik Liebrand, Claire Huck, Anya Crocker, Joe Stewart and Rosanna Greenop. Thanks also to Tim van Peer for your many thought-provoking conversations.

Last but by no means least, I'd like to thank all the other people who I was privileged to meet during my time in Southampton. In particular, thank you Jacob, Fran, Sam, Sam and Richard for helping to create so many fond memories.

Definitions and Abbreviations

$\Delta^{13}C$	Planktic-benthic $!^{13}C$ offset
$!^{13}C$	Stable carbon isotope composition: $^{13}C/^{12}C$ of the sample relative to that of the VPDB standard
$\delta^{13}C_{DIC}$	Stable carbon isotope composition of dissolved inorganic carbon: $^{13}C/^{12}C$ of dissolved inorganic carbon relative to that of the VPDB standard
$\Delta^{18}O$	Planktic-benthic $!^{18}O$ offset
$!^{18}O$	Stable oxygen isotope composition: $^{18}O/^{16}O$ of the sample relative to that of the VPDB standard
AABW	Antarctic Bottom Water
AMOC	Atlantic meridional overturning circulation
D-O	Dansgaard-Oeschger
DWBC	Deep Western Boundary Current
EOT	Eocene-Oligocene Transition
GCM	General circulation model
GTS	Geologic Time Scale
IODP	International Ocean Discovery Program
ITCZ	Inter-tropical Convergence Zone
kyr	Thousands of years
LC	Labrador Current
Ma	Millions of years ago
MTM	Multi-taper method
Myr	Millions of years
NAC	North Atlantic Current
NADW	North Atlantic Deep Water
NH	Northern hemisphere
NHG	Northern hemisphere glaciation
O-M	Oligocene-Miocene
OMT	Oligocene-Miocene Transition
pCO_2	Atmospheric concentration of carbon dioxide
SEM	Scanning electron microscope
SH	Southern hemisphere
SST	Sea surface temperature
VPDB	Vienna Pee Dee Belemnite
XRF	X-ray fluorescence

Chapter 1 Introduction

1.1 Motivations and thesis outline

Earth's climate is in a constant state of flux. While the current rate of greenhouse gas addition to the atmosphere is unprecedented since at least the start of the Cenozoic (Zeebe et al., 2016), if not even earlier in the Phanerozoic (Foster et al., 2017), studying how much, how quickly and in what ways Earth's climate changed in the past plays a vital role in predicting how Earth's climate may behave in the coming century (Stocker, 2014).

Much of our knowledge about Earth's climate in the past comes from investigation of sediment cores recovered from the sea floor. In this thesis, I present new results from the study of material drilled by International Ocean Discovery Program (IODP) Expedition 342 on the Newfoundland Ridge, in the North-West Atlantic (Norris et al., 2014). The North Atlantic is a region of critical importance for palaeoclimate records, because this is the primary region of deep water formation in the modern (Dickson and Brown, 1994). As a result, this region is highly sensitive to global changes in temperature, ocean circulation and continental- and sea-ice coverage. Significant volumes of deep water have formed in the sub-polar North Atlantic since at least the Eocene- Oligocene Transition, 34 Ma (Davies et al., 2001; Miller and Fairbanks, 1983; Scher and Martin, 2008), making this region well-suited to investigate the "trends, rhythms and aberrations" that have marked palaeoclimate history over the past 65 Ma and beyond (Bender, 2013; Zachos et al., 2001a).

Recovering sediments spanning much of the Cenozoic, some of the most intriguing material drilled by Expedition 342 was of Oligo-Miocene (33.9-23.0 Ma) age. This expedition was the first to drill sediments across the Oligocene-Miocene Transition (23 Ma) of sufficiently high sedimentation rate to permit generation not only of orbital-timescale palaeoclimate records, but also of higher-resolution (millennial timescale) datasets. The high sedimentation rates of this material, a consequence of drift sedimentation, have an additional benefit: the clay-rich sediment has enabled exceptional preservation of calcareous microfossils, in comparison to the moderate to poor preservation quality typical of pelagic sediments (Norris et al., 2014).

In this thesis, I begin by considering North Atlantic climate variability on sub-orbital (i.e., millennial-centennial) timescales in Chapter 3 ("Sub-orbital climate variability in the latest Oligocene"). Such variability is one of the most prominent features of Pleistocene (2.6 Ma-11.7 ka) climate. Dansgaard-Oeschger events (Dansgaard et al., 1993), Heinrich events (Heinrich, 1988) and Bond cycles (Bond et al., 1997) are associated with often-dramatic climatic variability on sub- orbital timescales, of particularly high magnitude in the North Atlantic. Identification of these cycles in palaeo-records requires highly expanded sequences, i.e., sequences characterised by a

very high sedimentation rate of more than several cm/kyr. However, it is rare to find such sediments in the marine realm dating from earlier than the Pliocene (i.e., >5.3 Ma) that have adequate age control. As a result, it is uncertain whether climate variability on sub-orbital timescales has been a pervasive feature of Earth's climate, or whether climate of earlier epochs was instead relatively stable. In this chapter I report investigations of stratigraphically expanded sedimentary sections of Oligo-Miocene age from the Newfoundland Margin at Site U1405. Here, sedimentation rates of >20 cm/kyr offer a rare opportunity to investigate whether climate varied on sub-orbital timescales in the pre-Pliocene. Did such variability occur even in the warmer world of the Oligocene? If so, is this variability more akin to the dramatic variability seen during Pleistocene glacials, or the lower amplitude variability observed during the Holocene?

In Chapter 4 ("Decoupling of surface and deep North Atlantic waters over the Oligocene-Miocene Transition"), I place this high-resolution record into context by presenting results which shed new light on one of the most striking episodes of the Cenozoic: the Oligocene-Miocene Transition (OMT). While this episode of major Antarctic ice-sheet expansion and retreat is relatively well studied from the perspective of a number of deep ocean records (Beddow et al., 2016; Lear et al., 2004; Liebrand et al., 2011; Pälike et al., 2006a; Zachos et al., 2001b), very little is known about the climate of the North Atlantic at this time, or more generally about climate from the perspective of the sea surface. In this chapter, a high-resolution (average sample spacing ~2 kyrs) sea surface stable isotope record is presented, using material collected at Site U1406. This record is also compared with an unpublished benthic stable isotope record from the same site (Liebrand et al., in prep) to enable direct comparisons of planktic-benthic offsets and (a)synchronicities, providing new insights into the potential mechanisms involved in the OMT climatic event. Was the sea surface response to the OMT stronger or more restrained than the deep water response? Did the surface and deep ocean respond simultaneously to the OMT, or did one lead the other?

All palaeoclimate reconstructions rely on proxy evidence; how can we improve the accuracy and fidelity of these proxies in the Oligo-Miocene? In Chapter 5 ("Taxonomy of Oligo-Miocene *Globigerina bulloides* and related forms: refinement using a multivariate statistical clustering method, and investigation of stable isotope behaviour"), I conduct a rigorous assessment of the planktic foraminiferal taxonomy of several species common around the OMT. As a result of the often-significant variability in stable isotope incorporation between different species of planktic foraminifera, generation of accurate records requires consistent and precise species identification. The most abundant surface-dwelling species present in material recovered by IODP Expedition 342 over the OMT is typically *Globigerina bulloides*. However, uncertainty exists over the taxonomy of this species and similar forms in the Late Oligocene and Early Miocene. Such individuals are typically classified as "*G. praebulloides*" when found earlier than the mid-Miocene, but this distinction between pre-mid-Miocene and modern forms has been suggested to be unnecessary (Pearson and Wade, 2009). In addition, while images of 'typical' specimens are easily divided into

different species in standard taxonomic works, in practice, the range of intra-species variation is often very large. Consequently, it can be very difficult to decide with certainty which species to assign to some individuals. With the aim of reducing both of these issues, in this chapter a set of morphometric measurements are made on all individuals that have an appearance strongly or moderately similar to *G. bulloides*. Without pre-assigning any taxonomic information to these morphometric measurements, a statistical clustering method (Ezard et al., 2010; Pearson and Ezard, 2014) is then used to determine the statistically most likely number of morphological groups (i.e., species and/or morphotypes) into which these individuals should be divided. The aim of this chapter is to provide a quantitative, unbiased, repeatable approach to delineating these forms into morphospecies, in a way that is useful to subsequent work both in this thesis and elsewhere.

1.2 Setting the scene: The Oligocene-Miocene Transition (OMT)

1.2.1 Introduction to the Oligocene-Miocene Transition (OMT)

The Oligocene (33.9-23.03 Ma), a stepping stone between the largely ice-free Palaeocene/Eocene and the extensively glaciated world of the Pleistocene, is bookended by episodes of significant Antarctic glacial expansion: the Eocene-Oligocene Transition (EOT), and the Oligocene-Miocene Transition (OMT). The EOT saw the initiation of sustained large-scale Antarctic glaciation (Coxall et al., 2005; Coxall and Wilson, 2011; Ehrmann and Mackensen, 1992; Kennett and Shackleton, 1976; Sagnotti et al., 1998; Shackleton et al., 1975), a result of a long-term Cenozoic decline in atmospheric pCO_2 (Beerling and Royer, 2011; DeConto and Pollard, 2003). Following the EOT, Antarctic glacial coverage waxed and waned cyclically, with a number of glacial events indicated by cyclicity in benthic $\delta^{18}O$ data (Figure 1.1a; Liebrand et al., 2017; Miller et al., 1991). The intensity (and also cycle "shape" in the time domain) of Antarctic glacial periods was not constant through the Oligocene: glacial extent was greatest during the Mid-Oligocene Glacial Interval (MOGI; Figure 1.1b)), peaking at ~27-28 Ma, before gradually decreasing until ~24 Ma (Liebrand et al., 2017). However, this gradual reduction in glacial coverage was abruptly interrupted at the end of the Oligocene by a dramatic expansion of Antarctic glaciation. Multiple benthic foraminiferal stable isotope records from the Equatorial Pacific and Equatorial and South Atlantic have shown that the OMT was a worldwide phenomenon, with a global rise in benthic $\delta^{18}O$ and $\delta^{13}C$ of ~1‰ over ~200 kyrs, followed by a recovery over a similar timespan (Figures 1.1 and 1.2; Beddow et al., 2016; Lear et al., 2004; Liebrand et al., 2011; Pälike et al., 2006a; Zachos et al., 2001b).

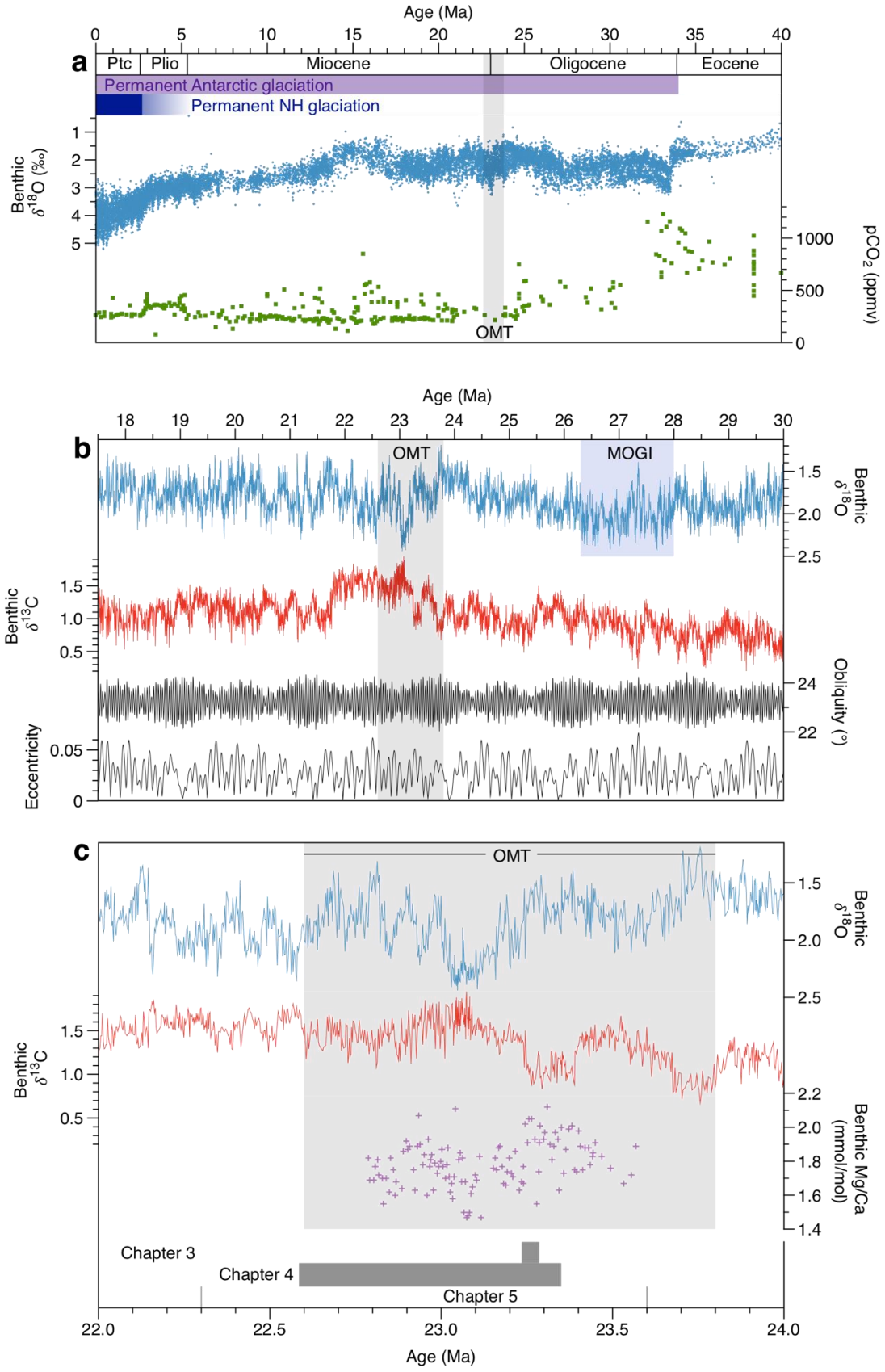
Age (Ma)
a
Ptc
Plio
Miocene
Oligocene
Eocene
Permanent Antarctic glaciation
Permanent NH glaciation
Benthic δ18O (‰)
pCO2 (ppmv)
OMT
Age (Ma)
b
OMT
MOGI
Benthic δ18O
Benthic δ13C
Obliquity (°)
Eccentricity
c
OMT
Benthic δ18O
Benthic δ13C
Benthic Mg/Ca (mmol/mol)
Chapter 3
Chapter 4
Chapter 5
Age (Ma)

Figure 1.1 (opposite) In all panels, the OMT interval proposed by Liebrand et al. (2017) is indicated by the grey shaded area. Panel **a**: global compilations of benthic foraminiferal $\delta^{18}O$ (Zachos et al., 2001a) and atmospheric pCO_2 (Beerling and Royer, 2011) records with purple and blue shaded areas indicating timing of onset of permanent Antarctic and Arctic glaciation, respectively. Panel **b**: benthic foraminiferal $\delta^{13}C$ and $\delta^{18}O$ records from Site U1264 (Walvis Ridge; Liebrand et al., 2016), with the duration of the Mid-Oligocene Glacial Interval (MOGI), as proposed by Liebrand et al. (2017), shaded in blue. Orbital solutions are those calculated by Laskar et al. (2004). Panel **c**: benthic foraminiferal $\delta^{13}C$ and $\delta^{18}O$ records from Site U1264 (Walvis Ridge; Liebrand et al., 2016), and a benthic foraminiferal Mg/Ca record from Site U926 (Mawbey and Lear, 2013). Shading/bars at base of this panel indicate the time intervals studied in each chapter of this thesis.

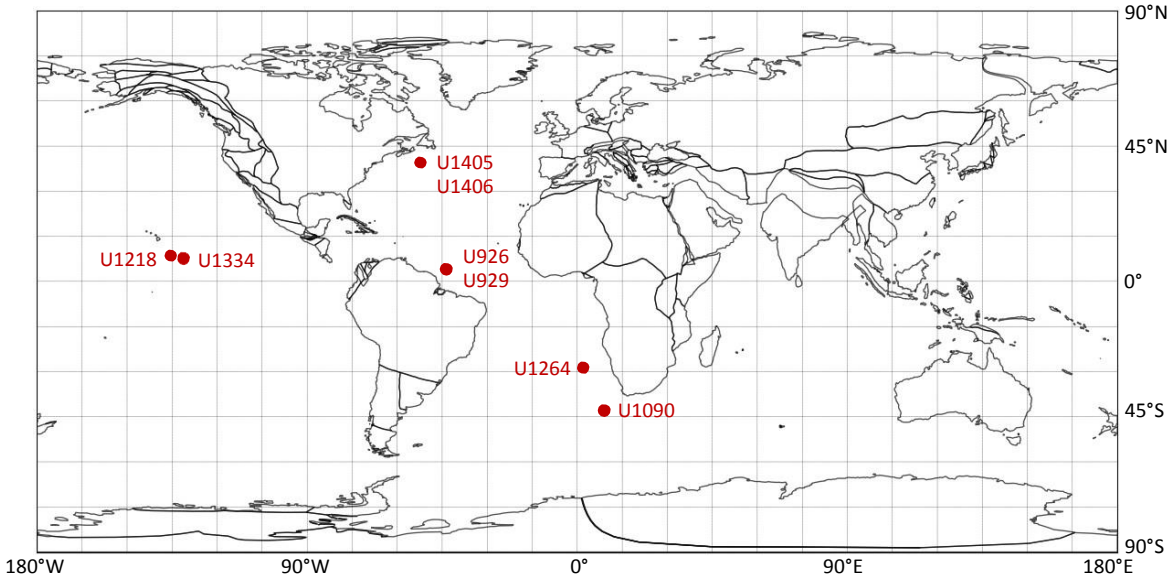

Figure 1.2 Global paleogeographic reconstruction for 23 Ma, constructed using GPlates (accessible online at http://portal.gplates.org/). Superimposed as red circles are all IODP sites from which orbital-resolution benthic stable isotope records have been generated across the OMT, plus Site 1405.

Since the initial identification of the "Mi-1" stable isotope event, the Cape Roberts Drilling Project has provided direct evidence of extensive Antarctic ice cover over the OMT, in the form of a 250 kyr erosional hiatus (Naish et al., 2001), supported by a major shift in the Chemical Index of Alteration of mudrocks that indicates associated physical erosion/mechanical weathering (Passchier and Krissek, 2008). Estimates of sea level change, from inverse modelling of benthic $\delta^{18}O$

(Liebrand et al., 2011) and backstripping of the New Jersey continental margin (Pekar et al., 2002; Pekar and DeConto, 2006) have been interpreted to indicate a sea level fall and rise of between 30 and 80 m across the OMT. It is noted, however, that while these lines of evidence suggest that Antarctic glaciation was extensive through the OMT, palynological evidence indicative of the persistence of *Nothophagus* (Southern Beech) and sparse tundra throughout the late Oligocene-early Miocene at Cape Roberts (Askin and Raine, 2000) suggests that at least small pockets of Antarctica remained at least transiently deglaciated throughout the OMT.

While initial attempts to deconvolve the benthic $\delta^{18}O$ change over the OMT into ice volume and temperature change (Lear et al., 2004) have been called into question because of poor foraminiferal preservation and the effects of carbonate saturation state (Elderfield et al., 2006) on foraminiferal Mg/Ca, a record of foraminiferal Mg/Ca record across the OMT at Sites U926 and U929 (Figure 1.1c; Mawbey and Lear, 2013) suggests that the OMT glaciation occurred in two steps, reminiscent of the two-step EOT (Coxall et al., 2005). In this interpretation, deep-water cooling preceded initial ice growth; ice growth then stalled as temperatures increased, before growing again as temperatures dropped (in both cases by 1-2°C). Thus, the total deep-water temperature drop was ~3°C, followed by an almost complete recovery in the deglaciation phase of the OMT. Given that deep-sea temperatures are set by surface temperatures at sites of water mass subduction, it is unsurprising that several direct records of surface temperature also indicate temperature change over the OMT. Palynological records from China and North America indicate cooling coincident with onset of the OMT (Kotthoff et al., 2014; Miao et al., 2013). Meanwhile, a dust record from the Equatorial Pacific suggests southward movement of the Inter-Tropical Convergence Zone (ITCZ) coincident with the OMT, also indicative of NH cooling (Hyeong et al., 2014).

1.2.2 What was the cause of transient glacial expansion and retreat over the OMT?

Taking these foraminiferal and sedimentological records into account, the glacial expansion over the OMT is postulated to have been equivalent to a change from ~0-50% to ~100% of the modern volume of ice on Antarctica (Beddow et al., 2016; Liebrand et al., 2017). Suggested explanations for the dramatic glacial expansion at the OMT typically invoke astronomical forcing, i.e., the periodic variability in Earth's rotation and orbit (Hays et al., 1976; Milankovitch, 1941). This variability can take three forms: cyclicity in the degree of ellipticity of the Earth's orbit around the Sun (eccentricity); cyclicity in the tilt angle of Earth's rotation axis (obliquity); and cyclicity in the position and rotation of the Earth's orbital path (precession). Astronomical forcing alters the magnitude and latitudinal/seasonal distribution of solar insolation on the Earth. For example, reduced obliquity and eccentricity reduce the effects of seasonality, resulting in milder summers. Given that the limiting factor for ice sheet growth is not winter accumulation rate but summer

melting rate (Raymo et al., 2006), a prolonged interval without warm summers as a result of the coincidence of a node of low variability in obliquity with low eccentricity aids ice sheet growth.

Records of Oligocene climate variability are typically dominated by eccentricity (100 kyr, 400 kyr) and obliquity (41 kyrs), and on longer timescales by nodes in both eccentricity (2.4 Ma) and obliquity (1.2 Ma; Liebrand et al., 2017; Pälike et al., 2006b; Wade and Pälike, 2004), although a single record from the high-latitude South Atlantic has a marked absence of strong obliquity forcing (Liebrand et al., 2011). The OMT is one of several intervals in the Oligocene where a 1.2 Myr node in obliquity coincides with a 400 kyr eccentricity minimum (Figure 1.1b), resulting in particularly low seasonality, which has been suggested as a potential cause of the OMT (Zachos et al., 2001b). However, this explanation is not entirely satisfactory, because intervals of similarly low (or even lower) seasonality, for example those centred on 19.7, 20.7, 24.4, 25.4 Ma (Laskar et al., 2004), do not appear to be associated with major Antarctic glacial expansions (Pälike et al., 2006a). Determining why the OMT occurred at the O-M boundary, rather than at one of the other intervals of low seasonality, remains an important unanswered question.

A crucial first step towards answering this question is understanding the mechanism through which orbital forcing drove climate in the Oligo-Miocene. The dominance of longer orbital periodicities in the Oligocene, especially the 400 kyr cycle in $\delta^{13}C$ and carbonate flux records, has been suggested to be a result of amplification associated with the carbon cycle, a consequence of the long residence time (~100 kyrs) of carbon in the ocean. Incorporation of such orbital modulation of organic carbon burial into models successfully reproduces the 400 kyr cyclicity seen in climate records (Mawbey and Lear, 2013; Pälike et al., 2006b).

The $\delta^{13}C$ change over the OMT is of a larger magnitude than that typical of the Oligocene (Figure 1.1), suggesting the operation of carbon cycle feedbacks associated with OMT cooling and glaciation. Firstly, blanketing of the Antarctic continent by ice has been suggested to have reduced global weathering rates, causing a doubling of pCO_2 and resultant increase in $\delta^{13}C_{DIC}$ (Lear et al., 2004). Conversely, a substantial addition of nutrients to the oceans over the OMT, a result of weathering of large areas of newly exposed continental shelves following eustatic sea level drop, has been suggested to have triggered an increase in productivity as evidenced by increased benthic foraminiferal accumulation rates over the OMT (Diester-Haass et al., 2011). Enhanced organic carbon burial associated with this productivity rise would have sequestered ^{12}C and increased $\delta^{13}C_{DIC}$. Enhanced productivity (and organic carbon burial) over the OMT has alternatively been postulated to have occurred because of intensified upwelling as a result of increased latitudinal temperature gradients associated with global cooling (Diester-Haass et al., 2011; Zachos et al., 1997).

The rapid retreat of Antarctic ice in the recovery phase of the OMT has long been difficult to reconcile with the results of coupled GCM-ice sheet model experiments. At the heart of this

problem is the ice sheet hysteresis effect (Figure 1.3): once formed, the top of a large polar ice sheet has high albedo and a surface elevation far above the snow-line. A small amount of warming may melt the ice sheet's margins, but substantial warming (i.e., pCO_2 rise) must occur to raise the snow-line sufficiently to trigger major melting of the ice sheet (Oerlemans, 1981; Oerlemans and Van Der Veen, 1984; Weertman, 1961). The results of ice sheet model experiments have suggested that pCO_2 higher than 500 ppmv (Gasson et al., 2016) or 800-1100 ppmv (Pollard and DeConto, 2005) would be required to cause significant melting of a large Antarctic ice sheet (Figure 1.3), yet, in existing records, there is little evidence of pCO_2 increase across the OMT (Figure 1.1a; Beerling and Royer, 2011).

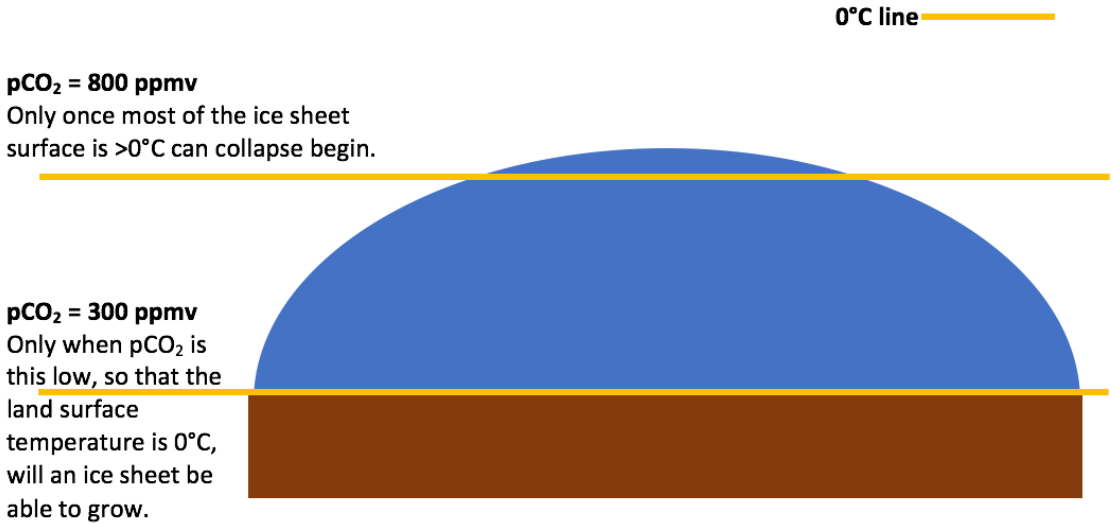

Figure 1.3 Schematic figure demonstrating the ice sheet hysteresis effect. pCO_2 levels are illustrative. Land surface is illustrated in brown, and the ice sheet in blue. Low pCO_2 levels are required to trigger ice sheet growth, because the freezing line (yellow line) must descend to the land surface. However, one this ice sheet has formed, almost all its surface area lies at least hundreds of metres above the land surface, so the freezing line must ascend dramatically (triggered by a substantial rise in pCO_2 levels) for significant ice sheet melting to occur.

Our increasingly extensive understanding of the glacial-interglacial cycles of the Plio-Pleistocene has come from exploitation of sediments that are sufficiently expanded to enable identification of orbital-timescale variability. Yet over the OMT, with the exception of benthic stable isotope records, almost no orbital-timescale climate records exist. For example, the highest resolution proxy records of ocean circulation (Scher and Martin, 2008) and pCO_2 (Beerling and Royer, 2011) have typical sampling intervals of >100 kyrs. Meanwhile only a single orbital-timescale planktic foraminiferal stable isotope record has been generated, and this is on thermocline-dwelling foraminifera (Beddow, 2016); not a single orbital-timescale published record of sea surface

conditions exists. The recovery of planktic foraminifera-rich expanded sections across the OMT by IODP Expedition 342 (Norris et al., 2014) offers a unique opportunity to gain insights into the OMT at resolutions traditionally restricted to more recent intervals of geological time.

Chapter 2 Materials and methods

2.1 Materials: IODP Sites U1405 and U1406

2.1.1 Site descriptions and splice/age model construction

All material studied in this thesis was recovered from IODP Sites U1405 and U1406 by IODP Expedition 342 (except for the SEM images from Site U926 in Chapter 4). At Site U1405 (40°08.30′N, 51°49.20′W; 4287 m water depth), 270 m, 220 m and 228 m of core were recovered from Holes A, B and C, respectively (88%, 101% and 98% recovery, respectively). A shipboard splice was generated using biostratigraphic and physical property data (Norris et al., 2014); this was subsequently refined using XRF elemental composition data as detailed in Chapter 3. Building on preliminary shipboard biostratigraphic (calcareous nannofossils, planktonic foraminifers and radiolarians) and palaeomagnetic age control, subsequent shore-based palaeomagnetic analyses on core u-channels (T. van Peer, pers. comm.), together with 2 cm resolution XRF scanning data (D. Liebrand, pers. comm.), were used to refine the age model.

At Site U1406 (40°21.0′N, 51°39.0′W; 3798.9 m water depth), 267 m, 241 m and 223 m of core were recovered from Holes A, B and C, respectively (94%, 95% and 94% recovery, respectively). A shipboard splice was generated using biostratigraphic and physical property data (Norris et al., 2014); this was subsequently refined using 2 cm resolution XRF elemental composition data (van Peer et al., in prep). Building on the preliminary shipboard biostratigraphic (calcareous nannofossils, planktonic foraminifers and radiolarians) and palaeomagnetic age control, subsequent shore-based palaeomagnetic analyses on core u-channels were used for initial refinement of the age model (T. van Peer, pers. comm.). This age model was then orbitally tuned by matching cycles in XRF-measured ln(Ca/K) to cycles in orbital forcing (specifically obliquity minus 0.6*eccentricity; T. van Peer, pers. comm.).

Almost the entirety of the material recovered at Site U1405 is of late Oligocene to early Miocene age; this short depositional duration means sedimentation rates are extremely high in parts of the record, sometimes exceeding 20 cm/kyr. However, this sedimentation is not continuous, with several short hiatuses. Meanwhile, material recovered at Site U1406 predominantly spans the mid- Eocene to early Miocene, with an additional small amount of Palaeocene material recovered (Norris et al., 2014). Sedimentation rates at Site U1406 are typically lower than those at Site 1405, but the record at Site U1406 is much more continuous, with only a single major hiatus, in the mid- Oligocene. Site U1405 is therefore more suited to the high-resolution study presented in Chapter 3, while Site U1406 is better suited to the longer, orbital-timescale study presented in Chapter 4.

2.1.2 Modern oceanographic setting

There are two primary controls on modern oceanography at Site 1405 (Expedition 342 scientists, 2012; Meinen and Watts, 2000; Pickart et al., 1999): cool Labrador Sea Water (LSW) heading south, and the warm North Atlantic Current (NAC) heading north (Figure 2.1). LSW, formed to the north of Site 1405 in the Labrador Sea, is a cool, low salinity, nutrient-rich water mass. It is transported southwards by the Labrador Current; during this transport much of the LSW sinks to form deep water as part of the Deep Western Boundary Current (DWBC) (Palter et al., 2008). The bathymetry of the Southeast Newfoundland Ridge forces the DWBC offshore and towards the surface. This causes the DWBC to encounter the overlying North Atlantic Current (NAC) at a depth of ~1500m (at the locations of Site 1405/1406; Figure 2.1). The NAC is a component of the Gulf Stream, which transports warm, high salinity, nutrient-poor waters northwards. Forms of the DWBC (Boyle et al., 2016; Davies et al., 2001; Miller and Tucholke, 1983), NAC (Pinet et al., 1981; Wade and Kroon, 2002) and LC (Barron and Peterson, 1991) have all been active since at least the Oligocene, when North Atlantic overturning was initiated (Boyle et al., 2016; Davies et al., 2001; Miller and Tucholke, 1983).

2.2 Foraminifera and their use as palaeoclimate proxies

A multitude of proxies are used to reconstruct past climate conditions, ranging from sedimentological to geochemical to ecological (Hillaire-Marcel and Vernal, 2007). Among the most utilized proxies in palaeoceanography are those relying on the geochemistry of benthic and planktic foraminiferal calcite. The stable isotope geochemistry of planktic foraminifera is discussed in Section 2.1.2. However, given the importance of accurate species identification for producing reliable stable isotope records, I first turn to the taxonomy of planktic foraminifera.

Figure 2.1 (opposite) Modern NW Atlantic temperatures. Top and middle: representative winter and summer SSTs, respectively; the LC-NAC front is the region where temperature contours (in °C) gather together immediately north of Sites U1405 and U1406. Data is from February and August 2016 for the winter and summer plots, respectively; the data source is the NOAA Optimum Interpolation (OI) Sea Surface Temperature (SST) V2 monthly 1° spatial resolution average dataset. Bottom: latitudinal depth profile of temperature at longitude of 51°45’ to 52°00’, the approximate latitude of Sites U1405 and U1406. Values are averaged from 1955-2012, and originate from the NOAA World Ocean Atlas 2013 version 2. All data plotted with NASA Panoply software. See Section 3.1 for further information about data sources used in this figure.

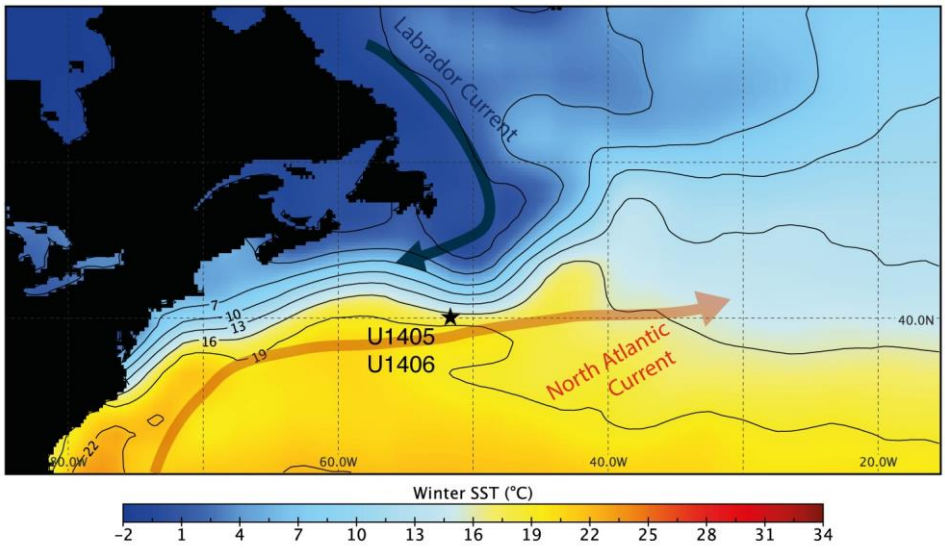
Labrador Current
North Atlantic Current
U1405
U1406
40.0N
60.0W
40.0W
20.0W
Winter SST (°C)
-2 1 4 7 10 13 16 19 22 25 28 31 34

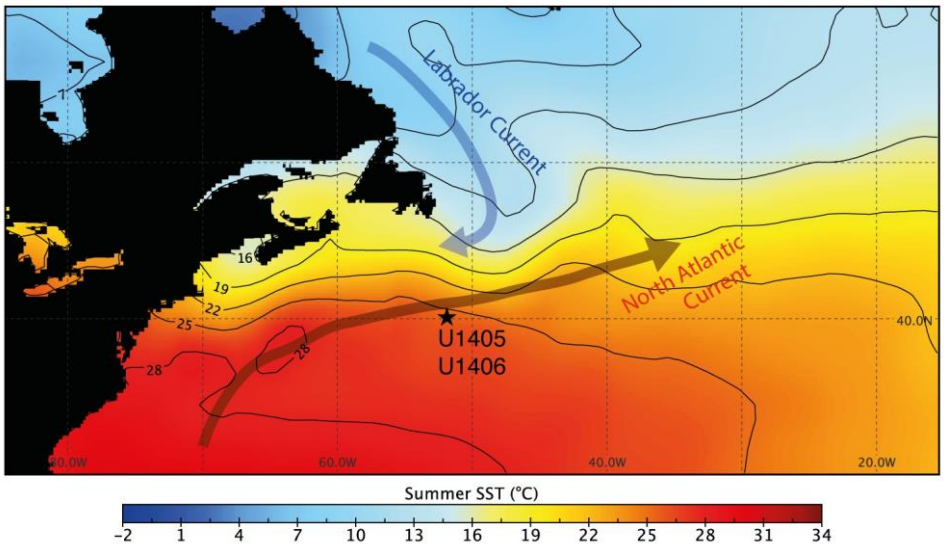
Labrador Current
North Atlantic Current
U1405
U1406
40.0N
60.0W
40.0W
20.0W
Summer SST (°C)
-2 1 4 7 10 13 16 19 22 25 28 31 34

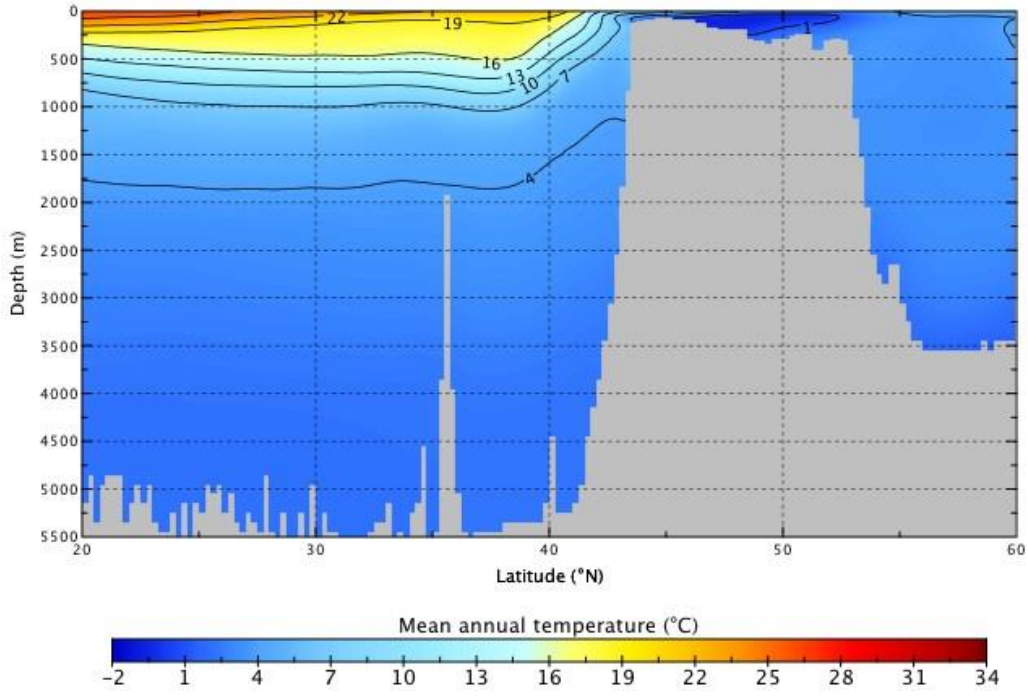
Depth (m)
0 500 1000 1500 2000 2500 3000 3500 4000 4500 5000 5500
20 30 40 50 60
Latitude (°N)
Mean annual temperature (°C)
-2 1 4 7 10 13 16 19 22 25 28 31 34

2.2.1 Planktic foraminiferal taxonomy

Planktic foraminifera are unicellular, heterotrophic zooplankton, some species of which host symbionts (Hemleben et al., 1989). Typically growing over the course of several weeks to months, planktic foraminifera form calcite shells, or 'tests', typically of size ~0.1-1.0 mm. Planktic foraminifera are highly abundant: their calcite tests account for around 25% of carbonate production in the modern oceans (Langer, 2008), and they are a significant component of many seafloor sediments (Seibold and Berger, 2013). Because the test is all that remains in fossil foraminifera, the taxonomy of these fossils relies entirely on the concept of "morphospecies", whereby species are delineated using shell morphology (Forey et al., 2004; Pearson et al., 2006; Smith, 1994). Forty-five such morphospecies exist in the modern oceans, but hundreds of now- extinct species have been identified throughout the geological record (Aze et al., 2011). While the morphospecies approach has recently been revealed to be overly simplistic, with many morphospecies in fact made up of several genetically distinct groups (Aurahs et al., 2011; Darling and Wade, 2008; Morard et al., 2009; Quillévéré et al., 2013; Vargas et al., 1999), the absence of genetic material in fossilized foraminifera means that the morphospecies approach remains the most suitable method for distinguishing fossil forms.

Morphospecies concepts are based around the holotype, i.e., the single individual on which the first formal definition of a species is based. In biology, species typically occupy distinct regions of morphospace (where 'morphospace' is a hypothetical three-dimensional set of axes containing all information about morphological variability), (see Dobzhansky and Dobzhansky, 1937; Mayr, 1963). However, many morphospecies of planktic foraminifera instead tend to occupy 'clouds' within morphospace that are not separated by 'empty' morphospace Tabachnick and Bookstein, 1990). This range of morphological variability within planktic foraminiferal species means that there is often significant debate within the micropalaeontological community as to how morphologies should be delineated into morphospecies (Aze et al., 2011). As a result, differing personal preferences over 'lumping' or 'splitting' of morphospecies mean that typical reference works, for example those describing planktic foraminifera in the Oligocene (Bolli and Saunders, 1985; Kennett and Srinivasan, 1983; Spezzaferri, 1994), are often not entirely consistent with each other.

In an attempt to make morphospecies delineation more quantitative and less subjective, there is a growing interest in the application of morphometric methods to planktic foraminiferal taxonomy. These methods, also frequently applied across a range of other biological fields (Adams et al., 2013; Rohlf and Marcus, 1993; Slice, 2007; Zelditch et al., 2012), quantify morphological differences and similarities between species in a repeatable, objective way. Early applications to planktic foraminifera took pre-defined species concepts and attempted to quantify the variability both within and between species (Healy-Williams, 1984; Malmgren and Kennett, 1976, 1977, Scott, 1976, 1975). While this approach is still applied to some taxonomic questions (e.g., Aurahs

et al., 2011; Quillévéré et al., 2013; Spezzaferri et al., 2015; Wade and Olsson, 2009), an alternative approach is to abandon pre-existing morphospecies concepts. In this approach morphological variability is assessed in a quantitative, objective way with no (or at least fewer) *a- priori* assumptions (e.g., Tabachnick and Bookstein, 1990; Wei, 1987). New statistical methods have since enabled determination of the statistically most likely number of clusters into which a group of measured individuals falls (Ezard et al., 2010), enabling quantitative determination not only of the morphological differences between individuals, but of the number of morphospecies into which they are most appropriately classified (Pearson and Ezard, 2014).

2.2.2 Planktic foraminiferal stable isotope measurements

The stable isotope composition of foraminifera is one of the oldest (Emiliani, 1954, 1955, Urey, 1947, 1948) and most widely used geochemical proxies in palaeoclimate. The widespread geographic distribution, long-ranging (over millions of years) fossil record, high abundance and easily preserved calcium carbonate shells of foraminifera make them ideal for constructing high-resolution oxygen and carbon stable isotope records that reveal valuable palaeoclimatic information (Pearson, 2012; Ravelo and Claude, 2007; Rohling and Cooke, 1999).

Oxygen exists as three stable isotopes on Earth, the two most abundant of which are ^{18}O (99.8%) and ^{16}O (0.2%) (Rosman and Taylor, 2009). When oxygen is incorporated into any natural material, including foraminiferal calcite, fractionation occurs. For convenience, in foraminiferal calcite this fractionation is generally expressed relative to a standard using "delta notation" (Equation 2.1), where the standard used is typically Vienna Pee Dee Belemnite (VPDB; Coplen, 2009). Positive $\delta^{18}O$ thus reflects enrichment in $\delta^{18}O$ relative to the VPDB standard.

$$\delta^{18}O_{carb} = \frac{(^{18}O/^{16}O)_{Sample} - (^{18}O/^{16}O)_{Standard}}{(^{18}O/^{16}O)_{Standard}} \times 1000$$

Equation 2.1 $\delta^{18}O_{carb}$ is the $\delta^{18}O$ value of foraminiferal calcite; Sample refers to foraminiferal calcite; Standard typically refers to VPDB

The extent to which oxygen in seawater is fractionated upon incorporation into foraminiferal calcite depends on the growth temperature of the test. This effect is primarily a result of kinetic fractionation – heavier isotopes are less reactive than lighter isotopes – but this difference becomes less significant with increasing temperature. In inorganic calcite, the relationship between

temperature and isotopic composition of precipitated calcite is easily calculated (Epstein et al., 1953; McCrea, 1950). However, foraminiferal calcite precipitation is biologically mediated, so the

relationship of $\delta^{18}O_{carb}$ to temperature is not the same in inorganic calcite (Bé and Donk, 1971; Grazzini, 1976; Shackleton et al., 1973). Differences in calcite precipitation between species mean that each species requires its own temperature-$\delta^{18}O_{carb}$ calibration in the form of Equation 2.2; the so-called "vital effects" that cause these inter-species differences are discussed in more detail below (Section 2.1.3).

$$T(°C) = a + b(\delta^{18}O_{carb} - \delta^{18}O_{sw}) + c(\delta^{18}O_{carb} - \delta^{18}O_{sw})^2$$

Equation 2.2 T is the average water temperature in which the foraminifera grew; $\delta^{18}O_{carb}$ is the average test $\delta^{18}O$ value; $\delta^{18}O_{sw}$ is the average $\delta^{18}O$ value of the seawater in which the foraminifera grew; a, b and c are species-specific constants

Temperature-$\delta^{18}O_{carb}$ calibrations are frequently determined using culture experiments (Bemis et al., 1998; Erez and Luz, 1983; Spero et al., 2003), which have the advantage that all parameters can be precisely controlled, but the disadvantage that the absence of a 'natural' environment can make it difficult to replicate the marine environment exactly. Alternatively, calibrations can be determined using foraminifera collected in sediment traps (Mulitza et al., 2003) and core tops (Duplessy et al., 2002), where the isotopic composition of individuals can be compared with buoy CTD sensor data.

As shown in Equation 2.2, $\delta^{18}O_{carb}$ also varies depending on the oxygen isotopic composition of the ambient seawater in which the foraminifer grows, $\delta^{18}O_{sw}$, which is affected by both local and global processes. The lighter atomic mass of ^{16}O relative to ^{18}O means that water molecules containing ^{16}O are preferentially evaporated; conversely, water molecules containing ^{18}O are preferentially precipitated in rainfall. $\delta^{18}O_{sw}$ is therefore reflective of the local evaporation/precipitation balance, and thus of salinity. This relationship can be complicated by additional factors such as river outflow, iceberg melting and thermohaline circulation (Rohling and Cooke, 1999). The precipitation bias towards ^{18}O also results in an accumulation of isotopically heavy water molecules in ice sheets at the poles, leaving the ocean isotopically light: the $\delta^{18}O$ values of modern average Antarctic ice and sea water have been estimated as -50 ‰ and -0.28 ‰, respectively, against the Pee Dee Belemnite standard (Shackleton et al., 1975). Because the timescales of ice sheet growth and retreat are greater than the mixing time of the ocean, the isotopic effects of changing ice sheet volume affect the whole ocean uniformly. On a longer timescale, changes in oxygen fractionation can also occur because of changes in the rock cycle (principally changes in chemical weathering), but given that these changes occur only on timescales of 10^8 years (Jaffrés et al., 2007; Veizer et al., 1999; Wallmann, 2001), they are typically assumed to be constant for the purposes of palaeoclimatic reconstructions.

Alongside stable oxygen isotopes, the other element typically measured in stable isotope analyses is carbon. With two stable isotopes: ^{12}C (98.9%) and ^{13}C (1.1%; Faure, 1986), the stable carbon isotope composition of foraminiferal calcite is generally reported as $\delta^{13}C$ for convenience (Equation 2.3).

$$!\,^{\#9}8 = \frac{^{\#9}8/\,^{\#:}8_{,\&--/0} - {}^{\#9}8/\,^{\#:}8_{,2\&34\&'4}}{^{\#9}8/\,^{\#:}8_{,2\&34\&'4}} \times 1000$$

Equation 2.3 $\delta^{13}C_{carb}$ is the $\delta^{13}C$ value of foraminiferal calcite; Sample refers to foraminiferal calcite; Standard typically refers to VPDB.

The effect of kinetic fractionation on $\delta^{13}C$ is minimal; $\delta^{13}C_{carb}$ therefore primarily reflects $\delta^{13}C$ of the seawater in which the test grows ($\delta^{13}C_{DIC}$; DIC = Dissolved Inorganic Carbonate) (Williams et al., 1977). During photosynthesis, $^{12}CO_2$ is preferentially fixed over its heavier counterpart $^{13}CO_2$ (Park and Epstein, 1960); as a result, $\delta^{13}C_{carb}$ can be used a proxy for a number of processes in the carbon cycle. Intervals of enhanced organic carbon burial are associated with a removal of ^{12}C from the ocean, and thus a rise in $\delta^{13}C_{DIC}$; conversely, oxidation of organic carbon is associated with a drop in $\delta^{13}C_{DIC}$ (Emerson and Hedges, 1988). Planktic-benthic gradients in $\delta^{13}C$ can also be used to estimate the strength of the biological pump, i.e., the intensity of primary productivity, given that ^{12}C-rich organic matter is progressively oxidized as it sinks to the sea floor (Boyle, 1988; Hilting et al., 2008; Hodell et al., 2003; Toggweiler, 1999). As with $\delta^{18}O$, care must be taken to account for the effects of changing ocean circulation and freshwater runoff. In addition, as with $\delta^{18}O$, there an offset between $\delta^{13}C_{carb}$ and $\delta^{13}C_{DIC}$ (Romanek et al., 1992; Turner, 1982), which is not constant between species, and so offsets must be applied in order for records from different species to be comparable (Ravelo and Fairbanks, 1995).

2.2.3 Vital effects and inter-species variability

In addition to inter-species variability, the range of $\delta^{18}O$ and $\delta^{13}C$ from individuals within the same species from the same sample can be significant. While some of this is a result of the time-averaging of geological sampling, even samples recovered over short time intervals from sediment cores or sediment traps typically show sizeable variability in both $\delta^{18}O$ and $\delta^{13}C$ (Billups and Spero, 1996, 1995; Ganssen et al., 2011; Killingley et al., 1981; Leduc et al., 2009; Schiffelbein and Hills, 1984). Consideration of the impact of the so-called "vital effects" (Berger et al., 1978; Rohling and Cooke, 1999; Wefer and Berger, 1991) that cause this variability is thus essential for production of accurate stable isotope records (Fraass and Lowery, 2017). The reasons for these vital effects are now considered.

Firstly, different species of planktic foraminifera are adapted to live in differing environmental conditions, and thus each have their own depth preference ranging between the surface and ~1000 m depth (Figure 2.2; Bé et al., 1977; Fairbanks and Wiebe, 1980; Hemleben et al., 1989; Lombard et al., 2011; Schiebel and Hemleben, 2005). Different species in the same sample may therefore have grown in water of markedly different temperature and $\delta^{13}C_{DIC}$. While determination of depth habitat is relatively simple with extant species, where species abundance is recorded in plankton tows at different depths (Fairbanks et al., 1982, 1980; Mortyn and Charles, 2003; Ravelo and Fairbanks, 1992), establishing the depth preference of extinct species is less simple. There is no way of quantifying the absolute depth range of an extinct species, but relative $\delta^{18}O$ values within an assemblage can be used to determine relative depth ranges (Pearson et al., 1997; Pearson and Wade, 2009; Stewart et al., 2012).

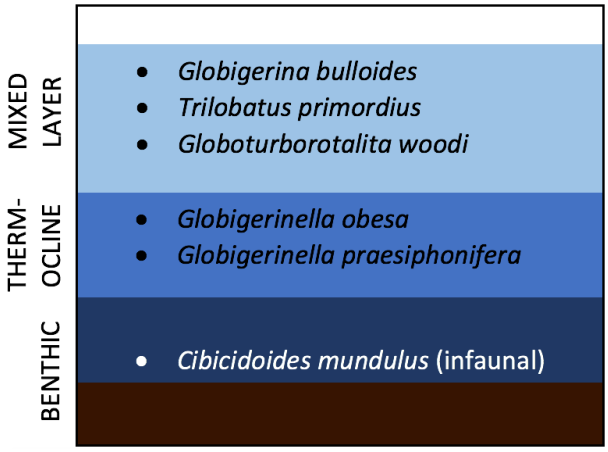

Figure 2.2 Depth habitats of all foraminifera mentioned in this thesis. Exact depths are unknown because most of these species are now extinct; these depths have been estimated based on relative $\delta^{18}O$ values (see Appendix 1 of Aze et al., 2011 for references). Many modern species move through the water column through ontogeny; this effect has not yet been accurately quantified for the Oligo-Miocene forms listed here.

Secondly, a number of processes cause a relationship between test stable isotope composition and ontogeny. Even if the typical depth habitat of a species is well established, most species also migrate through the water column, sometimes multiple times, over their lifespan (Hemleben et al., 1989). Each chamber may thus have grown at a different water depth; in addition, some species undergo a final gametogenesis step before death, associated with the addition of a thick calcite crust at a depth several hundred metres deeper than the typical habitat for the species (Duplessy et al., 1981), which consequently significantly changes the average $\delta^{18}O$ value of the whole test (Kozdon et al., 2009). All planktic foraminifera are postulated to experience decreasing rates of

growth with age; the consequent decrease in metabolic activity thus causes a reduction in carbon fractionation as test size increases. As a result, foraminiferal test $\delta^{13}C$ tends to increase with increasing test size (Berger et al., 1978; Birch et al., 2013; Kahn, 1979; Ortiz et al., 1996; Ravelo and Fairbanks, 1995; Spero et al., 1997; Vincent and Berger, 1981; Wefer and Berger, 1991). This relationship is particularly strong in species which host symbionts, postulated to be a result of an increase in the quantity of photosymbiotic organisms that the foraminifera hosts that is proportional to size. During photosynthesis, these symbionts preferentially remove ^{12}C from the seawater surrounding the foraminifera, raising the $\delta^{13}C_{sw}$ value of the local seawater from which the test calcite precipitates (Berger et al., 1978; Birch et al., 2013; Bouvier-Soumagnac and Duplessy, 1985; Norris, 1996; Ravelo and Fairbanks, 1995; Spero, 1992; Spero and Lea, 1993; Spero and Williams, 1988, 1989). Since the increase in symbiont abundance is proportional to the surface area of the test, a small increase in radius can cause a significant increase in foraminiferal test $\delta^{13}C$.

Thirdly, not all foraminifera within an assemblage will have grown during the same season. Some species have been shown to bloom when a certain temperature is reached, while others have peak blooms coinciding with maximum nutrient levels (Jonkers and Kučera, 2015; Schiebel et al., 1995; Schiebel and Hemleben, 2005). Even within a single species there may be multiple blooms per year. Several studies have exploited this behaviour to gain information about seasonality from foraminiferal assemblages (Tang and Stott, 1993; Wit et al., 2010).

Fourthly, "cryptic variability" within an apparently homogenous morphospecies, whereby one morphospecies in fact encompasses several genotypes, can cause significant intra-species stable isotope variability (Kucera and Darling, 2002). This variability typically arises because each genotype has a different habitat preference. While genetic material is not available for fossil foraminifera, the discovery of significant foraminiferal genetic variability has spurred attempts to more precisely delineate "morphotypes" within extant morphospecies (Aurahs et al., 2011; Darling et al., 2006; Morard et al., 2013; Quillévéré et al., 2013).

A number of strategies can be adopted to account for these "vital effects". Firstly, accurate and consistent species concepts are essential when picking foraminifera; morphometric methods can aid fulfilment of this objective, as discussed above. Secondly, picking individuals within a narrow size range reduces the effect of ontogenetic variability (Ezard et al., 2015). Thirdly, to minimize the intra-species variability within a single sample, it is preferable to measure samples containing as many individuals as possible. It has been estimated that >400 individuals would be required to produce a measurement with reproducibility of ≤0.1‰ with 90% confidence (Schiffelbein and Hills, 1984). While early mass spectrometers required a number of individuals of this order of magnitude in order to conduct a measurement, modern mass spectrometers used for stable isotope analysis require only a fraction of this number of individuals, with samples as small as single individuals now semi-routinely measured (Ganssen et al., 2011; Killingley et al., 1981; Koutavas et al., 2006; Leduc et al., 2009; Tang and Stott, 1993). As a result (and because of the time-

intensiveness of picking foraminifera), it is has become extremely uncommon to run hundreds of whole foraminiferal tests in the same analysis. However, several studies adopt an approach whereby a large number of tests are picked, broken into fragments that are then homogenized, with an aliquot taken for analysis (Bolliet et al., 2011; Brijker et al., 2007). This method relies on the aliquot selected being representative of the sample – an issue dealt with by repeat analysis of further aliquots as necessary.

2.2.4 Taphonomy

The final factor that must be considered when generating foraminiferal stable isotope records is taphonomy, which refers to any change that takes place in the calcite tests of foraminifera between their death and subsequent recovery from seafloor sediment. Production of stable isotope records that are faithful to the stable isotope composition of the original, pre-burial foraminiferal tests requires avoidance of foraminiferal tests which have undergone post-mortem alteration; a set of criteria for exceptionally preserved foraminifera was proposed by Pearson and Burgess (2008). The three primary mechanisms through which post-mortem alteration occurs – dissolution, inorganic precipitation, and recrystallization – are now discussed:

Dissolution can occur in the water column itself if the water is under-saturated with respect to carbonate; this effect is typically limited in shallow waters (Bissett et al., 2011), but occurs frequently as a result of corrosive bottom waters (Berger, 1971; Hemleben et al., 1989; Lipps, 1979). Dissolution also commonly occurs as soon as foraminiferal tests arrive at the seafloor where organic matter is oxidized to acidify porewaters (Jahnke et al., 1997; Jahnke and Jahnke, 2004; Self-Trail and Seefelt, 2005). The effects of dissolution are often readily visible under a binocular microscope, with foraminiferal tests damaged and fragmented (Dittert and Henrich, 2000; Peterson and Prell, 1985; Thunell, 1976); records of fragmentation and average shell weight can be used as quantitative proxies for dissolution (de Villiers, 2005; Le and Shackleton, 1992). Care must be taken when interpreting stable isotope records from foraminifera which have undergone dissolution, as different parts of the foraminiferal test can be more resistant to dissolution than others; given the ontogenetic variability in stable isotope composition outlined above, dissolution can therefore introduce bias to stable isotope measurements (Lohmann, 1995).

Secondly, foraminiferal tests can gain post-depositional inorganically precipitated calcite overgrowths, a result of pore waters infiltrating the sediment surrounding the calcite test; "exceptionally preserved" foraminifera typically come from clay-rich sediments, through which it is difficult for pore waters to permeate (Norris and Wilson, 1998; Pearson et al., 2001; Pearson and Wade, 2009; Stewart et al., 2004). Thirdly, foraminiferal tests can undergo recrystallization, whereby the original calcite crystals precipitated during foraminiferal growth are replaced by larger, secondary crystals formed after the test has been buried. This process results from neomorphism of the original crystals on a micron-scale, so original shell morphology is often

retained (Hodell et al., 2007; Pearson and Burgess, 2008; Sexton et al., 2006a). While calcite overgrowths and recrystallization are easily visible in SEM images, both can be difficult to identify under a binocular microscope. In particular, the retention of shell morphology (even down to the level of pores and spine bases) during recrystallization makes this a form of "cryptic diagenesis". The degree of translucency of the test has been suggested as a proxy for recrystallization: tests which have been well preserved typically have a 'glassy' appearance, whereas those which have undergone recrystallization appear more 'frosty' (Sexton et al., 2006a).

Overgrowths and recrystallization occur in different waters than those in which foraminifera grew, and so alter the foraminiferal test stable isotope composition (Kozdon et al., 2011, 2013; Schrag, 1999). This process typically only causes significant changes to foraminiferal $\delta^{18}O$ (Pearson et al., 2001, 2007; Sexton et al., 2006a; Williams et al., 2005); $\delta^{13}C$ is not strongly affected because the stable C isotopic composition of pore waters and foraminiferal calcite are usually similar (Pearson, 2012). While this would appear to render datasets generated on "frosty" foraminifera useless, it has been suggested that this diagenetic effect is typically sufficiently consistent at individual sites that overall trends in short records are generally faithful to the original biogenically precipitated calcite, even if the absolute values have been altered, though this is dependent on sedimentation rate (Sexton et al., 2006a).

2.3 XRF core scanning

Alongside foraminiferal geochemistry, X-Ray Fluorescence (XRF) core scanning is another widely used method for obtaining palaeoclimatological data. XRF scanning is a non-destructive method for analysing the elemental composition of sediment cores. Crucially, this method permits analyses at sufficiently high resolution (down to 1 mm in this thesis) to enable production of near- continuous records, as opposed to lower resolution records produced from analyses of the more widely spaced discrete samples typically used in palaeoclimate studies. XRF core scanning has been used to measure proxies for a diverse range of palaeoclimate applications including investigation of dust transport, lacustrine sedimentation, primary productivity and bulk carbonate content of marine sediments, as well as for stratigraphy (e.g., Bahr et al., 2005; Gebhardt et al., 2008; Jaccard et al., 2005; Kuhlmann et al., 2004; Richter et al., 2006; Rothwell and Croudace, 2015).

The process of XRF scanning involves an X-ray source at a 45° angle to the split sediment surface. The X-rays cause ionization of atoms in the sediment, i.e., one or more electrons are ejected from the ionized atoms. Immediately upon this ejection, an electron from a higher orbital shell falls to replace the displaced electron. In the process, this electron releases energy in the form of a photon. The frequency of this fluorescent radiation is proportional to the square of the atomic number,

following Moseley's Law (Moseley, 1914). The depth below the sediment surface to which the X-rays penetrate is dependent on atomic weight, and also on the chemical composition of the matrix. For "average marine sediments with significant amounts of Si, Al and/or Ca and some Fe", this penetration depth is 1 mm for Fe, 0.5 mm for Ca and 0.05 mm for AI (Richter et al., 2006). The emitted photons are recorded (in counts per second: cps) by a detector perpendicular to the source, with the number of counts at each frequency broadly proportional to the abundance of the corresponding element in the sediment. This relationship is not absolute because a number of factors can cause scattering of X-rays and/or the emitted photons.

The factors that cause scattering, and ways of minimizing these effects, are now considered. Surface roughness (Richter et al., 2006) is typically reduced by first smoothing the core surface using the edge of a microscope slide. This smoothing is across-core, not down-core, to avoid any up-/down-core contamination. The smoothed surface is then covered with a thin ultralene film in order to prevent contamination of the detector by the sediment, and to prevent sediment desiccation (Richter et al., 2006). Given that condensation on the sediment surface can bias XRF measurements, with water preferentially absorbing radiation emitted from lighter elements (e.g., Al, Si; Ge et al., 2005; Hennekam and de Lange, 2012; Koshikawa et al., 2003; Tjallingii et al., 2007), this film is not placed on the sediment until the core has equilibrated with room temperature. Nevertheless, additional factors that cause scatter, such as grain-size variability (Röhl and Abrams, 2000) and sediment inhomogeneities such as burrows (Jansen et al., 1998), cannot be compensated for. Thus while attempts have been made to calibrate XRF measurements to absolute elemental abundances (Lyle et al., 2012; Rousseau et al., 1996; Weltje and Tjallingii, 2008), XRF core scanning records are typically more cautiously interpreted as relative, rather than absolute, measurements.

The following chapter, entitled “Sub-orbital climate variability in the Oligocene North Atlantic Ocean”, is written in the style of a short-format research article, with the intention of future publication. While the manuscript was written entirely by Richard E. Smith, Paul A. Wilson also assisted with manuscript editing.

Chapter 3 Sub-orbital climate variability in the Oligocene North Atlantic Ocean

Major changes in atmospheric, marine and terrestrial climate at millennial and centennial timescales are best known from the circum-North Atlantic of the Pleistocene epoch (~2.5 million years ago to present) when the great ice sheets of the northern continents were in transition between their maximum and minimum extents. These rapid fluctuations in climate involved variability in Atlantic Meridional Overturning Circulation (AMOC). Vigorous AMOC is postulated to have been a feature of global thermohaline circulation since at least the Eocene-Oligocene Transition (~34 Ma), though the precise timing of its initiation is uncertain. Here, we present a record of palaeoceanographic variability in the North-West Atlantic during the latest Oligocene (~23.2 Ma). We find evidence of high frequency climate variability on millennial timescales from ~2000 to ~170 years) in sediment geochemistry, sea surface plankton ecology and temperature/salinity. Our results, from a time well before the development of large ice sheets in the northern hemisphere, suggest that millennial-centennial climate variability in the North Atlantic operates under a broader range of climatic states than previously observed.

In the Holocene, Earth's climate underwent pronounced changes in temperature, hydrology and ocean circulation on centennial-millennial timescales (Mayewski et al., 2004; Wanner et al., 2008, 2015). This variability is often cyclical, with cycle duration varying with latitude and environment. Variability on similar timescales extends back to glacial periods of the Late Pleistocene, where cyclical climatic behaviour is typically of higher amplitude and more globally synchronous. Here, Dansgaard-Oeschger (D-O) events (Dansgaard et al., 1993) are associated with climatic change of dramatic magnitude and extent: Greenland air temperature variability exceeded 10°C within as little as a few decades (Huber et al., 2006), and global teleconnections drove synchronous changes in terrestrial hydroclimate, for example by modulating the West African and East Asian monsoons and Southern Hemisphere storm tracks (Markle et al., 2017; Mulitza et al., 2008; Wang et al., 2001). These D-O events have been suggested to have similar periodicities (~1500 years) to 'Bond cycles' (Bond et al., 1997), the most pronounced and best-known example of sub-orbital periodicity in the Holocene, though this is debated (Obrochta et al., 2012). The largest amplitude sub-orbital shifts in the marine realm are observed in the North Atlantic, a result of its critical location as a site of deep water formation. Both Holocene (Chapman and Shackleton, 2000; Oppo et al., 2003; Thornalley et al., 2009) and Late Pleistocene (Clark et al., 2002; Gottschalk et al., 2015; Rahmstorf, 2002) records show a relationship between millennial-timescale temperature changes and the strength and/or flow path of North Atlantic thermohaline circulation, though the causality of this relationship is questioned (Barker et al., 2015). A variety of mechanisms have been

proposed to explain both Holocene millennial climate variability (Bond et al., 2001; Darby et al., 2012; Debret et al., 2007) and D-O events (Clark et al., 2002; Dima and Lohmann, 2009; Ganopolski and Rahmstorf, 2001; Kleppin et al., 2015; Peltier and Vettoretti, 2014; Petersen et al., 2013; Rahmstorf, 2002; Rasmussen et al., 2016; van Kreveld et al., 2000; Zhang et al., 2014), generally invoking periodicities arising from internal ocean and/or atmosphere dynamics, solar insolation variability, or in the case of D-O events only, periodic ice sheet and sea ice growth/retreat. However, a definitive pacemaker for millennial-timescale climate variability has yet to be established.

The range of climatic states in which high amplitude sub-orbital climate variability (i.e., D-O events) is expressed is reasonably well-established. Records indicate a temperature/ice volume threshold for high-amplitude sub-orbital variability in the Late Pleistocene that was only passed during glacial periods (McManus et al., 1999), with a reduced amplitude of sub-orbital variability and general climate stability in the Pliocene/early Pleistocene, when NHG was less extensive (Bartoli et al., 2006; Bolton et al., 2010; Draut et al., 2003; Friedrich et al., 2013). Sub-orbital variability is also of low amplitude when NHG is at a maximum; instead it is typically glacial periods of intermediate Northern Hemisphere ice volume in which the most pronounced sub-orbital variability is observed (Birner et al., 2016). Yet, the range of climatic states over which lower-amplitude, 'Holocene-type' sub-orbital variability takes place is not well established. While terrestrial varved sediments have been documented in records stretching back to the Late Oligocene (Fox et al., 2015) and further back through the Phanerozoic (de Winter et al., 2014), there is a paucity of marine records with sufficiently high sedimentation rates in the pre-Pliocene. The handful of such marine sedimentary sequences that have been studied lack the age control that enables precise identification of sub-orbital periodicities in Plio-Pleistocene records (Anderson, 1982; Elrick and Hinnov, 2007; Fischer et al., 1985). In particular, there is a sparsity of records from the North Atlantic, despite this region's critical role in more recent sub-orbital climate variability.

Here, we test for sub-orbital climate cycles in North Atlantic records from the latest Oligocene (~23.2 Ma), an interval which provides a novel set of background conditions in which to test for the presence of high frequency climate variability (Figure 3.1a). In the latest Oligocene, Antarctica was covered with a sizeable ice sheet, but this was only up to half the volume of its modern counterpart, with periodic, orbitally driven episodes of expansion and retreat (Liebrand et al., 2017). While there is limited evidence of Arctic sea ice (Darby, 2014) and localized mountain glaciers on Greenland (Bernard et al., 2016; Eldrett et al., 2007) as far back as the late Eocene (~44 and ~38 Myr ago, respectively), major NHG was not initiated until the Late Pliocene (~2.6 Myr ago; Bailey et al., 2013; Knies et al., 2014). Our records thus have the potential to shed light on the nature of millennial-centennial variability under a very different climate state to the one that prevailed during the Pleistocene and Holocene. At the same time, Late Oligocene tectonic

configuration, with an Atlantic Ocean of similar shape (if somewhat narrower) to today, enables comparison with modern records. Crucially, dominant pathways of ocean circulation in the Atlantic were, to a first order, similar to the modern; this is demonstrated by benthic foraminiferal stable isotope ratios (Miller and Fairbanks, 1983), seismic stratigraphy (Boyle et al., 2016; Davies et al., 2001; Miller and Tucholke, 1983) and radiogenic Nd isotopes (Scher and Martin, 2008; Via and Thomas, 2006), which indicate significant NADW production/AMOC at least as early as the Eocene-Oligocene Transition (~34 Ma) onwards.

Sub-orbital variability at the seafloor and sea surface

We present results from an 11.2 m interval of drift sediments at Integrated Ocean Drilling Program (IODP) Site U1405, located in the NW Atlantic off Newfoundland (40.1°N, 51.8°W, water depth 4287m). Based on our robust age model (constructed using magneto-, bio- and cyclo-stratigraphy; see Methods and Supplementary Figure 3.1) the duration of this interval is 51 kyrs, indicating an average sedimentation rate of 22 cm/kyr. This is an order of magnitude higher than typical Palaeogene records from pelagic sites, and is higher even than that of Iberian Margin Site MD01-2444/U185, where the planktic foraminiferal $\delta^{18}O$ record that is most similar to Greenland D-O variability is found. Site U1405 therefore provides a rare opportunity to test for the presence of sub-orbital climate cyclicity in the pre-Pliocene. We first present a high-resolution (1 mm scanning interval) record of $\%CaCO_3$ (Figure 3.1b), measured by X-Ray Fluorescence (XRF) core scanning and calibrated with discrete coulometric measurements (Supplementary Figure 3.2). This $\%CaCO_3$ record traces the proportion of the sediment composed of biogenic carbonate, generally ranging from 1 to ~20%, which is primarily composed of planktic foraminifera and coccolithophores (with no significant non-biogenic carbonate component). Clay, transported by the Deep Western Boundary Current (DWBC; Boyle et al., 2016), makes up most of the remainder of the sediment, along with a modest biogenic silica component (4 to 17% in 19 samples analysed; see Supplementary Information).

Close inspection of our $\%CaCO_3$ record reveals well-resolved cyclic features on sub-orbital timescales (Figure 3.1c, 3.2b,c), and multi-taper method (MTM) spectral analysis shows that these are regularly repeating (Figure 3.2a). When tested against a red noise model, three regular periodicities are found to have a statistical significance of over 99%: ~2000, ~1000 and ~320 years; and two have statistical significance above 95%: ~600 years and ~170 years. Carbonate dissolution cannot account for these changes: planktic foraminifera are exceptionally well-preserved in these clay-rich sediments (Figure 3.3). Cycles in $\%CaCO_3$ thus indicate cyclic changes in the relative balance between clay sedimentation and biogenic carbonate rain from the sea surface.

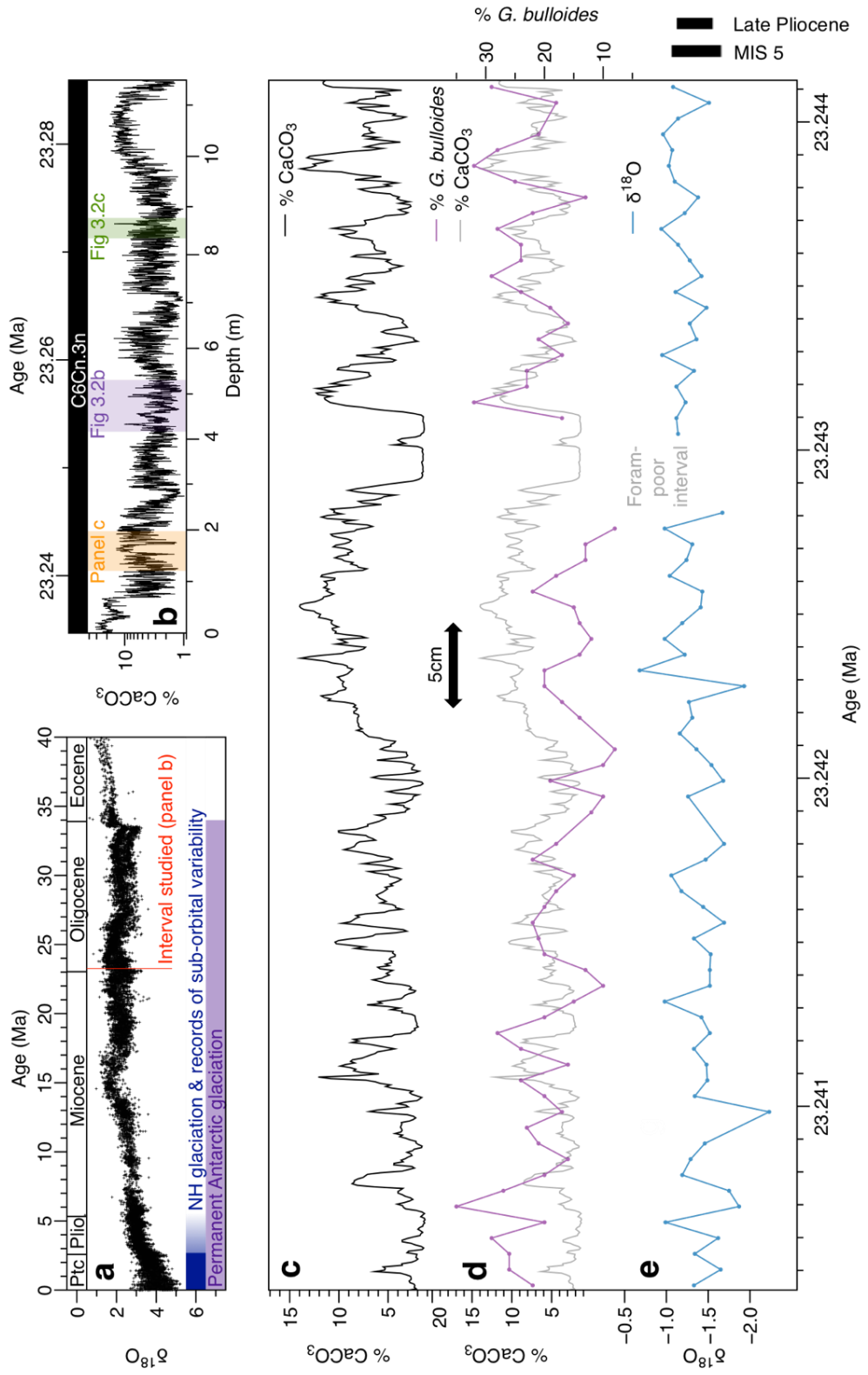

Figure 3.1 High resolution $\delta^{18}O$ and sediment $\%CaCO_3$ records from the latest Oligocene. **a**, Compilation of benthic $\delta^{18}O$ records from the Cenozoic (Zachos et al., 2001a), with the study interval presented in **b** shaded in red. **b**, Sediment $\%CaCO_3$, measured by X-Ray Fluorescence (XRF) core scanning. This ~11m interval spans ~50 kyrs. **c**, A zoomed interval (~6 kyrs) of the record highlighted in orange in **b**, showing

quasi-cyclic behaviour. **d**, In purple, 1 cm resolution record showing proportion of all planktic foraminifera that are surface-dweller *Globigerina bulloides*, demonstrating generally marked covariance with record **c**, which is reproduced here in grey. **e**, $\delta^{18}O$ of *G. bulloides* measured at 1 cm intervals. The black bars labelled 'MIS 5' and 'Late Pliocene' illustrate the approximate range of planktic $\delta^{18}O$ variability at these times in records from the Blake Outer Ridge (Oppo et al., 2001; Vautravers et al., 2004) and North Atlantic sub-tropical gyre (Bolton et al., 2010), respectively.

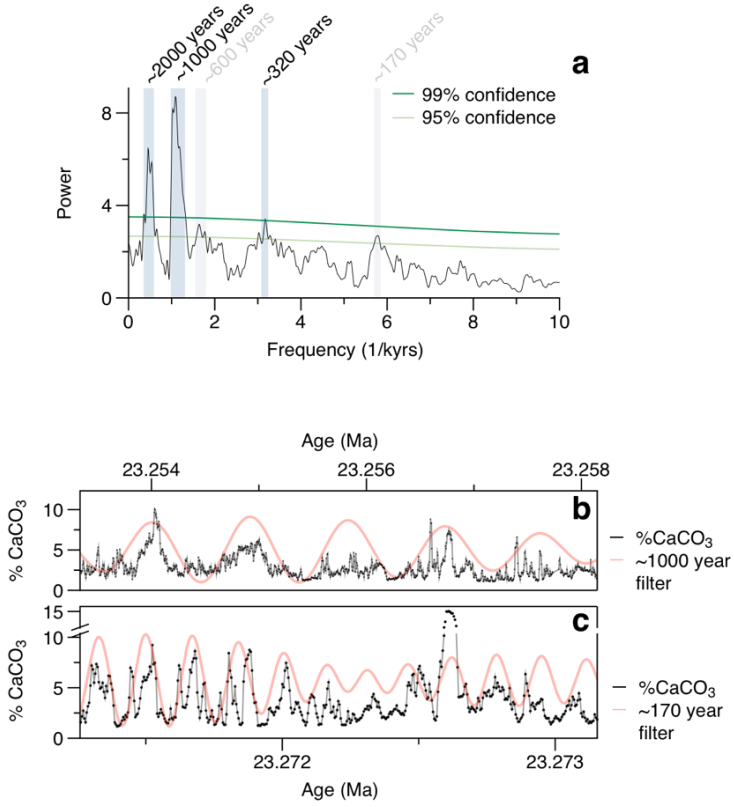

Figure 3.2 Spectral analysis of sediment $\%CaCO_3$. **a**, This multi-taper method spectral analysis (See Methods) of the record presented in **1b** reveals very strong periodicities (>99% confidence against a red noise model) at several frequencies (corresponding to ~2000 year, ~1000 year and ~320 year periodicities), and additional significant periodicities (>95% confidence) at frequencies corresponding to ~600 and ~170 years. **b** and **c**, ~5 kyr and ~2kyr zoomed interval of record **1b** in black, with filters of record **1b** in purple at periodicities of ~1000 and ~170 years.

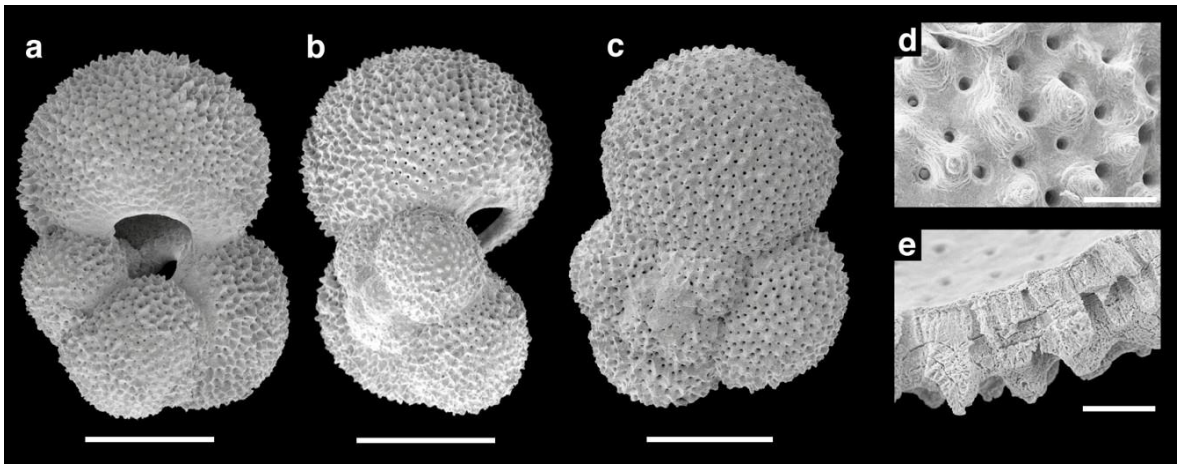

Figure 3.3 Scanning Electron Microscope (SEM) images of *G. bulloides*. **a,b,c,** Apertural, side and spiral SEM images, respectively, of *G. bulloides*. Scale bar is 100 µm. **d,e,** Close-up SEM images of *G. bulloides*, illustrating exceptional preservation, including retention of growth layers, visible in **e**. Scale bar is 10 µm.

First, we consider variable clay supply as a mechanism for controlling the observed changes in clay to carbonate burial. Such variability over longer (Myr) timescales is observed through the Cenozoic in integrated borehole-seismic records from the J-Anomaly and Newfoundland Ridges, implying changeable strength of the DWBC, and thus AMOC (Boyle et al., 2016). There is precedent for similar AMOC variability but on shorter, sub-orbital timescales in multiple records of the late Pleistocene, with a cooler Northern Hemisphere associated with reduced North Atlantic Deep Water (NADW) formation (Elliot et al., 2002; Rahmstorf, 2002). Our data show several strong periodicities in Al/Ti similar those seen in $\%CaCO_3$ (~2200, ~1000, ~300 and ~160 years; Supplementary Figure 3.3) consistent with mineralogical variability (Bahr et al., 2014) in response to changes in deep water current strength. This observation is consistent with variability in sediment provenance at periodicities from ~1-4 kyrs seen in K/Ti XRF core scanning record from the mid-Pleistocene North Atlantic (IODP Site U1314, 56°N; Grützner and Higgins, 2010). Variable clay sedimentation, and resultant cyclic dilution of biogenic carbonate, may therefore play a role in driving our $\%CaCO_3$ record.

Alternatively, variability in $\%CaCO_3$ could be driven by changes in sea surface carbonate productivity, which we assess by recording the proportion of the planktic foraminiferal assemblage made up by the surface-dwelling species *Globigerina bulloides* (Figure 3.1d). In the modern ocean, *G. bulloides*, an asymbiotic species, is often used as a productivity indicator because of its abundance in high northern/southern latitudes and low-latitude upwelling regions (Fraile et al., 2008). *G. bulloides* may have hosted symbionts in the Palaeogene (Pearson and Wade, 2009), and therefore had a different ecology to today, but the high-amplitude variability seen in our record (ranging from 8 to 35%) indicates highly variable surface water conditions on sub-orbital

timescales. Crucially, cycles in $\%CaCO_3$ and % *G. bulloides* are of the same sign: enhanced sediment carbonate content is associated with surface water ecology changes that favour *G. bulloides*.

Given the absence of an age model of much higher resolution, which would not be possible to generate using current techniques, it is not possible to assign either of the above mechanisms as the sole or dominant driver of changes in our $\%CaCO_3$ record. Instead, we note that regardless of their relative influence, and as a result of the proximity of Site U1405 to sites of formation of the same deep water that bathes the seafloor directly below, both of these mechanisms are indicators of the same process: cyclic change in surface oceanographic conditions at Site U1405. We now investigate this oceanographic variability in more detail.

Indicators of oceanographic change

Today, the surface ocean hydrography of Site U1405 is strongly influenced by the North Atlantic Current (NAC), a component of the Gulf Stream that transports warm, high salinity, nutrient-poor waters northwards (Figure 3.4a, b). However, Site U1405 also lies within the range of the frontal zone between waters of the NAC and the Labrador Current (LC), which transports cool, low salinity, nutrient-rich Labrador Sea Water southwards. Movement of this front is well documented in modern instrumental records, which reveal latitudinal shifts on annual and multi-decadal timescales (Han, 2007; Hirahara et al., 2013). We assume that both a proto-Labrador current (Barron and Peterson, 1991) and a proto-Gulf Stream (Pinet et al., 1981; Wade and Kroon, 2002) operated in the latest Oligocene, consistent with the Eocene-Oligocene origins of modern day North Atlantic circulation (Boyle et al., 2016; Davies et al., 2001; Miller and Fairbanks, 1983; Miller and Tucholke, 1983; Scher and Martin, 2008; Via and Thomas, 2006), and thus that the front operated broadly similarly to today. Movement of the front is also seen in Plio-Pleistocene records, shifting southwards during episodes of enhanced NHG, driving changes in productivity because of the higher primary productivity in the frontal zone relative to waters bathed by the NAC alone (Friedrich et al., 2013; Naafs et al., 2010; Taylor and Ferrari, 2011; Villanueva et al., 2001). The cyclical pattern in carbonate export productivity we observe in the latest Oligocene suggests periodic variability in the influence of the frontal zone on hydrography at Site U1405. This suggests cyclical variability in the southerly reach of the frontal zone, and thus in the relative strengths of the NAC and LC.

To better assess the magnitude of temperature/salinity variability at Site U1405, we present planktic foraminiferal stable isotope records generated on *G. bulloides* (Figure 3.1e). The planktic

record demonstrates variability in $!^{18}O$ typically of ~0.6‰ (but up to 1‰) on centennial timescales similar to those on which the planktic foraminiferal faunal assemblage varies. This magnitude of

$!^{18}O$ variability is comparable to that at nearby locations associated with sub-orbital variability in times of modest Arctic glaciation during the Plio-Pleistocene. These include planktic foraminiferal

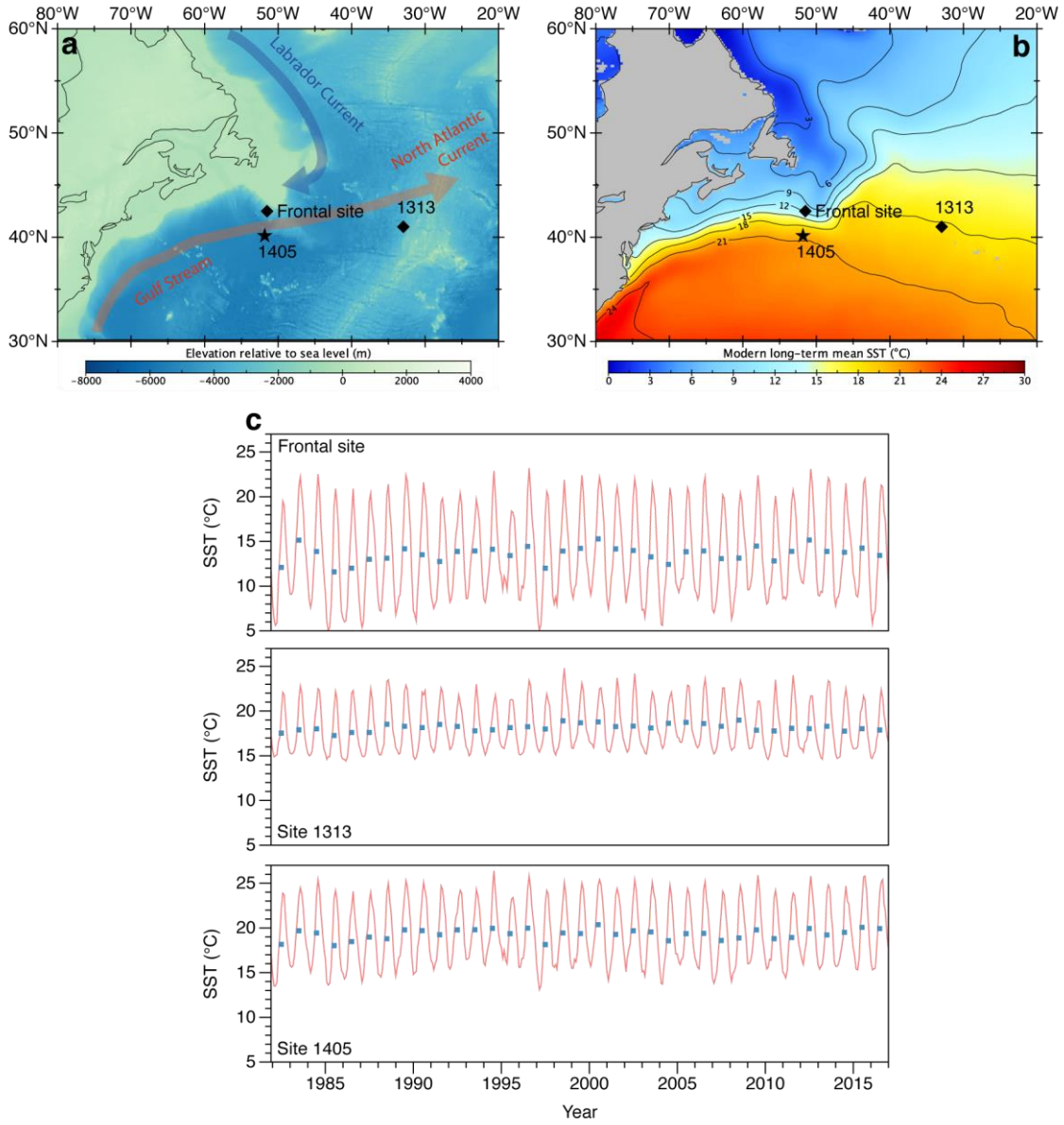

Figure 3.4 Bathymetry and sea surface temperature (SST) in the modern North-West Atlantic. **a**, Bathymetry of the modern North Atlantic, with the locations plotted of IODP sites U1405 and U1313, and a site (42.5°N, 51.5°W) lying in the North Atlantic Current-Labrador Current front. Schematic paths of the modern Gulf Stream/North Atlantic Current and Labrador Current are also shown. **b**, Average SST from 1955-2012. **c**, Average monthly (red line) and annual (blue markers) SST at sites marked in **a** and **b**. See Methods for data sources.

!^{18}O variability of ~0.5-0.7‰ during Marine Isotope Stage (MIS) 5 at the Blake Outer Ridge (32°N), south-west of Site U1405 and directly underneath the flow path of the NAC (Oppo et al., 2001; Vautravers et al., 2004), and ~0.3-0.6‰ at sub-tropical gyre IODP Site U1313 during the Late Pliocene (Bolton et al., 2010).

Foraminiferal abundance is not high enough in our samples to generate a paired Mg/Ca temperature proxy record for *G. bulloides*. Therefore, to assess the relative contributions of temperature and salinity near Site U1405, we consider SST-!$^{18}O_{sw}$ relationships in the northwest North Atlantic today. We use !^{18}O calibrations of modern *G. bulloides* to estimate the approximate influence of temperature and salinity on !$^{18}O_{G.\ bulloides}$ (Bemis et al., 1998; Supplementary Figure 3.4). Salinity changes only dominate !$^{18}O_{G.\ bulloides}$ variability south of Site U1405, where latitudinal temperature change is minimal, and only changes !$^{18}O_{G.\ bulloides}$ by ~0.3‰. Temperature changes have a much larger effect, being the dominant control on estimated foraminiferal !^{18}O north of Site U1405, changing !$^{18}O_{G.\ bulloides}$ by 1.3‰. We therefore infer that the majority (>75%) of !^{18}O variability observed is caused by temperature change.

To determine the extent to which temperature changes at Site U1405 are representative of broader regional temperature changes, we compare satellite-derived sea surface temperature records from the years 1981 to 2017 at Site U1405 with those at a location ~260 km north (i.e., in the middle of the frontal zone) and at IODP Site U1313, ~1600 km east, an archetypal North Atlantic sub-tropical gyre site (Figure 3.4c). Variability at the frontal location is significant, with the range of seasonal variability typically ~15 °C and an inter-annual range of ~3.7 °C, while at Site U1313 variability is greatly reduced, with seasonal and inter-annual variability of ~7 °C and ~1.7 °C respectively. Variability at Site U1405 is intermediate, with seasonal and inter-annual variability of ~10 °C and ~2.3 °C respectively, indicating that variability at Site U1405 is influenced somewhat, but not dominated, by the NAC-LC frontal zone. As a result, temperature changes here in the modern are indicative of temperature variability in the sub-tropical gyre, suggesting that our record indicates sub-orbital temperature variability in the wider North Atlantic and is not simply a function of a frontal zone.

Sub-orbital climate cyclicity: a persistent feature of Earth's climate

Next, we consider the broader regional implications of our results. Surface water density (i.e., temperature and/or salinity) in the modern high latitude North Atlantic is closely associated with AMOC strength in instrumental records (Latif et al., 2004; Rahmstorf et al., 2015) and model experiments (Roberts et al., 2013). Specifically, enhanced AMOC is associated with significantly cooler than average temperatures just north of Site U1405 in the Labrador Sea but mildly warmer than average temperatures just south of Site U1405, where NAC influence is stronger. The flow path of the NAC is also seen to change with AMOC strength in instrumental records and model experiments, moving further south with intensified AMOC (Joyce and Zhang, 2010; Sanchez-Franks and Zhang, 2015). Changes in surface water density (indicated in our record by !^{18}O variability) and the relative influence of the NAC and LC (indicated by ecological variability) at Site U1405, together with potential changes in DWBC strength (indicated by mineralogical variability of clay sedimentation) therefore imply changes in the strength of AMOC on sub-orbital timescales in the latest Oligocene. This relationship is not necessarily surprising given the

relationship between North Atlantic temperature and AMOC strength over millennial timescales in both the Holocene (Thornalley et al., 2013) and latest Pleistocene (Clark et al., 2002; Rahmstorf, 2002), with cooler intervals typically associated with weakened AMOC.

Our observations indicate that Earth's climate has several sub-orbital periodicities which act over a wider range of background climate states than previously observed. The similarity of the ~1000 and ~2000 year cycles we observe to the range of variability of 'Bond cycles' and D-O events hints at a common pacemaker acting in the Late Pleistocene and latest Oligocene, as does the similarity of a variety of Late Pleistocene/Holocene centennial climate cycles to the smaller length cycles we observe (e.g., 192 year [Prasad et al., 2004], 205 year [Neff et al., 2001], ~200 year [Raspopov et al., 2008] and 169 year [McDermott et al., 2001] cycles as potential equivalents to the ~170 year cycles we observe). But what is the ultimate pacemaker of these cycles? While most proposed mechanisms for late Pleistocene millennial climate variability involve internal oceanic/glacial/atmospheric dynamics, others suggest an external solar forcing, which could provide a mechanism without requiring significant NHG. Gleissberg (~87 year) and DeVries-Suess (~210 year) cycles, generally attributed to solar variability (Peristykh and Damon, 2003; Wagner et al., 2001), have been modelled to produce cyclic climate behaviour on periods of ~1500 years (Bond et al., 2001; Braun et al., 2005; Dima and Lohmann, 2009; though this is debated [Muscheler and Beer, 2006]) and ~200 years (Seidenglanz et al., 2012; Weber et al., 2004). However, in the absence of a causal mechanism both for the cycles themselves and for their interaction with Earth's climate, such a connection remains speculative. Regardless of the identity of the pacemaker, the existence of centennial and millennial cycles in both the Pleistocene/Holocene and latest Oligocene is indicative of a driver which acts over a wide range of climatic states, or a range of drivers which vary in influence as climatic parameters change. Our results call for new records from additional climate states (e.g., in greenhouse climates) to determine whether this range of climatic states is even broader than we have identified here.

3.1 Methods

Age model

All ages referred to herein refer to the GTS 2012 timescale (Gradstein et al., 2012), unless otherwise stated. In the Late Oligocene and Early Miocene, twelve magnetic reversals were identified shipboard across a 135 m interval stretching from the top of subchron C6AAr.3r (age 21.688 Ma) to the base of subchron C6Cn.3n (23.295 Ma; Expedition 342 scientists, 2012). We use this interval as the basis of our age model. Reversal positions between the top of subchron C6Br.1r

(22.268 Ma) and the base of C6Cn.3n were refined with measurements made at NOCS-University of Southampton (T. van Peer, pers. comm.).

XRF core-scan data were collected across the whole study interval (C6AA.3r to C6Cn.3n) at 2 cm resolution. When placed on the shipboard magnetostratigraphic age scale, several terrigenous elemental ratios (which we interpret as proxies for lithology) show periodic behaviour, with particularly clear cycles in Si/Al and Ti/Fe (Supplementary Figure 3.1a). Multi-taper method spectral analysis of these ratios indicates the presence of several strong periodicities of length ~20.5 kyrs, ~33 kyrs and ~100 kyrs. Given the similarity of these periodicities to orbital cycles of precession (~21 kyr), obliquity (~41 kyr) and eccentricity (~100 kyr), we interpret them as originating from the orbital forcing that is a pervasive feature of climate change on 10^3-10^5 year timescales throughout the Cenozoic (Hays et al., 1976; Zachos et al., 2001a).

Having detected the footprint of orbital variability in an extended Late Oligocene-Early Miocene interval of Site U1405, we generated a detailed age model for our specific study interval, subchron C6Cn.3n. There are nearly 3 complete cycles in Si/Al and Ti/Fe during subchron C6Cn.3n (Supplementary Figure 3.1c). The estimated range of duration of this subchron falls between 62 and 106 kyrs, with uncertainty arising from differing cyclostratigraphic interpretations (Supplementary Table 3.1) indicating that these three cycles in the XRF data series are either precession- or obliquity-driven. We interpret the cycles to be precession- (not obliquity-) driven, based on three lines of evidence. First, we note that the ~33 kyr "obliquity" signal seen in our spectral analysis is weaker than the ~20.5 kyr precession signal, as well as being at a periodicity >15% shorter than the expected obliquity periodicity. Second, a precession signal is consistent with the stronger relative influence of the North Atlantic Current relative to the Labrador Current at our site today (see main text), which would favor a low-latitude (precession) over high- latitude (obliquity) orbital forcing. Such behaviour is seen in Late Pleistocene North Atlantic records, with precessional influence on clay mineralogy at latitudes as high as 51.9°N (Bout-Roumazeilles et al., 1997). We also note the high carbonate content of Site U1405 and other Sites on the J-Anomaly Ridge (Expedition 342 scientists, 2012); in the modern, sediment carbonate content is higher on sea floor under the NAC than that under the LC (Biscaye et al., 1976). Third, a ~60 kyr duration of subchron C6Cn.3n is consistent with a greater number of literature estimates (Supplementary Table 3.1) than a duration of ~120 kyrs (Beddow, 2016; Billups et al., 2004; Gradstein et al., 2012; Liebrand et al., 2016). We therefore subsequently assign a precessional forcing to the cycles in Si/Al and Ti/Fe, with a spacing of 20.5 kyrs between each precessional peak. We also note that, regardless of whether the duration of subchron C6Cn.3n is ~60 or ~120 kyrs, there is no doubt that the variability we observe in our record (Figures 3.1, 3.2) takes place on sub-orbital timescales.

To account for short-term changes in sedimentation rate through our record we tune our record spanning subchron C6Cn.3n to the precessional maxima and minima identified in filtered Si/Al and

Ti/Fe (dashed lines in Supplementary Figure 3.1c). Note that we use a splice that is modified from the shipboard splice for logistical reasons; see the Appendix. Based on the spectral analysis peak in these records at 20.5 kyrs, we assign a duration of 10.25 kyrs (i.e., half a precessional cycle) between each maxima and minima when tuning. The tuned record, on a floating timescale, lies between the first and last of the precessional maxima/minima that fall in subchron C6Cn.3n (i.e., the left- and right-most dashed vertical lines in Supplementary Figure 3.1c). In Figures 3.1 and 3.2 we assign absolute ages to our floating timescale based on the age of the top of subchron C6Cn.3n on the GTS 2012 timescale but, because of the uncertainty in this age (Supplementary Table 3.1), we stress that, although our study is not concerned with issues of absolute age, the absolute ages that we assign are associated with some uncertainty.

XRF core scanning

For the XRF core scan data presented in the Age Model section above (i.e., the 2 cm resolution data presented in Supplementary Figure 3.1), data were collected using an Avaatech (Serial No. 19) instrument at the Gulf Coast Repository, Texas A&M University. Measurements were made every 2 cm down-core over a 1.2 cm^2 area with a down-core slit size of 10 mm, using generator settings of 10 kV, a current of 1 mA, and a sampling time of 20 seconds. For the data presented in the main text of this article (i.e., the 1 mm resolution data presented in Figures 3.1 and 3.2), data were collected at using an Avaatech (Serial No. 12) instrument at MARUM, Bremen University. Measurements were made every 1 mm down-core over a 12 mm^2 area with a down-core slit size of 1 mm, using generator settings of 10 kV, a current of 1.0 mA, and a sampling time of 20 seconds. In both cases the split core surface was covered with a 4 µm thin SPEXCerti Prep Ultralene1 foil to avoid contamination of the XRF measurement unit and desiccation of the sediment. The data reported here were acquired by a Canberra X-PIPS Silicon Drift Detector (SDD; Model SXD 15C-150-500) with 150eV X-ray resolution, the Canberra Digital Spectrum Analyzer DAS 1000 and an Oxford Instruments 100W Neptune X-ray tube with rhodium (Rh) target material. Raw data spectra were processed by the Analysis of X-ray Spectra by the Iterative Least Square (WIN AXIL) package from Canberra Eurisys.

Spectral analysis

XRF records (on the tuned age scale) were first linearly interpolated to fill in gaps from data removed because of sample disturbances at the top and bottom of each section, and where occasional samples had been taken prior to XRF core scanning. The interpolated record has an artificial sampling interval of 5 years. This record was then detrended with a Gaussian notch filter (frequency 0 yrs^{-1}, bandwidth 0.0003 yrs^{-1}). Linear interpolation and detrending was performed using Analyseries software (Paillard et al., 1996). Next, outliers lying more than 5 standard deviations from the mean of this de-trended data were removed. Using this method, 0.5% of the Al/Ti data points were removed; no outliers were identified in Ca counts. A second linear

interpolation (again with artificial sampling interval of 5 years) was performed to fill in gaps left by removed data points. Following these data preparation steps, a spectral analysis was performed using SSA-MTM Toolkit software (Ghil et al., 2002; Figure 3.2a and Supplementary Figure 3.2b). Filters of selected frequencies were then generated in Analyseries (Figure 2b,c) using a Gaussian filter.

Estimation of sediment $\%CaCO_3$ content

To obtain a high-resolution proxy for $\%CaCO_3$, we first measured $\%CaCO_3$ using an AutoMate + CM5015 coulometer at the National Oceanography Centre, University of Southampton. 78 discrete 1 cm crushed samples were measured, with carbonate content ranging from 1 to 29 %. We then calculated the average XRF-measured Ca counts over the corresponding interval in the other core half. A linear regression of coulometry data to XRF data shows strong positive correlation (R^2 = 0.88; Supplementary Figure 3.2). This regression ($\%CaCO_3$ = 0.00018428 × Ca counts) was subsequently applied to the whole record shown in Figures 3.1 and 3.2 to generate a record of $\%CaCO_3$.

Taxonomy of *Globigerina bulloides*

Although forms similar to modern *Globigerina bulloides* are, in the Oligocene, typically assigned to the ancestral species *Globigerina praebulloides* (Blow, 1979; Bolli and Saunders, 1985; Kennett and Srinivasan, 1983), the individuals we observe show only minor differences from the modern species. We therefore use the modern species name, following Pearson and Wade (2009), adopting a conservative taxonomic definition in which only individuals with a 'bulloides-type' (Hemleben and Olsson, 2006), rather than cancellate, wall texture were included.

Foraminiferal faunal assemblage counts

Samples were freeze-dried, soaked in Calgon and washed over a 63 µm sieve with de-ionized water. The coarse fraction was retained, and oven-dried at 40°C. This sample was then dry-sieved to retain all material in the >180 µm size fraction. All samples contained >70 planktic foraminifera (>100 individuals in 82% of samples). The total numbers of a) individuals of *Globigerina bulloides* and b) individuals of all other remaining planktic foraminiferal species were recorded; the ratio of these is presented in Figure 3.1d.

Planktic foraminiferal stable isotopes

From the same washed samples, 3-20 individuals of *G. bulloides* were picked in the 180-212 µm size fraction, with 3-20 individuals picked depending on abundance (≥6 individuals in 77% of samples). Picked individuals were transferred to reaction vials and analysed using a Kiel IV Carbonate Device attached to a Thermo Finnigan MAT 253 dual inlet mass spectrometer at NOCS,

University of Southampton. Analytical precision is 0.08‰ (1σ) for $!^{18}O$. Data were calibrated

using a two-point calibration to standard NBS 18 and an internal standard (GS1). Results are reported relative to the Vienna Pee Dee belemnite (VPDB) standard.

Modern oceanographic data

All maps are plotted using NASA Panoply software (https://www.giss.nasa.gov/tools/panoply/). Bathymetry data (Figure 3.4a) is the General Bathymetric Chart of the Oceans (GEBCO) 30 arc-second grid, version GEBCO_2014 (20150318) (obtained from https://www.bodc.ac.uk/data/hosted_data_systems/gebco_gridded_bathymetry_data/gebco_30_second_grid/). Sea Surface Temperature (SST) map data (Figure 3.4b) is taken from the NOAA World Ocean Atlas 2013 version 2 (https://www.nodc.noaa.gov/OC5/woa13/woa13data.html). Values are averaged from 1955-2012, and are interpolated from their 0.25° spatial resolution. SST time-series (Figure 3.4c) are from NOAA Optimum Interpolation (OI) Sea Surface Temperature (SST) V2 (https://www.esrl.noaa.gov/psd/data/gridded/data.noaa.oisst.v2.html) monthly 1° spatial resolution averages. This data originates from satellites, ships and buoys. Because the SST data is interpolated to a 1° x 1° grid, data for Site U1313 is for co-ordinates 41.5°N, 32.5°W (67 km NE of the true location of Site U1313) and data for Site U1405 is for 40.5°N, 51.5°W (49 km NE from the true location of Site U1405).

3.2 Supplementary Figures

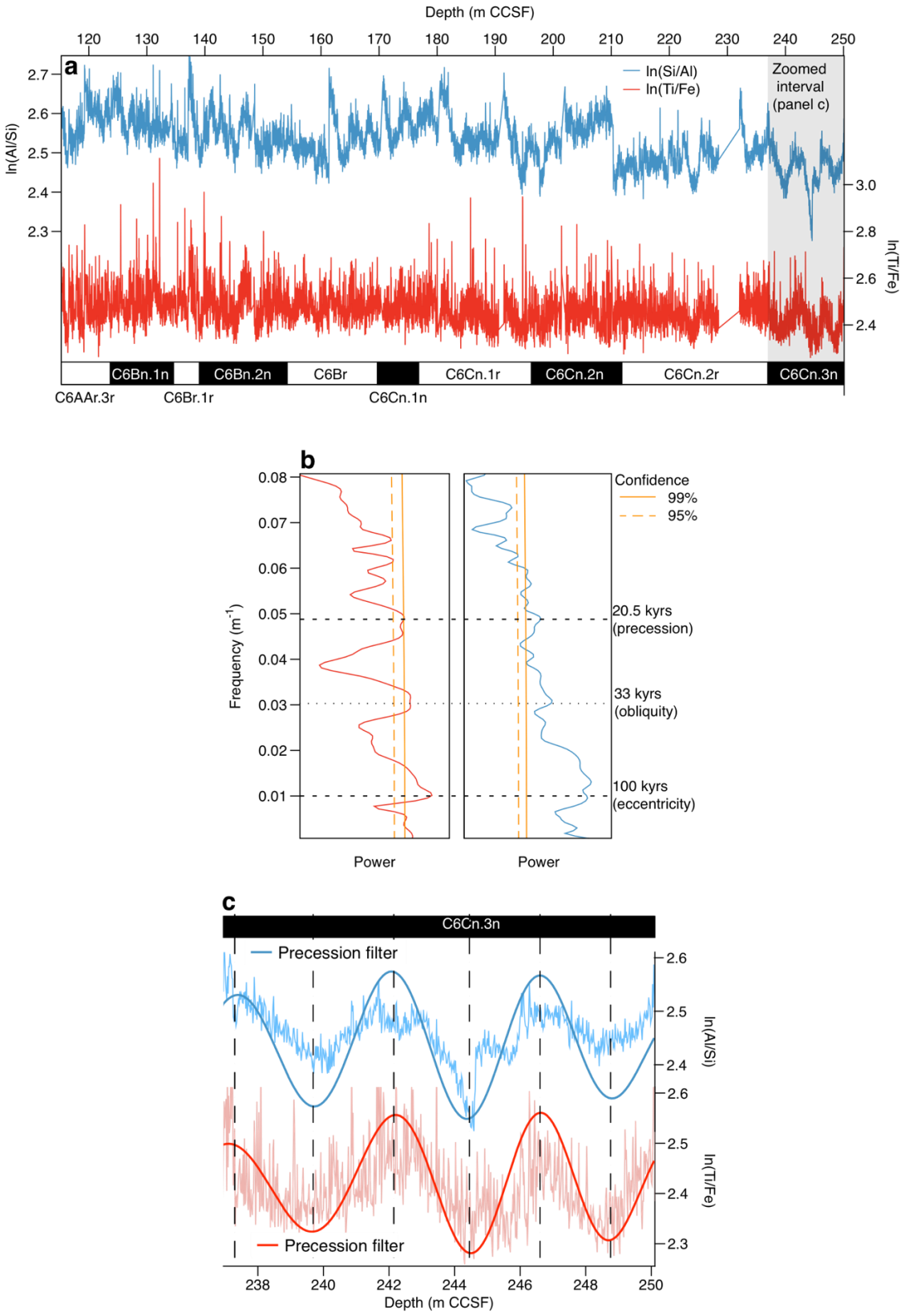

Supplementary Figure 3.1 (previous page) Construction of age model. **a**, 2 cm resolution Al/Si and Ti/Fe records, generated by XRF core scanning. **b**, MTM spectral analysis of the records shown in **a**, revealing three periodicities close to precession, obliquity and eccentricity. **c**, A zoomed interval of **a**, showing only subchron C6Cn.3n (the study interval; see Figure 3.1b). Overlain in heavy blue and red are 20.5 kyr Gaussian filters of the data. Dashed lines align with maxima and minima in the data, and are used (with a spacing of 10.5 kyrs) to tune the record detailed in the main text.

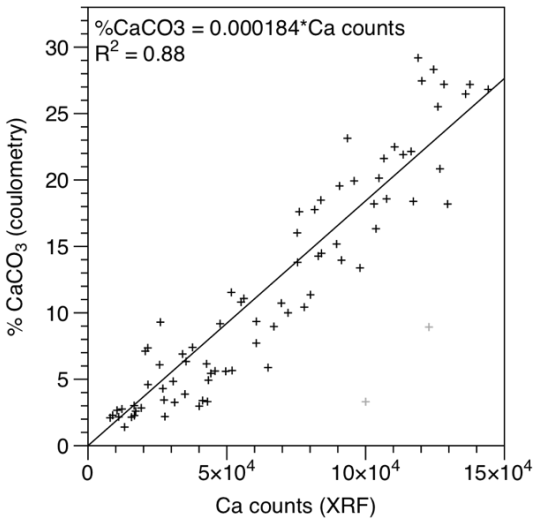

Supplementary Figure 3.2 %$CaCO_3$ calibration. Cross-plot of %$CaCO_3$, as measured in discrete 1 cm samples by coulometry, and Ca counts, as measured by XRF core scanning. The fit is a straight line, with a forced y intercept of zero. The two grey data points were deemed outliers and excluded from calculation of the best fit line.

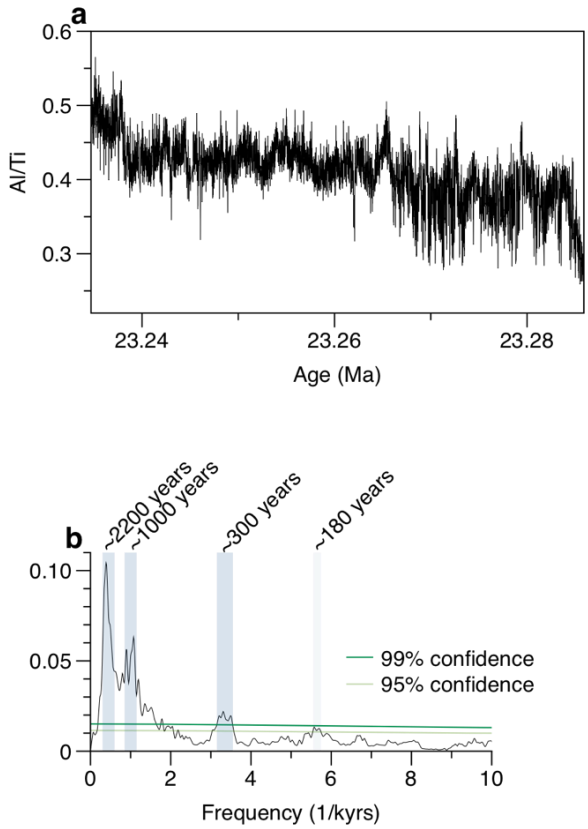

Supplementary Figure 3.3 Al/Ti record. **a,** ln Al/Ti, measured by XRF core scanning. **b,** Spectral analysis of the Al/Ti record, revealing several very strong periodicities (>99% confidence interval) at ~2200, ~1000 and ~300 years, and a strong periodicity at ~180 years.

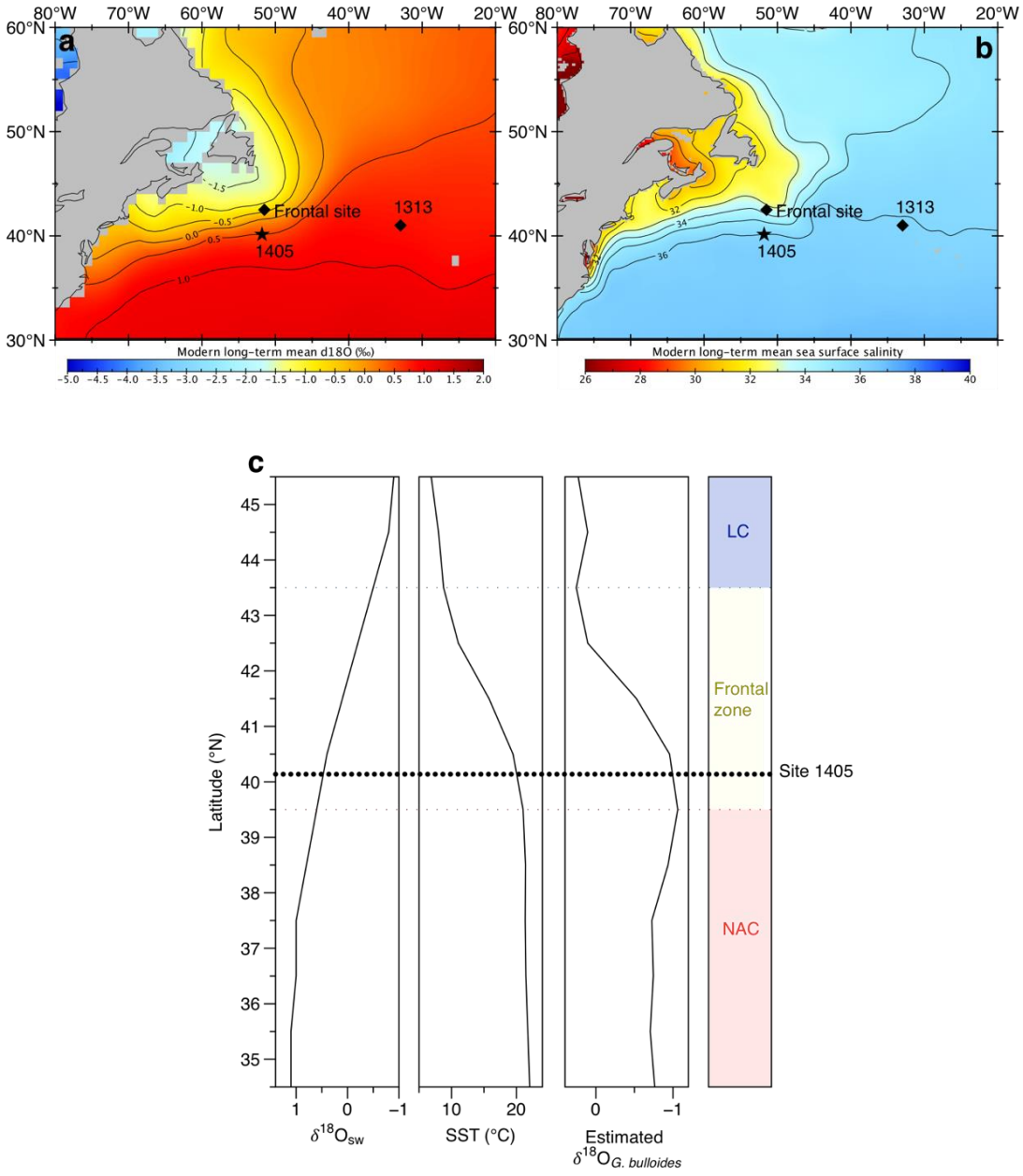

Supplementary Figure 3.4 Modern NW Atlantic surface $!^{18}O_{sw}$ and salinity. **a,** Estimated modern surface water $!^{18}O$ on an interpolated 1° spatial grid (LeGrande and Schmidt, 2006; Schmidt et al., 1999). **b,** Modern Average sea surface salinity 1955-2012 (same data source as Figure 3.4b; see Methods). **c,** Latitudinal transect (1° latitudinal resolution) at 51.5°W of estimated $!^{18}O_{sw}$, SST and predicted $!^{18}O_{G.\ bulloides}$, using a culture calibration for 11-chambered *G. bulloides* (Bemis et al., 1998).

3.3 Supplementary Table

Reference	**Site**	**Start**	**End**	**Subchron length**
GTS 2012 (Gradstein et al., 2012)	1218: Equatorial Pacific	23.233	23.295	**62 kyrs**
Billups et al., 2004	1090: South Atlantic	23.237	23.299	**62 kyrs**
Beddow et al., 2016 (based on !^{13}C)	U1313: Equatorial Pacific	23.211	23.286	**73 kyrs**
Liebrand et al., 2016	1264, 1265, 1266: Walvis Ridge	23.247	23.332	**85 kyrs**
Beddow et al., 2016 (based on $CaCO_3$)	U1313: Equatorial Pacific	23.212	23.318	**106 kyrs**

Supplementary Table 3.1 Literature estimates of the duration of magnetic subchron C6Cn.3n.

The following chapter, entitled “Decoupling of surface and deep North Atlantic waters over the Oligocene-Miocene Transition”, is written in the style of a research article, with the intention of future publication. While the manuscript was written entirely by Richard E. Smith, Paul A. Wilson also assisted with manuscript editing.

Chapter 4 Decoupling of surface and deep North Atlantic waters over the Oligocene-Miocene Transition

4.1 Abstract

The Antarctic ice sheet was highly dynamic in the Oligocene and Miocene, with orbitally-forced cycles of expansion and retreat. The Oligocene-Miocene Transition (OMT; ~23 Ma) stands out as one of the largest of these cycles. The OMT terminated the late Oligocene warming trend with a pronounced transient glaciation in which Antarctic ice volume is generally inferred to have increased and subsequently decreased by at least half its modern volume over several hundred thousand years. Here we present a ~0.8 Myr-long (23.4-22.6 Ma) high-resolution planktic stable isotope ($\delta^{18}O$ and $\delta^{13}C$) record across the OMT from IODP Site U1406 in the North-West Atlantic, a critical region for modern ocean circulation. Our record benefits from excellent preservation of clay-hosted foraminiferal calcite and high sedimentation rates (~2 cm/kyr), and has an average sampling interval of ~2 kyrs. We identify substantial short and medium-term (10^3-10^4 years) variability in planktic $\delta^{18}O$ of up to ~1.5‰, interpreted to be the product of significant regional surface-ocean temperature changes and latitudinal shifts of the front between the North Atlantic Current and Labrador Current. Comparison of our results to an unpublished benthic stable isotope record from the same site reveals that changes in the surface ocean generally lead those on the sea floor by tens of thousands of years. This finding indicates a previously undetected decoupling of surface and bottom waters over the OMT that implies that the North Atlantic played a role in triggering Antarctic glaciation and deglaciation.

4.2 Introduction

The Oligocene and Miocene epochs are characterised by recurring benthic foraminiferal $\delta^{18}O$ cycles, interpreted as episodes of high latitude climate change involving the growth and retreat of major Antarctic ice sheets (Liebrand et al., 2017; Miller et al., 1991; Pälike et al., 2006b; Wade and Pälike, 2004) following the initiation of major glaciation at the Eocene-Oligocene Transition ~34 Ma (Coxall et al., 2005; Coxall and Wilson, 2011). The boundary between the Oligocene and Miocene epochs (23.03 Ma) coincides with a particularly high amplitude benthic $\delta^{18}O$ shift of ~1‰ observed in records worldwide (Beddow et al., 2016; Billups et al., 2002; Liebrand et al., 2011; Pälike et al., 2006a; Zachos et al., 2001b), known as the Oligocene-Miocene Transition (OMT). The OMT is interpreted to reflect Antarctic glacial expansion (Naish et al., 2001; Passchier and

Krissek, 2008) to around its present volume over ~200 kyrs, from a baseline of up to half of its current volume (Gasson et al., 2016; Liebrand et al., 2011) or even a deglaciated state (Liebrand et al., 2017). This glacial expansion is equivalent to ~30-80 m of sea level change (Liebrand et al., 2011; Miller et al., 1991; Pekar et al., 2002); meanwhile a low resolution Mg/Ca data set indicates that deep water temperatures cooled by about 3°C associated with this transient event (Mawbey and Lear, 2013). Low resolution terrestrial records indicate surface cooling in North America and Asia over the OMT (Kotthoff et al., 2014; Miao et al., 2013), but an absence of high-resolution surface records means the timing of this cooling relative to Antarctic glacial expansion is poorly constrained.

While the glaciation stage of the OMT has been linked to an orbital configuration favouring low seasonality and thus cool polar summers (Pälike et al., 2006a; Zachos et al., 1997, 2001b), the relatively rapid deglaciation stage of the OMT has long proven difficult to reconcile with the results of coupled GCM-ice sheet model experiments. This rapid (~150 kyrs) inferred deglaciation is at odds with the strength of CO_2 hysteresis associated with large Antarctic ice sheets in initial coupled numerical experiments (Pollard and DeConto, 2005) in the context of apparently modest changes in pCO_2 levels (Beerling and Royer, 2011). This picture may be beginning to change, with recent work suggesting that large Antarctic ice sheets may have been sensitive to smaller pCO_2 changes than previously suggested (Gasson et al., 2016); meanwhile a terrestrial record indicates that there may have been a brief pCO_2 rise associated with the deglaciation stage of the OMT (Reichgelt et al., 2016). However, high resolution records, necessary for investigation of the precise timing of climatic change over the OMT, are sparse, especially from the marine realm. The only published record of surface ocean conditions for the OMT comes from the Equatorial Atlantic Ocean; this record is of modest temporal resolution (~4 kyr sampling interval), and shows relatively little change in sea surface conditions, with inferred temperature variability less than that seen in bottom waters (Paul et al., 2000; Pearson et al., 1997). This picture of modest change in the surface Equatorial Atlantic contrasts with a record of pronounced thermocline cooling of 4-5°C over the OMT in the Equatorial Pacific (Beddow, 2016). Arguably the biggest OMT data gap is the absence of records from the North Atlantic Ocean, a critical site of deep water formation today and, as it is widely suggested, since the Eocene-Oligocene Transition (Davies et al., 2001; Miller and Fairbanks, 1983; Via and Thomas, 2006).

4.3 Methods

4.3.1 Site description and oceanography

A sedimentary sequence spanning the Oligocene-Miocene Boundary was recovered by IODP Expedition 342 at Site U1406 in the North-West Atlantic sediment drifts on the Newfoundland

Margin (Figure 4.1). Here, clay-rich sediments give rise to relatively expanded sections (~2 cm/kyr) benefiting from excellent age control (van Peer et al., in prep) and superbly preserved calcareous microfossils from a location proximal to the sites of deep ocean convection today (Norris et al., 2014). Present day surface waters at Site U1406 lie on the southerly edge of the front between the Labrador Current (LC), transporting cool, less saline water southwards, and the North Atlantic Current (NAC), a component of the Gulf Stream bringing warm, more saline water northwards. We refer the reader to (Smith, 2017a) for an assessment of the modern front and its behaviour in the Oligo-Miocene. At depth, Site U1406 is bathed by the Deep Western Boundary Current, inferred to have flowed since the early-/mid-Eocene, which transported the clay that makes up a large component of our samples (Boyle et al., 2016). Surface and deep water currents bathing Site U1406 during the Oligo-Miocene were thus broadly similar to their modern counterparts.

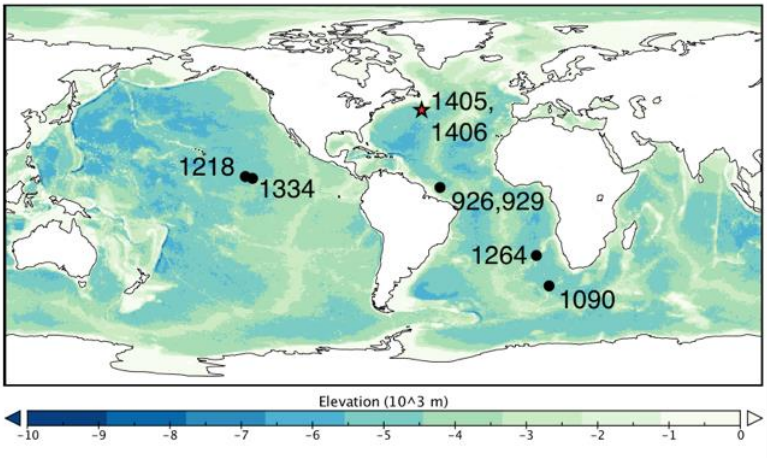

Figure 4.1 Locations of all existing high-resolution benthic stable isotope records across the OMT. See main text for references. Site U1406, the focus of this study, is highlighted (together with nearby Site U1405) by a red star. Colours represent bathymetry.

Consideration of the relationship of these currents to the wider ocean in the Oligo-Miocene must take into account tectonic differences from the present day, and the resultant differences in ocean circulation. In the present day, the only connection from the Atlantic to the Pacific Ocean is the Drake Passage and so deep water formation is active in the highly saline North Atlantic, with a secondary component in the Southern Ocean; meanwhile the low surface-salinity North Pacific is highly stratified. Salinity is therefore the primary control on the location of deep water formation. In the late Oligocene/early Miocene, the open Tethys Seaway (Woodruff and Savin, 1989) and Panama Gateway (Haug and Tiedemann, 1998) enabled significant low latitude inter-basinal

exchange. As a result, models indicate that the high latitude salinity gradient between the Atlantic and Pacific basins was greatly reduced relative to today (von der Heydt and Dijkstra, 2008, 2006). Consequently, the influence of temperature on the geographic distribution of deep water formation was elevated at the expense of salinity, with these models indicating resultant deep water formation in both the North Atlantic and North Pacific, as well as the Southern Ocean. It is thus likely that the NAC and DWBC were weaker than their modern counterparts.

4.3.2 Sampling

We use the revised splice and age model of van Peer et al. (in prep). Approximately 400 discrete 2 cm samples were taken every 4 cm along a part of the revised splice corresponding to an interval from 22.59 to 23.34 Ma. Sedimentation rate varies from 1.0 to 3.2 cm/kyr (mean 2.2 cm/kyr), being generally higher after than before and during the OMT. Samples were oven-dried, soaked in Calgon and washed over a 63 µm sieve with de-ionized water. The coarse fraction was retained, and oven-dried at 40°C.

4.3.3 Stable isotope analyses

Where possible (47% of samples), we picked a large number (40) of individuals of planktic foraminifera *Globigerina bulloides* (Figure 4.2; Smith, 2017b) from each sample, broke their chambers open and mixed them together before removing an aliquot for analysis, leaving enough material for subsequent re-runs as needed (Bolliet et al., 2011; Brijker et al., 2007). This same approach was taken for samples with only 11-39 individuals (31 % of samples); in order to retain enough material for analysis, samples with 10 or less individuals (16% of samples) were not crushed. The range of stable isotope variability among individuals from the same sample reflects seasonality, depth zonation and the time-integration inherent in geological sampling (Fraass and Lowery, 2017; Schiffelbein and Hills, 1984). The variability arising from these factors can be minimized in favour of a cleaner down-core record of mean environmental change by analysing a large number of individuals per sample, which the crushing and homogenization method we use facilitates.

The remaining samples (7%) contained fewer than three individuals in the 212-250 µm fraction, and so individuals were instead picked in the 180-212 µm fraction, where possible. As many species of planktic foraminifera have isotopic offsets between size fractions (Friedrich et al., 2012),

to assess the magnitude of this effect in our data we measured $!^{13}C$ and $!^{18}O$ across foraminifera from four size fractions: 150-180 µm, 180-212 µm, 212-250 µm and 250-300 µm in four samples (Supplementary Figure 4.1). This analysis reveals no offset of consistent sign between the 180-212 µm and 212-250 µm fractions in $!^{18}O$ (the range of offsets of the small relative to large fraction is -0.15 to +0.08‰) but an average offset of +0.22‰ (range +0.14 to +0.32‰) in $!^{13}C$. We therefore

add 0.22‰ to all $!^{13}C$ data generated in the 180-212 µm fraction in order to make the data comparable to the rest of our record.

Samples were analyzed using a Kiel IV Carbonate Device attached to a Thermo Finnigan MAT 253 dual inlet mass spectrometer at NOCS, University of Southampton. Analytical precision is 0.08‰ (1σ) for $!^{18}O$ and 0.06‰ (1σ) for $!^{13}C$. Data were calibrated using an internal standard (GS1). Results are reported relative to the Vienna Peedee belemnite (VPDB) standard. Our results were compared with a benthic stable isotope dataset generated on the same samples (Liebrand et al., in prep).

4.3.4 Time series analysis

Stable isotope records (on the tuned age scale) were first linearly interpolated to account for changes in sedimentation rate, with the interpolated record having an artificial sample spacing of 1 kyr. This record was then de-trended with a Gaussian notch filter (frequency 0.0 $Myrs^{-1}$, bandwidth 4.0 $Myrs^{-1}$); both of these steps were performed using *Analyseries* software (Paillard et al., 1996). Following these data preparation steps, spectral analyses were performed on both benthic and planktic $!^{13}C$ and $!^{18}O$, as well as on the benthic-planktic offsets ($\Delta^{13}C$ and $\Delta^{18}O$) using *SSA-MTM Toolkit* software (Ghil et al., 2002). Coherency and phase differences between the planktic and benthic records were also calculated using *Analyseries*, with a 95% confidence level for coherency.

4.4 Results

4.4.1 Foraminiferal ecology and preservation

Based on interspecies stable isotope comparisons, *Globigerina bulloides* and *Globigerina primordius* are consistently interpreted to have dwelled in the surface waters of the OMT ocean (Greenop et al., submitted; Pearson et al., 1997; Pearson and Wade, 2009). We chose to generate our record on the former because of its more consistent abundance through our record. However, the $!^{18}O_{G.\ bulloides}$ record we present here is consistently ~1‰ more positive than $!^{18}O_{G.\ primordius}$ we measured on foraminifera from the same samples (Supplementary Figure 4.2). A similar offset is seen between $!^{18}O_{G.\ bulloides}$ here at Site U1406 and both $!^{18}O_{G.\ bulloides}$ (Smith, 2017a) and $!^{18}O_{G.\ primordius}$ (O. Friedrich, pers. comm.) at nearby Site U1405. The restriction of the interspecies offset to Site U1406 may be attributable to a slight gradient in planktic foraminiferal preservation between the two sites, and indicates that one species is more resistant to diagenesis than the other. Inspection by binocular microscope indicates that the OMT planktic assemblage at Site U1405 is truly "glassy" following the terminology of Sexton et al. (2006) whereas at Site U1406, planktics from the OMT section show signs of incipient diagenetic alteration, with a generally opaque

appearance and occasional partially-dissolved foraminifera. These interpretations are substantiated by SEM analysis (Figure 4.2; all images generated at NOCS, University of Southampton, as part of the present study). Material from U1405 shows an exceptional taphonomy with smooth wall surfaces, well-defined pores and pronounced vertical growth layering seen in both *G. primordius* and *G. bulloides* (Figure 4.2: panels 2a-b). This contrasts somewhat with Site U1406: here, growth banding is sometimes obscured by secondary calcite precipitation (i.e., recrystallization), which gives the test surface and pore boundaries a rougher appearance (Figure 4.2: panels 1d-e). We note the greater wall thickness of *G. primordius*, and suggest that this thick, fairly cancellate wall structure gives *G. primordius* an enhanced resistance to diagenesis relative to *G. bulloides*, which has a thinner, "*bulloides*-type" wall (Pearson and Wade, 2009).

If dissolution was the primary mechanism of diagenesis in *G. bulloides*, preferential removal of outer layers of calcite (which would likely have grown during a life stage lived in deeper, and thus cooler, waters) would cause a shift to more negative $\delta^{18}O$ (Lohmann, 1995). That the offset of $\delta^{18}O_{G.\ bulloides}$ we observe is instead towards higher values suggests that recrystallization dominated post-depositional $\delta^{18}O$ changes, with cooler bottom waters relative to the sea surface favouring overgrowths with more positive $\delta^{18}O$ (Schrag et al., 1995). While this diagenesis precludes absolute quantification of surface water $\delta^{18}O$ and temperature, the effects of diagenesis are typically fairly constant over short records (Sexton et al., 2006a), meaning that the primary signal is most likely large enough (with a range in our record of >2.0‰) that its amplitude and sign are preserved.

There is no significant difference in $\delta^{13}C$ in *G. bulloides* between comparable intervals at Sites U1405 and U1406 (Supplementary Figure 4.2), which is unsurprising given that foraminiferal $\delta^{13}C$ is generally much less susceptible to diagenesis than $\delta^{18}O$ (Sexton et al., 2006a). However, it is striking that $\delta^{13}C$ in our *G. bulloides* record is generally more negative than benthic $\delta^{13}C$, by ~0.4 ‰. This differs from typical planktic-benthic gradients, where the biological pump causes a decrease in $\delta^{13}C$ with depth. The $\delta^{13}C$ difference between fellow surface dweller *G. primordius* and *G. bulloides* (Supplementary Figure 4.2) suggests *G. bulloides* in the Oligo-Miocene had a large isotopic offset from seawater $\delta^{13}C$, similar to its modern counterpart, rather than that surface waters were unusually isotopically light (Greenop et al., submitted).

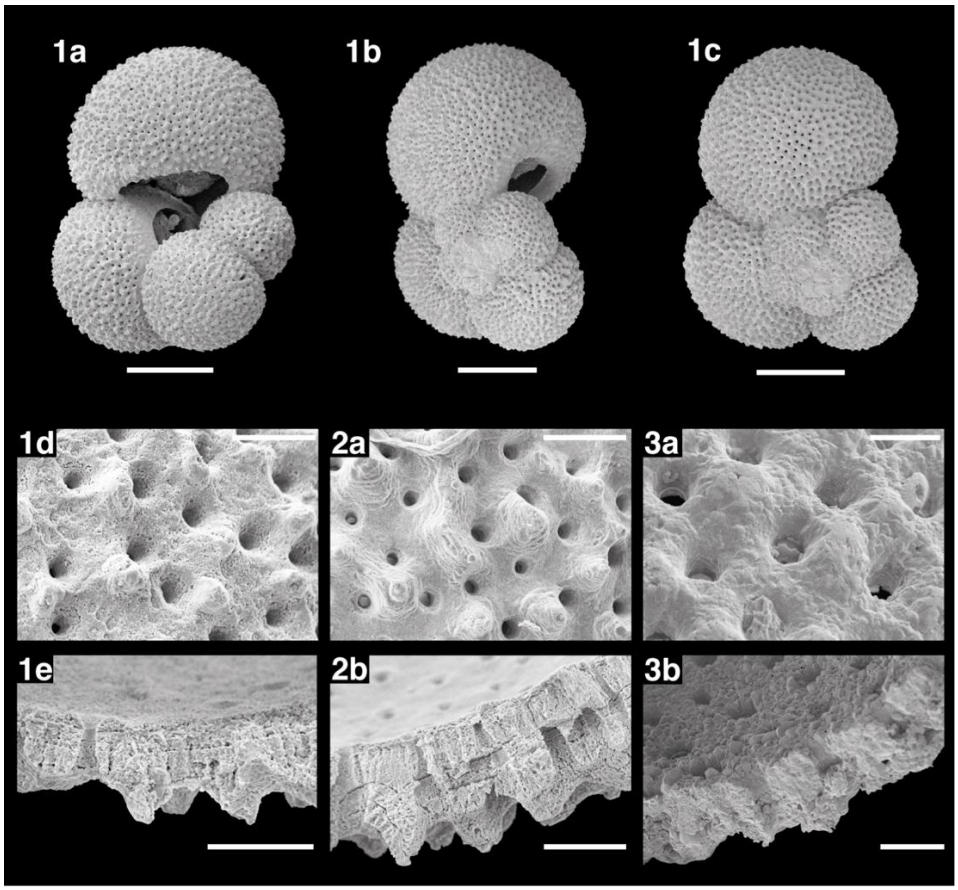

Figure 4.2 Scanning Electron Microscope (SEM) images of late Oligocene/early Miocene *G. bulloides* from Sites U1406, U1405 and 926. 1a-e: Individuals from Site U1406, showing good preservation but with early signs of diagenesis visible in close-up view. 2a-b: Individuals from Site U1405, showing exceptional preservation, including retention of growth layers in 2b. 3a-b: Individuals from Site U926, showing moderate recrystallization. Scale bar is 100 µm for 1a-c, and 10 µm for 2a-b and 3a-b. Foraminifera were picked from samples U1406C 9H 4W 102-104 cm (within the study interval presented here), U1405C 20H 5A 89-90 cm and U926B 51H 4W 28-30 cm. All images were produced at NOCS, University of Southampton, as part of the present study.

4.4.2 Planktic stable isotopes

Extended records have revealed a strong ~405 kyr eccentricity 'heartbeat' in Earth's carbon cycle in the Oligocene (Pälike et al., 2006b; Wade and Pälike, 2004); we also observe this pacing in our records, with approximately two complete cycles of this length in both $!^{13}C$ and $!^{18}O$ (Figure 4.3; Supplementary Figure 4.3). The OMT is marked by transient positive shifts in both planktic and benthic $!^{13}C$ and $!^{18}O$ (Figure 4.3; Supplementary Figure 4.3), consistent with other records. Taking values at 23.30 Ma as a baseline, the magnitude of the shift over the OMT is ~1.0‰ in

planktic $!^{13}C$ and ~1.5‰ in planktic $!^{18}O$. Following full recovery by ~22.9 Ma, planktic $!^{18}O$ then gradually increases until ~22.7 Ma, reaching several maxima only ~0.3‰ lower than those attained during the OMT. While planktic $!^{13}C$ follows broadly similar patterns on long (~400 kyr) timescales, post-OMT values never completely recover to those seen pre-OMT. This baseline shift from one side to other of the OMT matches similar shifts seen in benthic $!^{13}C$ records elsewhere (Beddow et al., 2016), attributed to a global shift in the carbon cycle causing enhanced export productivity over the OMT (Diester-Haass et al., 2011; Mawbey and Lear, 2013).

Superimposed on these broad shifts is pronounced variability (amplitude >1.0‰ in $!^{18}O$ and >0.8‰ in $!^{13}C$) on timescales of thousands to tens-of-thousands of years. This higher frequency variability is particularly clearly defined during the descent into the OMT (~23.25-23.12 Ma; between points A-C on Figure 4.4 and Supplementary Figure 4.3), but it is dampened during the peak of the OMT (between points C-F), before reappearing post-OMT (point F and younger).

Variability on ~10^{3-4} kyr timescales is particularly strong in $!^{18}O$ post-OMT. This is likely due in part to a higher sampling frequency (because of higher sedimentation rate) post-OMT than pre-OMT; this is demonstrated by a 4 kyr resampling of the data (Supplementary Figure 4.4).

Figure 4.3 (opposite) New and previously published palaeoclimate records across the OMT. From top to bottom: the top panel illustrates a benthic $!^{18}O$ record from Site U1264 (Liebrand et al., 2016), with the OMT shaded in purple. The main panel shows a compilation of data from the interval studied in this chapter, which encompasses most but not all of the OMT interval (as suggested by Liebrand et al. (2016) shaded in the top panel. The global benthic $!^{18}O$ stack (Beddow et al., 2016) is a stack of records from (I)ODP Sites U926, U929, U1090, U1218, U1264 and U1334. Bottom water temperature data was calculated from *O. umbonatus* Mg/Ca data in Mawbey and Lear (2013). This data was first converted to temperature using the *O. umbonatus* calibration in Lear et al. (2002), assuming a modern seawater Mg/Ca ratio. The data was then normalized by removing the average (calculated using only data in the interval presented here) for each record. Sources of atmospheric pCO_2 data are given in the key. U926 planktic $!^{18}O$ data is from Pearson (1997). The U1406 planktic $!^{18}O$ dataset is the primary new data presented in this chapter. For comparison, a benthic $!^{18}O$ record generated on the same samples (Liebrand et al., in prep) is also plotted at the base of this figure.

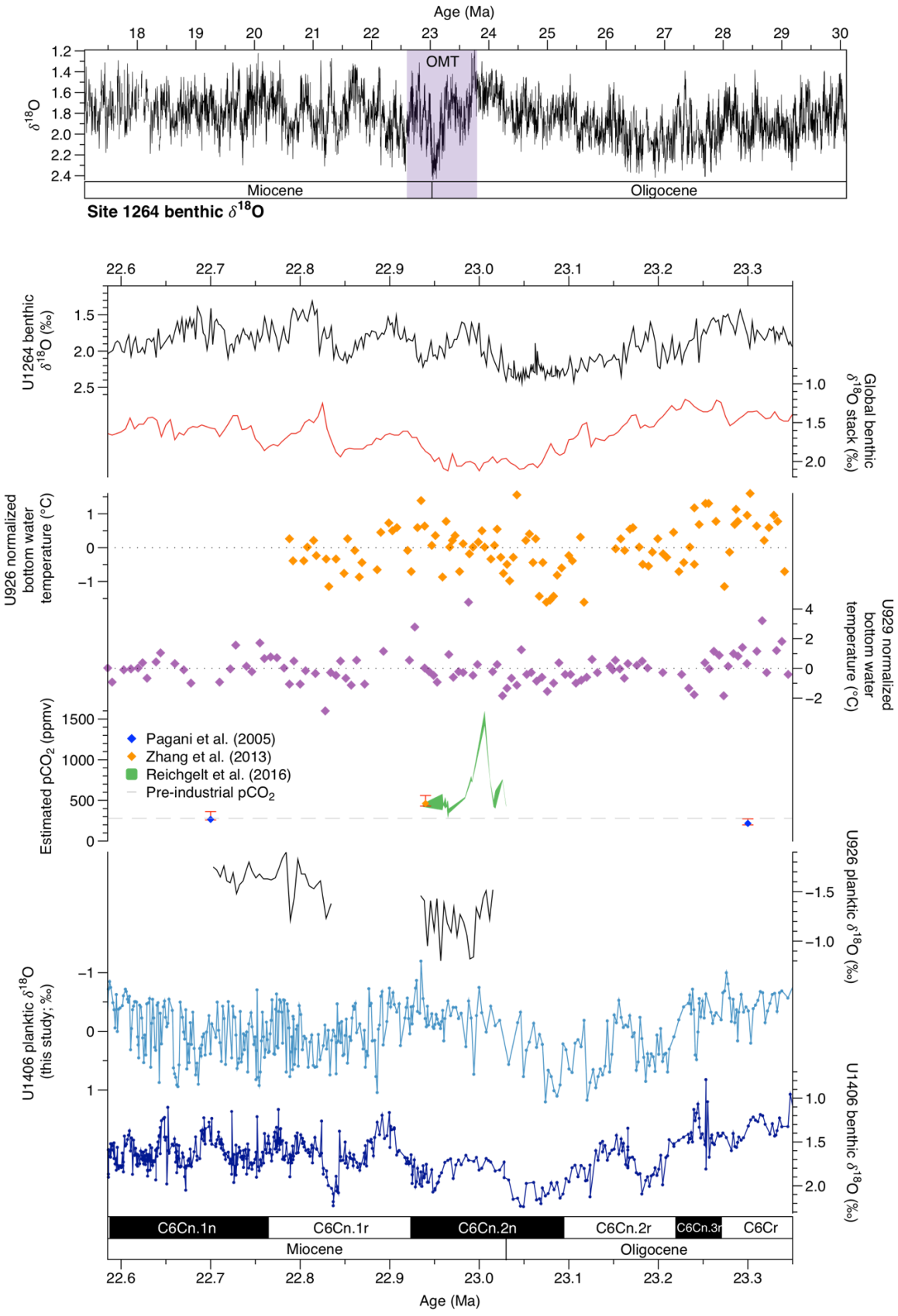
Age (Ma)
OMT
Miocene
Oligocene
Site 1264 benthic δ18O
U1264 benthic δ18O (‰)
Global benthic δ18O stack (‰)
U926 normalized bottom water temperature (°C)
U929 normalized bottom water temperature (°C)
Estimated pCO2 (ppmv)
Pagani et al. (2005)
Zhang et al. (2013)
Reichgelt et al. (2016)
Pre-industrial pCO2
U1406 planktic δ18O (this study; ‰)
U926 planktic δ18O (‰)
U1406 benthic δ18O (‰)
C6Cn.1n
C6Cn.1r
C6Cn.2n
C6Cn.2r
C6Cn.3r
C6Cr
Miocene
Oligocene
Age (Ma)

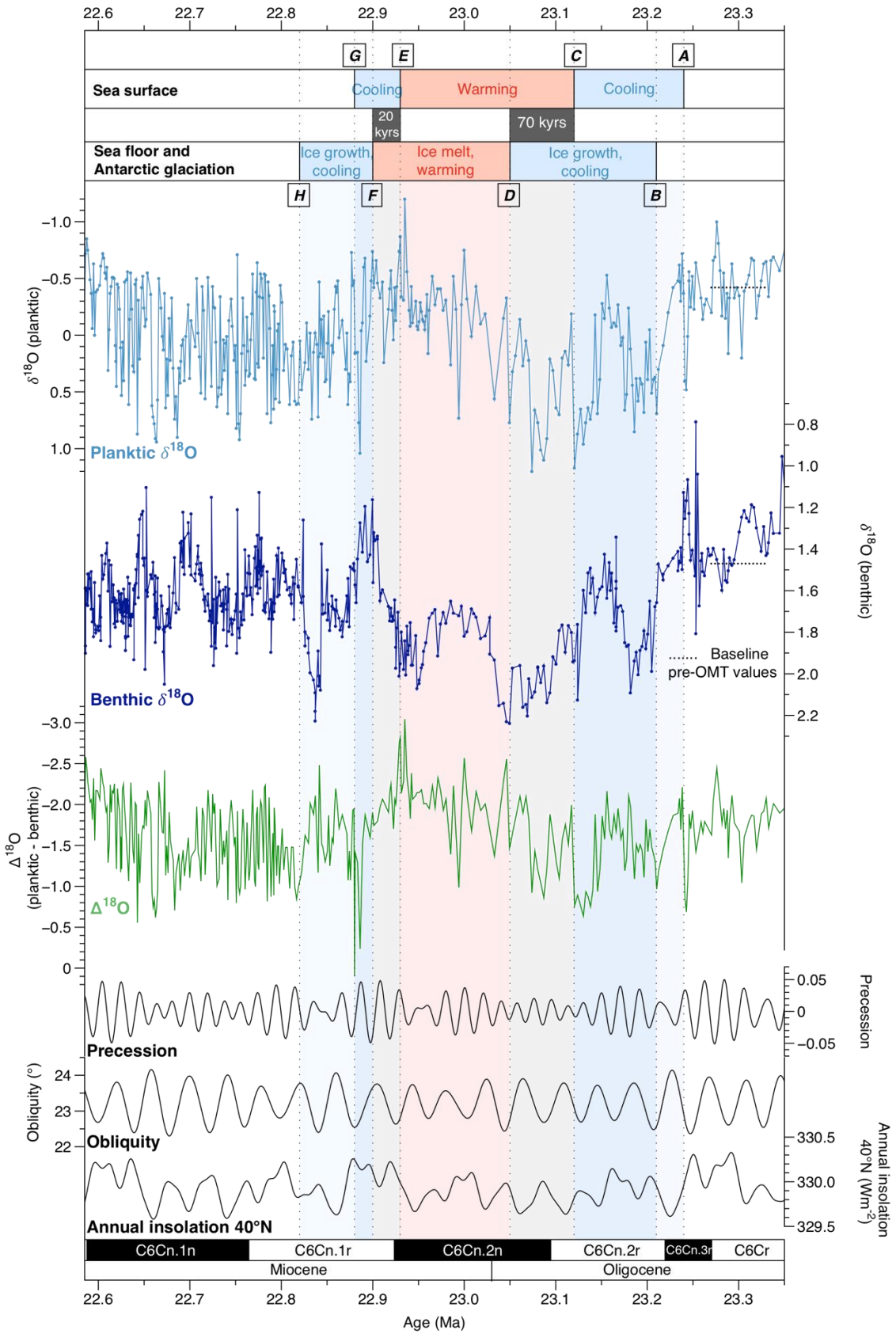
22.6
22.7
22.8
22.9
23.0
23.1
23.2
23.3
G
E
C
A
Sea surface
Cooling
Warming
Cooling
20 kyrs
70 kyrs
Sea floor and Antarctic glaciation
Ice growth, cooling
Ice melt, warming
Ice growth, cooling
H
F
D
B
δ18O (planktic)
Planktic δ18O
δ18O (benthic)
Benthic δ18O
..... Baseline pre-OMT values
Δ18O (planktic - benthic)
Δ18O
Precession
Obliquity (°)
Obliquity
Annual insolation 40°N
Annual insolation 40°N (Wm-2)
C6Cn.1n
C6Cn.1r
C6Cn.2n
C6Cn.2r
C6Cn.3r
C6Cr
Miocene
Oligocene
Age (Ma)

Figure 4.4 (opposite) Comparison of planktic and benthic $\delta^{18}O$ records from Site U1406 across the OMT. The interval presented in this figure lies entirely within the duration of the OMT interval as suggested by Liebrand et al. (2016). From top to bottom: Labels denoting 'cooling' and 'warming' at the sea surface and sea floor are based on interpretation of planktic (this study) and benthic (Liebrand et al., in prep) $\delta^{18}O$ records. $\Delta^{18}O$ is calculated only when planktic and benthic stable isotopes have been measured in the same sample. Orbital solutions are from (Laskar et al., 2004).

4.4.3 Comparison of planktic and benthic δ^{18} records

Foraminiferal $\delta^{18}O$ is a function of seawater temperature and local seawater $\delta^{18}O$, with changes in the latter driven by changes in local salinity and global ice volume. Variability of global ice volume affects planktic and benthic $\delta^{18}O$ equally; in the absence of SST data and modelling of $\delta^{18}O_{seawater}$ of the whole ocean, changes in surface conditions are therefore best represented not by planktic $\delta^{18}O$ alone, but by the residual change in the planktic record relative to the benthic record, i.e., the planktic-benthic offset, $\Delta^{18}O$. We ascribe all changes in $\Delta^{18}O$ to variability in surface temperature and/or salinity; these are minimum estimates which likely underestimate the true surface variability, hidden because synchronous temperature changes in benthic records would change $\delta^{18}O$ without changing $\Delta^{18}O$. Conversely, it is possible that changes in $\Delta^{18}O$ could instead reflect static surface conditions and highly variable bottom water temperatures. While we cannot rule this out without independent temperature proxies at Site U1406, the magnitude of change of $\Delta^{18}O$ is sufficiently large (>2‰) that it would require very large deep water temperature changes (approaching 10°C). This would be very difficult to reconcile with the modest (2-3 °C) bottom water temperature change reconstructed from both Mg/Ca estimates (Figure 4.3; Mawbey and Lear, 2013) and inverse modelling of benthic $\delta^{18}O$ (Liebrand et al., 2011).

Comparison of planktic and benthic records reveals leads and lags on the scale of individual orbital cycles. For example, while the large increase (~0.9‰) in planktic $\delta^{18}O$ between ~23.24 and 23.20 Ma (starting at 'A' in Figure 4.4) is associated with a ~0.5‰ increase in benthic $\delta^{18}O$ (indicating synchronous benthic-planktic behaviour that is amplified in surface waters), the next major planktic $\delta^{18}O$ increase (by ~1.5‰) at 23.15 Ma (preceding point 'C') is not followed by an increase in benthic $\delta^{18}O$ until ~20 kyrs (i.e., one precession cycle) later at 23.13 Ma (point 'C'). As a result, $\Delta^{18}O$ at 23.13 Ma rises to ~-0.6‰, an increase of ~1.0‰, indicating a significant decrease in temperature and/or rise in salinity at the sea surface of sufficient magnitude to raise residual planktic $\delta^{18}O$ values by ~1.0‰.

This shift to peak planktic $\delta^{18}O$ values is followed by a longer-term recovery (23.12-22.93 Ma) of $\Delta^{18}O$ of ~2.1‰, which strikingly begins (at point 'C') ~70 kyrs before peak benthic $\delta^{18}O$ is reached

at 23.05 Ma (point 'D'). These results suggest that, while the initial stages of expansion of Antarctic glaciation over the OMT were associated with cooling and/or salinity increase in the North Atlantic, this trend was reversed tens of kyrs before maximum glacial expansion/deep water cooling. This warming phase appears to have ended mid-way through the OMT deglaciation, when a rise of planktic $!^{18}O$ coincident with a fall of benthic $!^{18}O$ (and consequent rise of $\Delta^{18}O$ by ~1.3‰) from 22.93-22.89 Ma (between points 'E' and 'F') indicates renewed cooling/salinity increase in North Atlantic surface waters.

4.4.4 Spectral analysis

To assess whether a lead of the planktic record over the benthic record is also found on shorter timescales, and to investigate the relationship of both planktic and benthic records to orbital forcing. we present results of multi-taper method (MTM) spectral analysis (Ghil et al., 2002) and wavelet analysis (Meyers, 2014). Both planktic and benthic $!^{13}C$ and $!^{18}O$ records reveal strong spectral power corresponding to the three dominant drivers of orbital forcing (eccentricity, obliquity and precession) in benthic $!^{18}O$ (Figure 4.5) and $!^{13}C$ (Supplementary Figure 4.5). We note that the spectral peaks we identify do not have their frequencies as tightly constrained as those identified in existing benthic records; this is an artefact of the relatively short duration of our record.

While planktic $!^{13}C$ also has strong spectral power at frequencies corresponding to eccentricity, obliquity and precession, planktic $!^{18}O$ lacks significant spectral power corresponding to obliquity, and power at the frequency corresponding to eccentricity is not strong. A wavelet analysis through the duration of the record indicates that the most clearly defined cycles of the whole record – those between 23.24-23.07 Ma (between points 'A' and 'D' on Figure 4.4) – unfairly bias the spectral analysis; strong eccentricity and weaker obliquity and precession forcing are visible through the duration of the wavelet analysis. The three cycles in this interval do not appear to be paced by any of the dominant orbital forcings. This may be due to a small error in the age model (T. van Peer, pers. comm.).

We assess the relative pacing of our planktic and benthic records by orbital forcing by calculating coherency and phase offsets between the records. The records are coherent (>95% confidence) at all orbital frequencies, except for obliquity in $!^{18}O$, which is as expected given the weakness of obliquity forcing in planktic $!^{18}O$. Planktic records lead benthic records in all cases, by ~10-17 kyrs over eccentricity cycles, ~3-4 kyrs over obliquity cycles ($!^{13}C$ only) and ~1-9 kyrs over precession cycles (with a single exception in $!^{18}O$ at ~17.5 kyrs periodicity, where the planktic record lags the benthic record by ~6 kyrs). This analysis therefore reveals that the lead of the planktic record over the benthic record does not only occur on the timescales of whole orbital cycles, but also on millennial timescales.

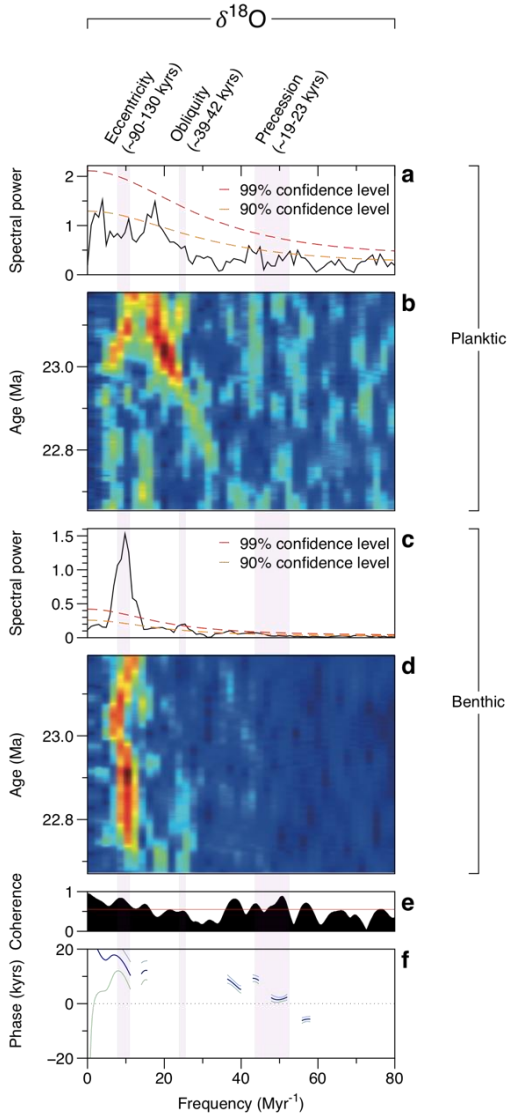

Figure 4.5 Time series analysis of Site U1406 planktic and benthic !^{18}O records. Panels **a and c**: Multi-Taper Method (MTM) spectral analyses of planktic and benthic records, respectively, with confidence levels in red (99%) and orange (90%). Ranges of dominant periodicities of orbital forcing are indicated in purple shading. Panels **b and d**: wavelet analysis of planktic and benthic stable isotope records, respectively. Warmer colours indicate higher spectral power. Panel **e**: coherence between planktic and benthic records. Red line indicates 95% confidence level. Panel **f**: phase offsets of planktic relative to benthic stable isotope records. The dark purple line represents the mean phase offset estimate; pale blue and green lines represent the upper and lower estimates of this range, respectively.

4.5 Discussion

4.5.1 Interpretation of planktic $\delta^{18}O$ variability: salinity or temperature?

To determine the relative influence of salinity and temperature on these large planktic $\delta^{18}O$ shifts, we compare the changes in each of these properties indicated by the planktic $\delta^{18}O$ shift with the oceanography of the modern North Atlantic. The modern salinity-$\delta^{18}O$ relationship in the North Atlantic is approximately: $\delta^{18}O_{seawater} = (0.5823*salinity) - 19.969$ (R^2=0.64; relationship determined from a linear regression of all sea surface salinity and $\delta^{18}O_{seawater}$ data from 30-50°N, 40-60°W from the Global Seawater Oxygen-18 Database v1.21 [Bigg and Rohling, 2000; Schmidt et al., 1999]; the relationship between temperature, salinity and $\delta^{18}O$ in *G. bulloides* is illustrated in Supplementary Figure 4.6). Thus, the residual (i.e., benthic/ice-volume component removed) planktic $\delta^{18}O$ rise (i.e., rise in $\Delta^{18}O$) of ~1.0‰ during the initiation of the OMT and the $\Delta^{18}O$ fall of ~2.1‰ during the recovery phase would result from salinity changes of ~+1.7 and ~-3.6 respectively, assuming no temperature change and modern salinity (Supplementary Figure 4.6). To put the magnitude of these changes in context, they are several times higher than (and of opposite sign to) the large, sea-ice driven salinity anomalies of this region at the LGM relative to the modern (Vernal et al., 2000). While salinity changes may have been amplified by the position of Site U1406 near the NAC-LC front, across which the amplitude of salinity variability is several salinity units, the relationship of higher (lower) salinity with higher (lower) temperature across this front precludes front-driven salinity changes from being a driver of large-amplitude $\delta^{18}O$ variability, following discussion in Smith et al. (2017a). In summary, we infer that regional changes in salinity, even when amplified at Site U1406 because of its frontal location, most likely had only a limited influence on planktic $\delta^{18}O$ in our record. Thus, while salinity may have contributed to some of the smaller amplitude (typically higher-frequency) planktic $\delta^{18}O$ variability we observe, another mechanism is required to explain the large, 10^4 kyr-timescale changes in planktic $\delta^{18}O$ that we observe over the OMT.

We now consider the effect of variability of temperature on planktic $\delta^{18}O$. The temperature sensitivity of modern *Globigerina bulloides* is ~4.9°C per 1‰, determined in culture (Bemis et al., 1998) and plankton tow (Mulitza et al., 2003) experiments. While uncertainty remains over whether ancestral forms of *G. bulloides* hosted symbionts (Greenop et al., submitted; Pearson and Wade, 2009), we discount this as having more than a small effect on SST sensitivity of $\delta^{18}O$, based on the similar sensitivities to *G. bulloides* of modern symbiotic species like *Globigernoides sacculifer* or *Orbulina universa* (Bemis et al., 1998; Mulitza et al., 2003). The $\Delta^{18}O$ rise of ~1.0‰ going into the OMT (between points 'A' and 'C' on Figure 4.4) thus reflects an SST drop of at least ~5°C (possibly more if the benthic $\delta^{18}O$ increase also incorporates temperature change, though possibly less if planktic $\delta^{18}O$ incorporates small salinity changes, as discussed above). The subsequent fall in $\Delta^{18}O$ of ~2.1‰ associated with deglaciation (between points 'C' and 'E') would

thus be associated with a ~10°C warming, i.e., to a temperature ~5°C higher than pre-OMT; the subsequent 1.3‰ rise in $\Delta^{18}O$ (from point 'E') would correspond to a ~6°C temperature drop, i.e., to a temperature ~1°C lower than pre-OMT.

Given the proximity of Site U1406 to the NAC-LC front, it is likely that any temperature signal recorded here is amplified in comparison to the wider North Atlantic. The dominance of precession over obliquity in the spectral analysis of our planktic $!^{18}O$ record indicates a dominant lower latitude influence, suggesting that Site U1406 lay south of the front during the OMT as it does today; large front-associated temperature changes at Site U1406 would thus suggest southward movement of the front. Significant southward shifts of the Arctic Front have precedent, at least in intervals of NHG, having been inferred from records both in Pleistocene glacial periods (McIntyre and Molfino, 1996; Villanueva et al., 2001) and during the intensification of NHG in the Late Pliocene (Naafs et al., 2010), though the latter is debated (Friedrich et al., 2013).

To assess the extent to which such frontal movements may have amplified the temperature signal at Site U1406, we consider $\Delta^{13}C$, the offset between planktic and benthic $!^{13}C$. Global changes in the carbon cycle drive changes in planktic and benthic records simultaneously and cause no change in $\Delta^{13}C$; any change in $\Delta^{13}C$ variability is thus indicative of changes in either the source of surface or deep waters, or in local surface water export productivity. In the present day there is a strong surface water $!^{13}C$ gradient across the front, of magnitude ~0.5‰ (Tagliabue and Bopp, 2008). A change in frontal position resulting in enhanced (reduced) LC influence at Site U1406 would therefore result in higher (lower) planktic $!^{18}O$ and lower (higher) $\Delta^{13}C$, based on the modern salinity-temperature relationships of the LC and NAC, and assuming constant surface productivity.

We therefore infer that where changes in $\Delta^{13}C$ and planktic $!^{18}O$ are coincident, for example the ~0.7‰ fall in $\Delta^{13}C$ at 23.22 Ma (point 'A' in Figure 4.4 and Supplementary Figure 4.3) coincident with a ~0.9‰ rise in $!^{18}O$, this may reflect frontal movement. The planktic $!^{18}O$ change would thus represent frontal amplification of a weak regional signal. However, these simultaneous oxygen and carbon changes are only associated with higher frequency (< ~100 kyrs) variability; there is no longer-term $\Delta^{13}C$ change concurrent with the broad cooling and warming periods we infer from planktic $!^{18}O$ over the OMT (see warming, cooling labels in Figure 4.4). We therefore infer that these intervals of surface cooling and warming likely reflect sizeable regional surface temperature changes, rather than just a small regional signal amplified by the frontal proximity of Site U1406.

4.5.2 Comparison with existing records

The Northern Hemisphere cooling we infer over the OMT follows similar observations in terrestrial records (Kotthoff et al., 2014; Miao et al., 2013) and inferences from dust records indicative of a temporary southward shift of the Intertropical Convergence Zone (ITCZ) over the OMT (Hyeong et al., 2014). NH cooling over the OMT is also predicted by inverse modelling of

benthic $\delta^{18}O$, which estimates a ~10°C cooling of NH mean annual temperature over the OMT followed by warming to a full recovery (Liebrand et al., 2011), though we note that this cooling estimate is an average over all latitudes 40-80°N, and is thus likely an overestimate for temperature change at Site U1406. Similar NH surface cooling was also recorded at the LGM, where Site U1406 was ~3.5°C cooler than the modern (Annan and Hargreaves, 2013); and at the Eocene-Oligocene Transition (EOT), when the cooling step preceding ice growth is associated with a ~5°C cooling in high latitudes (45-70°N; Liu et al., 2009), alongside tropical cooling of ~2-3°C (Wade et al., 2012).

However, the significant planktic $\delta^{18}O$ variability we observe at Site U1406 is markedly different to the minimal variability seen in the only other surface-dwelling planktic foraminiferal record generated to date over the OMT (Paul et al., 2000; Pearson et al., 1997). In this record, generated on surface dweller *Globigerinoides primordius*, the planktic $\delta^{18}O$ shift of ~0.6‰ over the OMT itself (Figure 4.3) is dwarfed by the change of >2.0‰ in our record. The magnitude of the planktic OMT shift at Site U926 is so small that it is less than the benthic change at the same location, an observation interpreted by Pearson (1997) to be indicative of bottom water cooling and constant surface temperatures. This interpretation is not consistent with the significant temperature variability we observe at Site U1406. It is also not consistent with the only other existing high resolution planktic $\delta^{18}O$ record over the OMT, generated on the thermocline-dwelling species *Dentoglobigerina venezuelana* at Site U1334 in the Equatorial Pacific (Beddow, 2016). Here, a $\delta^{18}O$ change of ~1.9‰ is recorded over the OMT, although the high variance of the record, noted by the author, may make this an overestimate (Beddow et al., 2016). We note the moderate diagenetic recrystallization seen in foraminifera at Site U926, in contrast to the generally good preservation, with only minor recrystallization, at Site U1406 (Figure 4.2). We thus suggest that the Site U926 record is artificially 'flat' as a result of post-depositional diagenesis, and that equatorial Atlantic SST may have in fact been more variable than this record suggests.

The tens-of-kyrs lead of planktic over benthic $\delta^{18}O$ through the OMT at North Atlantic Site U1406 is markedly different to the timing of changes at equatorial sites 1334 and U926. After an approximately synchronous onset of the OMT in both planktic and benthic records at Site U1334, planktic $\delta^{18}O$ increases more slowly than its benthic counterpart, but continues to increase for 50-100 kyrs after benthic $\delta^{18}O$ has peaked. This means that, in contrast to the rapid cooling and subsequent (pre-peak benthic $\delta^{18}O$) surface warming at Site U1406, Equatorial Pacific thermocline waters underwent little temperature change during Antarctic ice growth/bottom water cooling, but cooled substantially (estimated by the paper's authors as ~4-5°C) during the benthic recovery phase. Likewise, at Site U926 planktic $\delta^{18}O$ does not appear to begin its OMT recovery ~50 kyrs after that of the benthic record (though we note that the gap in data may mask some changes; Figure 4.3), indicating that a lag of planktic $\delta^{18}O$ over benthic $\delta^{18}O$ was a pervasive feature of

equatorial latitudes during the recovery phase of the OMT, in stark contrast to the mid-latitude North Atlantic, where surface waters began their recovery ~70 kyrs before bottom waters.

4.5.3 Wider oceanographic change

We now consider the processes that may have caused these temperature changes. We first consider the interval of glacial expansion and surface ocean/terrestrial cooling during the descent into the OMT. We suggest that the initial surface cooling seen between points 'A' and 'B' (Figure 4.3) was a result of the sharp drop in annual insolation at Site U1406 (Figure 4.4). Similar cooling episodes are seen coinciding with the two other intervals with particularly low insolation, at 22.66 and 22.74 Ma. However, this does not explain why this NH surface cooling was sustained, and even strengthened, between points 'B' and 'C', where insolation is no longer at a minimum.

We interpret point 'B', where benthic $!^{18}O$ falls significantly, as being associated with major bottom water cooling and Antarctic glacial expansion. There are a number of mechanisms via which this Antarctic glacial expansion could have caused sustained NH surface cooling. While glacial expansion in this interval was most likely a result of an orbital configuration favouring reduced seasonality, with consequent reduced summer glacial melting enabling sustained ice sheet growth (Pälike et al., 2006a; Zachos et al., 1997, 2001b), the reason for the cooling is less clear. Once potential scenario involves pCO_2 drawdown as a result of glacial expansion (Liebrand et al., 2011; Mawbey and Lear, 2013); while no such change has been identified in published pCO_2 records, the low resolution (tens of kyrs) of these records (Beerling and Royer, 2011; Zhang et al., 2013) may mask brief changes over the OMT.

Given that OMT pCO_2 estimates are not significantly higher than those required in models to initiate Arctic ice sheet growth (Figure 4.3; Beerling and Royer, 2011; DeConto et al., 2008), significant Arctic land- and sea-ice growth may thus have occurred over the OMT; evidence for Arctic sea ice (Darby, 2014, 2008; Krylov et al., 2008) and localized mountain glaciers on Greenland (Eldrett et al., 2007) stretches back to the Eocene. This would likely have strengthened the LC relative to the NAC, thus shifting the front between them southwards, as observed during episodes of NH glacial expansion in the Plio-Pleistocene (McIntyre and Molfino, 1996; Naafs et al., 2010; Villanueva et al., 2001). Such a process at Site U1406 would amplify the global signal associated with pCO_2 decrease, contributing to the significant cooling of surface waters we infer in our record.

Alternatively, given the significant extent of SH sea ice modelled following continental glaciation over the EOT (DeConto et al., 2007), it is reasonable to suggest that similarly large amounts of Antarctic sea ice were associated with the OMT. Antarctic sea ice expansion is associated with enhanced AABW production in the Pleistocene, because of cooling and enhanced salinity as a result of brine rejection (Ferrari et al., 2014). We suggest that a similar strengthening of AABW

over the OMT, as suggested based on comparison of benthic $\delta^{18}O$ and sea level (Pekar and DeConto, 2006), could have increased net heat transport towards the SH, thus leading to NH cooling. Records providing better constraints on the extent of Antarctic sea ice over the OMT are required to test this hypothesis.

We now consider the surface warming in our record from ~23.12 Ma (point 'C' in Figure 4.3), which is followed ~70 kyrs later (point 'D') by the deglaciation stage of the OMT. In the last glacial termination, regional leads and lags in temperature were typically associated with the bipolar seesaw, and semi-periodic strengthening and weakening of NADW formation (Broecker, 1998; Denton et al., 2010). However, these mechanisms operate over thousands, not tens of thousands of years, and cannot explain our results. We instead consider the possibility of a brief pCO_2 rise, such as a ~20 kyr rise at the OMT glacial termination recently inferred from a terrestrial record (Figure 4.3; Reichgelt et al., 2016). Large ice sheets have an inertia to climatic changes; for example, the lag of benthic $\delta^{18}O$ to orbital forcing is estimated as 5-15 kyrs in the Plio-Pleistocene (Lisiecki and Raymo, 2005) and up to 25 kyrs during the Oligo-Miocene (Pälike et al., 2006a); it would therefore not be surprising for a CO_2-induced warming to cause the planktic $\delta^{18}O$ recovery to begin before the benthic recovery (although a 70 kyr lead would be unusually large). However, while we do not rule out a brief spike in pCO_2, and some subsequent warming, this is difficult to reconcile with records of deep water (Figure 4.3; Mawbey and Lear, 2013) and thermocline (Beddow, 2016) cooling over the interval between initiation of planktic and benthic recovery at Site U1406. We also note that proposed mechanisms for carbon storage changes over the OMT deglaciation, for example carbonate platform formation (Opdyke and Walker, 1992) and organic carbon oxidation (Mawbey and Lear, 2013), can only explain pCO_2 rise once the deglaciation has begun, not ~70 kyrs before this.

Alternatively, Antarctic meltwater could have caused NH warming. The rapidity of Antarctic deglaciation following glacial expansion over the OMT, with an average sea level rise of ~30 cm/kyr (Liebrand et al., 2011; Miller et al., 1991; Pekar et al., 2002), would have added large amounts of buoyant freshwater to the Southern Ocean, likely decreasing AABW formation. As a result, the relative proportion of deep water formed in high northern latitudes would increase, as demonstrated in a numerical Earth system model studying rapid Antarctic melting associated with anthropogenic warming (Swingedouw et al., 2008). The resultant net increase in heat flow to northern latitudes would warm the North Atlantic. Modelling work is required to establish whether such a scenario is plausible given Antarctic melting rates in the OMT recovery. In addition, while this mechanism may have sustained NH warming once Antarctic melting had begun, it is hard to explain how this mechanism would cause warming at Site U1406 ~70 kyrs before benthic $\delta^{18}O$ begins to fall. If such a mechanism explained our results, it would indicate that the latter part of the benthic $\delta^{18}O$ rise was dominated by a sustained deep water temperature decrease coinciding with initiation of Antarctic melting ~70 kyrs before deep water temperatures (and benthic $\delta^{18}O$) reached

their minimum (maximum). However, this is not consistent with deep water temperature estimates and $!^{18}O_{sw}$ estimates from the Ceara Rise (Mawbey and Lear, 2013). Additional globally distributed benthic temperature records are thus required to test this hypothesis.

Finally, we consider whether orbital forcing could have caused NH warming. Such a mechanism could in turn explain why Antarctic deglaciation follows NH warming: given the importance of temperature in determining locations of deep water formation in the Oligo-Miocene (see Section 4.3.1), NH warming would most likely reduce NH deep water formation. This would enhance the relative proportion of deep water formed in the Southern Ocean, thus enhancing heat transport towards the SH and perhaps playing a role in initiating Antarctic deglaciation. However, there is no marked rise in insolation at 40°N over this interval in current astronomical models (Figure 4.4), although we note that uncertainty still remains in the precise timings of obliquity and precession cycles in the Oligocene (Laskar et al., 2004).

4.6 Conclusions

Our results demonstrate that the OMT was associated with significant surface $!^{18}O$ variability in the North Atlantic, which we interpret as reflecting high-amplitude surface temperature variability. Crucially, this North Atlantic cooling and warming leads Antarctic glacial expansion and retreat by tens of kyrs, implying that processes in the North Atlantic may have played a role in triggering Antarctic glacial expansion and retreat over the OMT. While climate variability around Antarctica has been suggested to drive variability in the North Atlantic in the Pleistocene, particularly in AMOC strength (Patara and Böning, 2014), our inference that this connection has also operated the other way round on tens-of-kyrs timescales has important ramifications for our understanding of both past and future climates. The North Atlantic plays a dominant role in modern climate because it is a site of significant deep water formation, but does it retain this role at times when large amounts of deep water are also formed elsewhere, and when Northern Hemisphere glaciation is only of modest extent? Is behaviour similar to what we observe also found during the lower-amplitude benthic $!^{18}O$ cycles that are pervasive throughout the Oligocene (Liebrand et al., 2017), or does its restriction to the OMT explain why this cycle was of particularly high amplitude? Our data highlight the pressing need for additional high-resolution records of temperature, ocean circulation and pCO_2 over the OMT.

4.7 Supplementary Figures

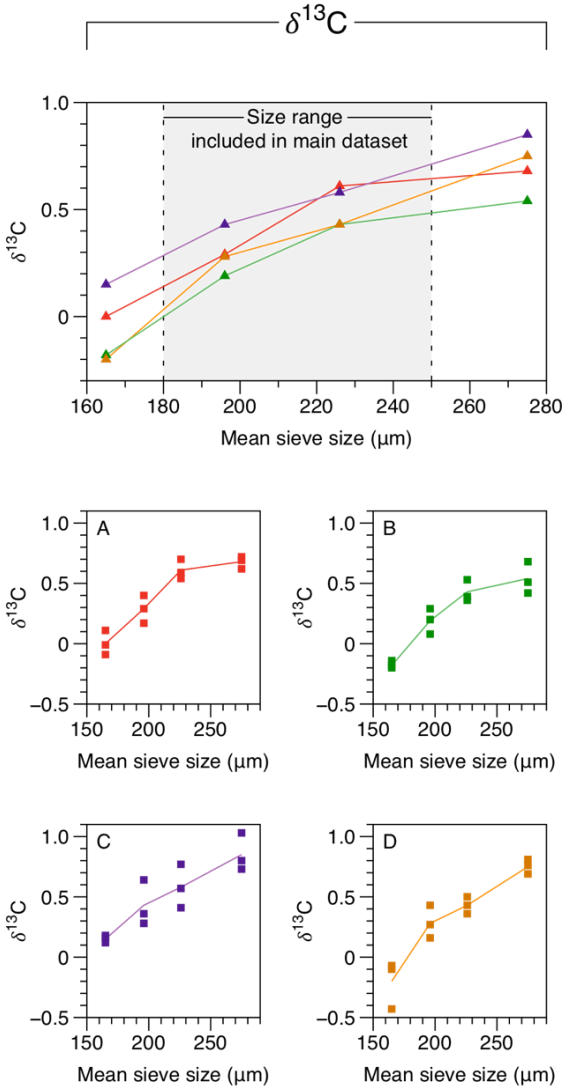

Supplementary Figure 4.1 (figure spans both pages) Relationship between foraminiferal stable isotope composition and size. All panels on the left refer to $\delta^{13}C$; all panels on the right refer to $\delta^{18}O$. Bottom panels show data from four different samples (A, B, C and D), with three measurements made for each size fraction (150-

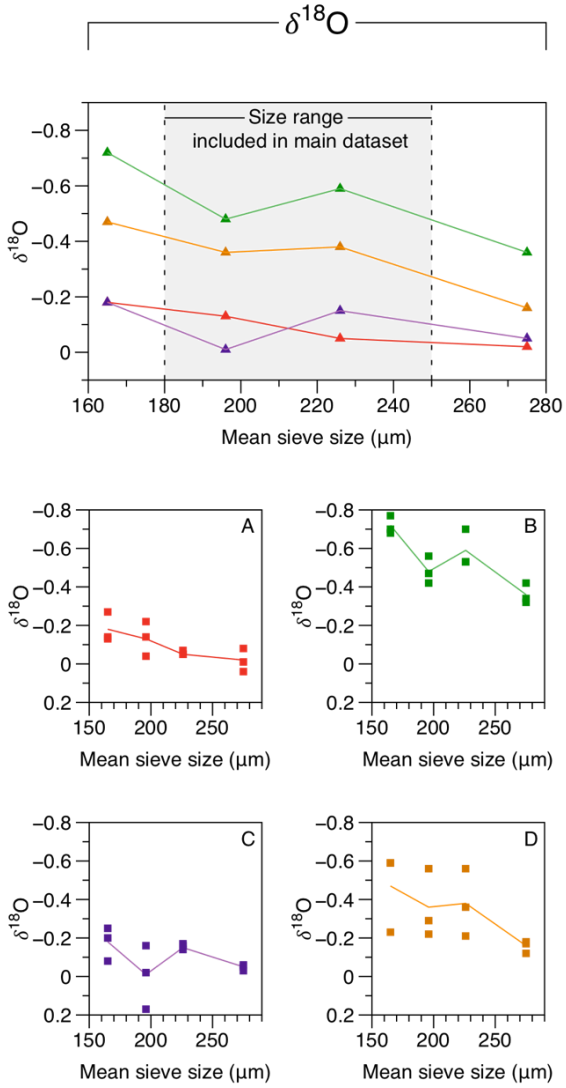

180 µm, 180-212 µm, 212-250 µm, 250-300 µm). Line represent average values for each size fraction. These same lines are combined in the top panels. The shaded area in the top panel indicates the size fraction range of foraminifera included in the main dataset presented in Figures 4.3 and 4.4.

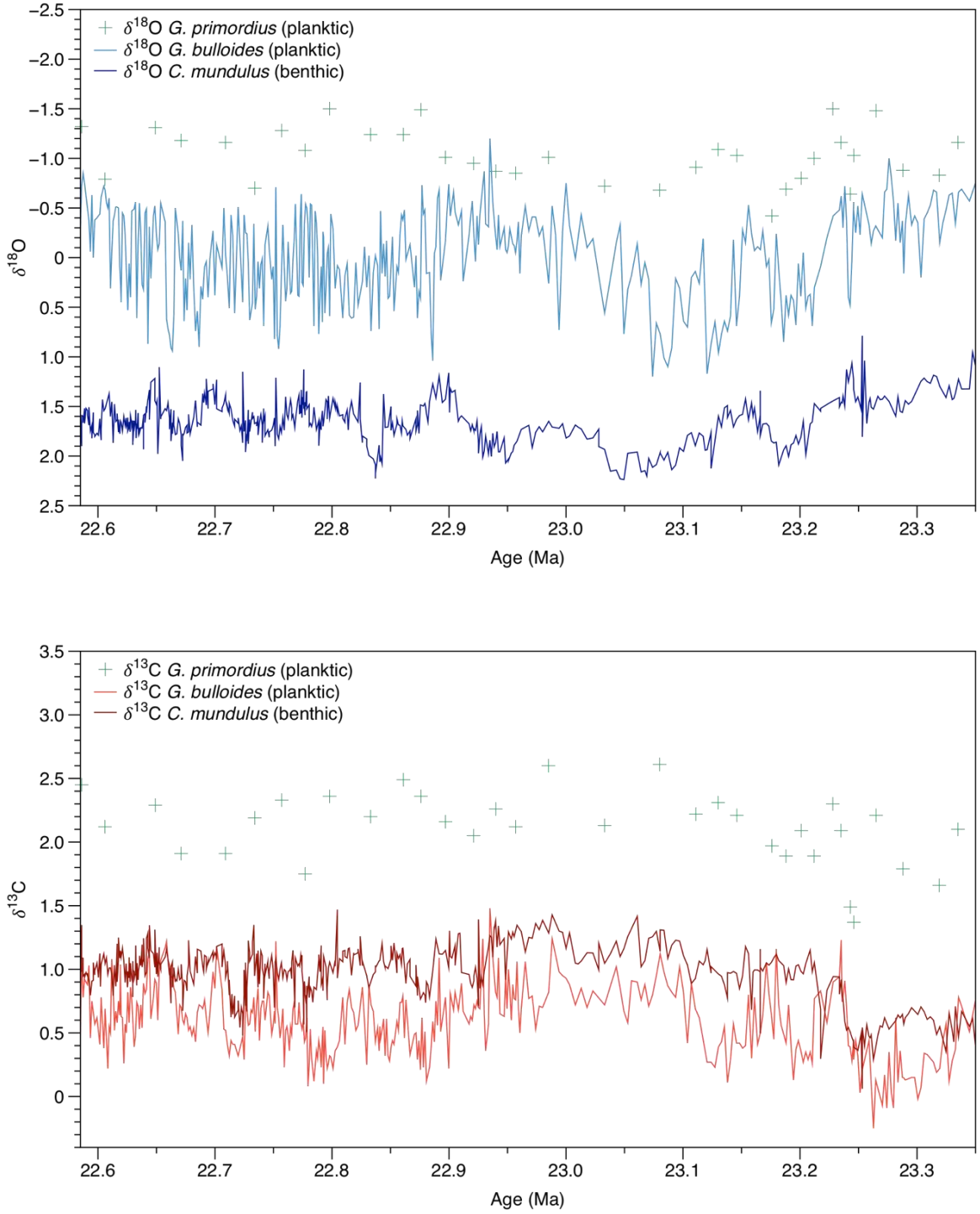

Supplementary Figure 4.2 Comparison of stable isotope measurements in *G. bulloides*, *G. primordius* and *C. mundulus* from Site U1406. *C. mundulus* data from Liebrand et al. (in prep).

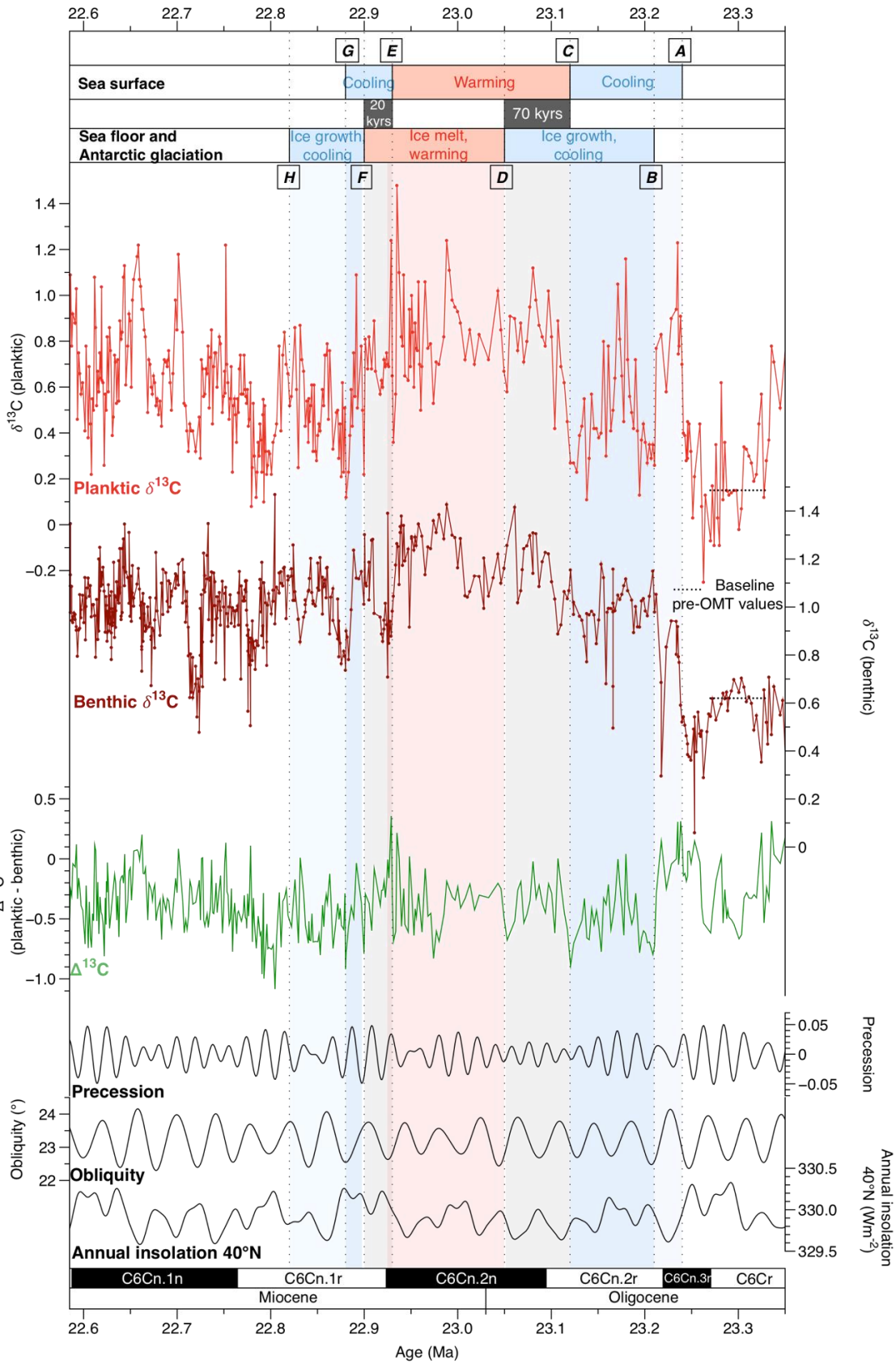
G
E
C
A
Sea surface
Cooling
Warming
Cooling
20 kyrs
70 kyrs
Sea floor and Antarctic glaciation
Ice growth cooling
Ice melt, warming
Ice growth, cooling
H
F
D
B
δ13C (planktic)
Planktic δ13C
Benthic δ13C
Baseline pre-OMT values
δ13C (benthic)
Δ13C (planktic - benthic)
Δ13C
Precession
Obliquity (°)
Obliquity
Annual insolation 40°N
Precession
Annual insolation 40°N (Wm-2)
C6Cn.1n
C6Cn.1r
C6Cn.2n
C6Cn.2r
C6Cn.3r
C6Cr
Miocene
Oligocene
Age (Ma)

Supplementary Figure 4.3 (previous page) Comparison of planktic and benthic !^{13}C records from Site U1406 across the OMT. This figure lies entirely within the duration of the OMT interval as suggested by Liebrand et al. (2016). From top to bottom: Labels denoting 'cooling' and 'warming' at the sea surface and sea floor are based on interpretation of planktic (this study) and benthic (Liebrand et al., in prep) !^{18}O records. Δ^{18}C is calculated only when planktic and benthic stable isotopes have been measured in the same sample. Orbital solutions are from (Laskar et al., 2004).

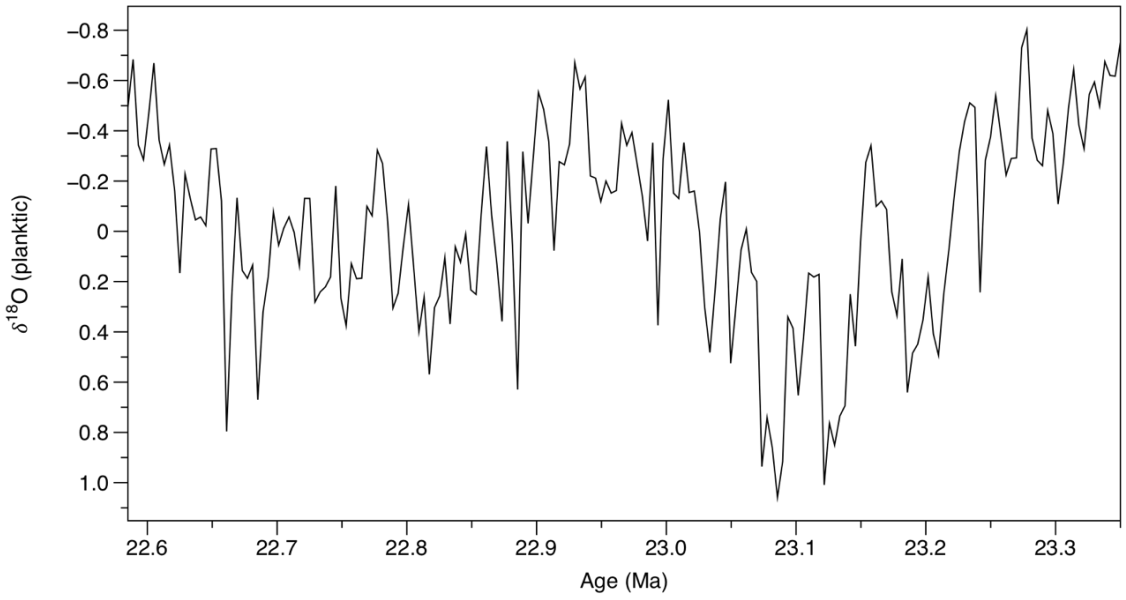

Supplementary Figure 4.4 Site U1406 planktic !^{18}O (see Figure 4.3) resampled at 4 kyr resolution. The sampling interval is variable in the main record presented in Figure 4.3. This figure is the same planktic !^{18}O record as that presented in Figure 4.3, but resampled at 4 kyr resolution to give an artificially uniform sample spacing.

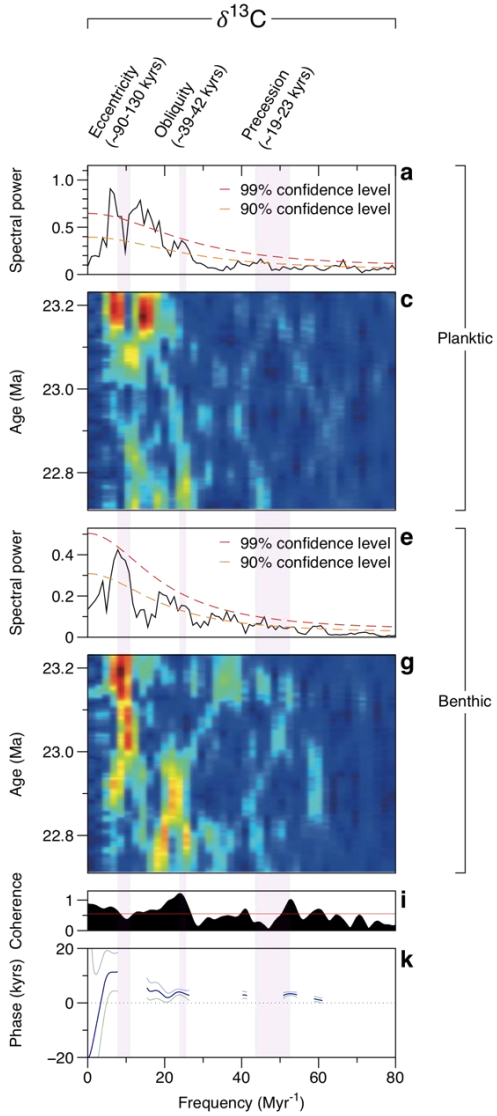

Supplementary Figure 4.5 Time series analysis of Site U1406 planktic and benthic !^{13}C records. Panels **a and c**: Multi-Taper Method (MTM) spectral analyses of planktic and benthic records, respectively, with confidence levels in red (99%) and orange (90%). Ranges of dominant periodicities of orbital forcing are indicated in purple shading. Panels **b and d**: wavelet analysis of planktic and benthic stable isotope records, respectively. Warmer colours indicate higher spectral power. Panel **e**: coherence between planktic and benthic records. Red line indicates 95% confidence level. Panel **f**: phase offsets of planktic relative to benthic stable isotope records. The dark purple line represents the mean phase offset estimate; pale blue and green lines represent the upper and lower estimates of this range, respectively.

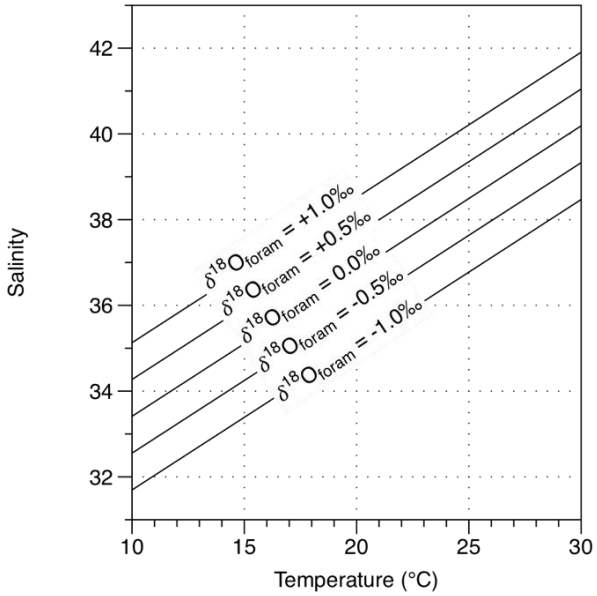

Supplementary Figure 4.6 Illustration of possible temperature-salinity-$\delta^{18}O$ relationships for given values of foraminiferal $\delta^{18}O$. Salinity estimation first requires estimation of the $\delta^{18}O_{seawater}$-salinity relationship; see Section 4.5.2 for details. $\delta^{18}O$ is here calculated using the *Globigerina bulloides* (11-chambered shell) calibration of Bemis et al. (1998).

The following chapter, entitled "Taxonomy of Oligo-Miocene *Globigerina bulloides* and related forms: refinement using a multivariate statistical clustering method, and investigation of stable isotope variability", is written in the style of a research article, with the intention of future publication. The manuscript was written entirely by Richard E. Smith, but Paul. N Pearson, Thomas H. G. Ezard and Paul A. Wilson also assisted with manuscript editing.

Taxonomy of Oligo-Miocene Globigerina bulloides and related forms: refinement using a multivariate statistical clustering method, and investigation of stable isotope variability

Chapter 5 Taxonomy of Oligo-Miocene *Globigerina bulloides* and related forms: refinement using a multivariate statistical clustering method, and investigation of stable isotope variability

5.1 Abstract

Globigerina bulloides d'Orbigny is an abundant modern species of planktonic foraminifer, used extensively in palaeoceanography to reconstruct past environmental change. However, uncertainty exists over the taxonomy and ecology of supposedly ancestral forms from the late Oligocene and Miocene that have often been included in '*Globigerina praebulloides*' Blow. While *G. bulloides* is commonly assumed to have evolved from '*G. praebulloides*' in the mid-Miocene, recently, foraminifera from the latest Oligocene have been described as being morphologically similar to modern *G. bulloides*. Given the often-significant inter- and intra-species variability encountered when generating stable isotope records, accurate taxonomic identification and species delineation is critical for generation of reliable records. Here, we take a quantitative approach to taxonomic classification. Approximately four hundred individuals with test forms similar to *G. bulloides* were selected from two deep sea samples from the Newfoundland Margin of Oligocene-Miocene boundary age. A suite of morphometric measurements was made on these individuals, then a statistical clustering method was applied to determine the most likely number of distinct morphological groups into which the individuals are best classified. Our analysis suggests that *G. bulloides* had two morphotypes in the Oligo-Miocene (one of which is typically larger and slightly more elongate with a slightly less arched aperture), but that these morphotypes are sufficiently similar to be assigned to a single species. Single-specimen foraminiferal stable isotope measurements indicate that these two morphotypes of *G. bulloides* show similar stable isotopic characteristics, yet this species displays a significant stable carbon isotope offset from the morphologically similar species and fellow surface dweller *G. woodi*. Our results underscore the importance of accurate taxonomic delineation for the creation of consistent stable isotope records.

5.2 Introduction

5.2.1 Identifying species of planktonic foraminifera in the fossil record

Planktonic foraminifera are widely used to reconstruct past surface ocean conditions, with their relative abundance and geochemical properties used as indicators of properties including temperature, salinity and primary productivity. Different species of foraminifera inhabit different regions of the water column and build their shells in a variety of ways (with some utilizing symbiotic relationships), resulting in inter-species variability in palaeoceanographic signals (e.g., Ezard et al., 2015; Hemleben et al., 1989; Kucera, 2007). For modern foraminifera, different species (and sub-species/genotypes) are increasingly differentiated by genetic analysis (Darling and Wade, 2008; Roberts et al., 2016). However, reconstructions based on fossil foraminifera, particularly extinct species, rely entirely on the concept of morphospecies, whereby is it assumed that morphologically similar individuals are members of the same species (Aze et al., 2011; Fordham, 1986), and thus had similar ecological preferences. This approach is complicated by the substantial intra-specific morphological variability typical of many species of planktonic foraminifera (André et al., 2012). While such variability has typically been interpreted as being ecophenotypic, work with extant species has revealed the presence of distinct morphotypes, each associated with one or more different genotypes, and with different ecological preferences (e.g., Aurahs et al., 2011; Darling et al., 2006; Huber et al., 1997; Morard et al., 2009; Quillévéré et al., 2013). These discoveries suggest that renewed emphasis on the accurate delineation of species in the fossil record has the potential to enhance the fidelity of palaeoceanographic reconstructions (Kucera and Darling, 2002).

Deciding whether the extent of morphological variability within a single species is sufficient to justify a split into more than one morphospecies (or conversely if the species definition is too narrow and should be joined with another morphospecies) is typically a highly subjective task, with interpretations often differing between workers (Olsson et al., 1999; Pearson et al., 2006). Quantitative morphometric methods, rather than subjective determinations, offer the potential for highly repeatable, non- (or at least less-) subjective determination of the range of morphological variability typical within a morphospecies (Zelditch et al., 2012). However, morphometric methods typically pre-assign species identifications to analyzed individuals, which introduces the bias of the worker who identifies the species (for a compilation of existing studies see the Appendix of Pearson and Ezard, 2014).

An alternative approach involves analysis of all individuals that fall within a broad morphological description, and then uses statistical clustering methods to determine whether the range of morphological variability within the sample set falls on a continuum (i.e., all individuals are part of a single, morphologically variable species) or into several discrete morphological groups (i.e.,

multiple morphospecies or morphotypes; Ezard et al., 2010). This method was used to distinguish between gradual evolutionary change (anagenesis) and the emergence of two morphologically distinct contemporaneous forms (i.e., speciation: cladogenesis), in Eocene *Turborotalia* (Pearson and Ezard, 2014). Ancestral forms similar to the palaeoceanographically important species *Globigerina bulloides*, among which there is a high ratio of morphological variability within-species relative to between-species, stand out as forms for which a statistical method offers potential for more accurate delineation into morphospecies and/or morphotypes.

5.2.2 Taxonomic issues surrounding ancestral forms of *Globigerina bulloides*

G. bulloides, an abundant modern species of planktonic foraminifera widely used for palaeoceanographic reconstructions in the Pleistocene, shows a wide range of morphological variability (Malmgren and Kennett, 1976, 1977; Shrivastav et al., 2016). This has led to suggestions that the species is a "wastebasket taxon" (Aze et al., 2011; Lamb and Beard, 1972). Recent genetic studies have begun to decipher some of this variability, revealing that typical *'G bulloides'* morphology encompasses several genotypes (Darling and Wade, 2008) that may be associated with different ecological niches (Darling et al., 2003; Morard et al., 2013). Two morphotypes of *G. bulloides*, distinguished by different pore densities and wall thicknesses, were recently identified (Osborne et al., 2016). However, uncertainty remains over the taxonomy and habitat of supposedly ancestral forms of *G. bulloides*, particularly in the late Oligocene and early Miocene. These forms are typically included in *'Globigerina praebulloides'* Blow (Blow, 1979; Bolli and Saunders, 1985; Kennett and Srinivasan, 1983), from which *G. bulloides* is commonly inferred to have evolved in the mid-Miocene. Yet foraminifera from the latest Oligocene have recently been described as being morphologically similar to modern *G. bulloides* (Pearson and Wade, 2009). In addition, the wide range of morphological variability among individuals of '*G. praebulloides*' and similar species (e.g., *Globigerina officinalis*, *Globigerinella obesa*, *Globoturborotalita woodi*) is not illustrated in standard taxonomic works, each of which typically display only a single individual. As a result, it is often hard to decide which species name to assign to individuals which differ slightly from the handful of individuals illustrated in taxonomic literature.

Here, in addition to test morphology, we also consider the wall textures of the individuals analysed. All planktonic foraminifera have one of several distinct wall textures, while individuals with the same texture may show a range of variability in porosity or pore size (Huber et al., 1997; Osborne et al., 2016; Vargas et al., 1999). These textures are sufficiently distinct that they are generally regarded as being a more conservative indicator of the genus to which a particular foraminiferal species belongs than gross test morphology. Wall textures are thus frequently used to distinguish between forms which are otherwise morphologically similar (Hemleben and Olsson, 2006). For

example, while some forms typically assigned to *Globigerina* and *Globoturborotalita* appear morphologically similar (e.g., Pearson and Wade, 2009), the former is associated with a '*bulloides*-type' wall with raised spine collars connected by ridges, whereas the latter is associated with a cancellate wall texture with pores arranged in a regular symmetrical 'honeycomb' texture (Figure 5.1). A morphometric approach offers an opportunity to determine whether these individuals also have consistent subtle morphological differences, or whether wall texture is truly the only distinguishing feature, in which case the assumption that such forms have distinct evolutionary lineages would perhaps be called into question.

Here, we use morphometric measurements, a statistical clustering method and single-test stable isotope measurements to investigate the morphology and ecology of '*G. praebulloides*' and similar forms in the Late Oligocene and Early Miocene. We aim to establish a) whether '*G. praebulloides*' is a wastebasket taxon requiring division, or if it is a single taxon with a large and continuous range of variability; and b) which morphological features are the most consistently distinct between morphospecies and therefore best relied upon when selecting planktonic foraminifera for palaeoenvironmental studies.

5.3 Methods

5.3.1 Site, oceanographic setting and sampling

Two samples were obtained from material recovered at IODP Site U1406 in the NW Atlantic (40.4°N, 51.7°W). Foraminifera at this site are generally excellently preserved, with only minor post-depositional recrystallization and dissolution (Smith, 2017c). Site U1406 lies near the boundary between the modern Labrador Current and North Atlantic Current, a frontal zone suggested to have existed since at least the Oligo-Miocene (Smith, 2017a). Given the large temperature gradient typically associated with oceanic fronts, these areas are typically avoided for evolutionary studies (Pearson and Ezard, 2014) because of the potential complexity added by different morphotypes/genotypes living on either side of the front (Darling et al., 2006; Morard et al., 2016). However, given the aim of our project to understand the full range of morphological variability within *G. bulloides* and similar species, the frontal location of Site U1406 is, if anything, advantageous. The two samples selected are dated to 22.4 Ma (Sample 1; U1406A-7H-CC-26 to 34 cm) and 23.6 Ma (Sample 2; U1406A-10H-5W-50 to 52 cm; van Peer et al., in prep). We note that Sample 1 is a 'core catcher' sample, and may therefore also include foraminifera from further up in the core (as young as 22.1 Ma); the advantage of the sample being a core catcher is that it contains abundant planktic foraminifera.

5.3.2 Selection of individuals for study

While our study aims to reduce subjectivity wherever possible, it nevertheless remains necessary to first decide which foraminifera should be included in our analysis. With the aim of including all species that show a moderate resemblance to (and may be confused with) *G. bulloides*, we produced a set of criteria for inclusion that is as broad as possible, while being sufficiently restrictive to enable a single set of morphological parameters to define the variability between individuals in a readily repeatable way. The criteria for inclusion of individuals in the study is as follows:

> *Macroperforate, 3 to 5 chambers in final whorl, chambers globular to subglobular. Sutures depressed and radial to slightly curved. Umbilicus small to medium. Primary aperture umbilical to umbilical-extraumbilical, very low to high arch. Any macroperforate wall texture and both presence/absence of supplementary aperture permitted. Kummerforms not picked. All individuals selected from >180 µm size fraction.*

The size fraction criterion of >180 µm size fraction was determined to produce images of sufficient quality for accurate measurements. Given that this limit is similar to the modal size of adult populations of *G. bulloides* from the Recent and Last Glacial (Peeters et al., 1999), this criterion also likely has the benefit of restricting our study to adult individuals. Kummerforms are generally split from normalforms in morphometric studies because of the different (and smaller) shape of the final chamber (Malmgren and Kennett, 1976); here they did not make up a significant number of individuals in the sample material, and so we opted to exclude them completely from our analysis. We also avoided individuals showing evidence of reworking (e.g., pyrite overgrowths) or significant diagenesis; the former may be of significantly different age, and the latter may obscure wall texture (Constandache et al., 2013) and introduce post-depositional bias into stable isotope measurements (Sexton et al., 2006a). In total, 186 and 210 individuals were selected from samples 1 and 2, respectively, for inclusion in the study.

5.3.3 Discrete parameters

While automated measurements (i.e., measurements made by computer software) are suitable for most of the parameters we measure, several non-subjective parameters are more easily determined by eye: 1) coiling direction (dextral/sinistral); 2) presence or absence of a supplementary aperture on the spiral side; 3) number of chambers in the final whorl, to the nearest half. Pore size was also determined manually, which we now explain.

Visual inspection of all individuals picked suggested a clear distinction between either ‘large’ or ‘small’ pores, verified with accurate pore size measurements (measured in ImageJ) from SEM

images. Only pores near-perpendicular to the plane of view were included in the analysis; in order to fulfil this criterion while using only a single image of each individual, 4 to 15 (median 6) pores were measured per individual. In some individuals, the wall texture of the final-formed (F) chamber differed from earlier-forming chambers, so for consistency we only considered pore size of the penultimate-formed (F-1) chamber. Our manual determination of pore size was (necessarily) made from the exterior wall of the foraminifer. Measurements of pore size have been suggested to be more accurate when taken from the interior of broken foraminiferal fragments, primarily because the effects of diagenesis are more pronounced on exterior shell walls (Constandache et al., 2013), but also because of effects resulting from the convex shape of the shell (Bé, 1968). To test whether these effects bias our determination of pore size we measured the pore size on SEM images of both the interior and exterior walls of broken fragments of the same individuals, after cracking these individuals between two glass slides. We find no marked or consistent difference between interior and exterior measurements (Supplementary Figure 5.1), which we suggest is largely a result of the excellent foraminiferal preservation at Site U1406.

Our results indicate that our visual approximation of 'large' versus 'small' pore size is highly accurate, showing very strong correlation with measured pore diameter (Figure 5.1). Individuals identified as having 'small' pores all have a mean pore diameter between 1.9-3.3 µm, apart from one individual with mean pore diameter 4.0 µm. Individuals with 'large' pores have a mean pore diameter of 4.4-8.2 µm. The relative range of variability is approximately the same for both 'small' and 'large' pore sizes, when considered relative to the mean pore diameter.

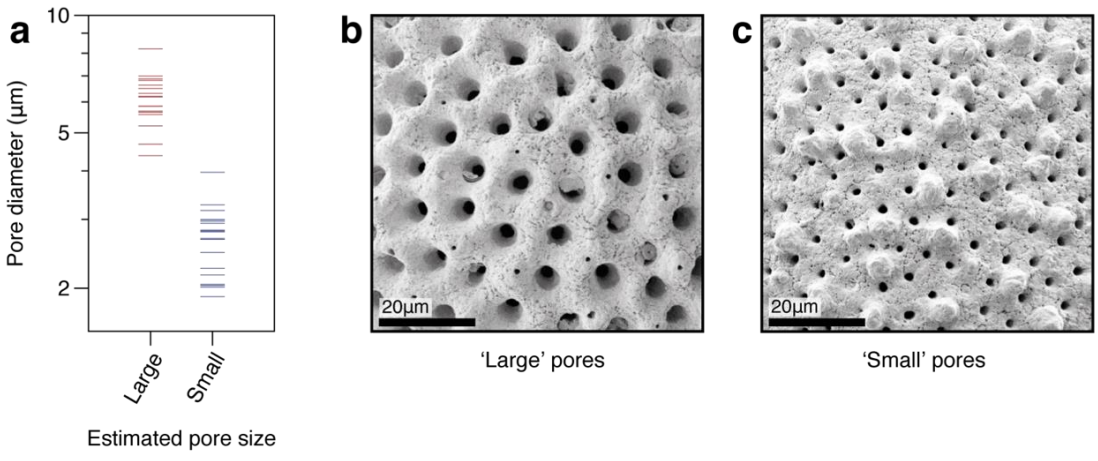

Figure 5.1 Comparison of pore size estimations with measurement on SEM images. SEM images were taken of individuals estimated by eye with a light microscope to have 'large' (red) or 'small' (blue) pores. Pore size was then measured on the SEM images (y-axis). The values presented here are the average for each foraminifer; see Supplementary Figure 5.1 for raw (i.e., individual pore) data.

SEM images reveal that there is a relationship between pore size and wall texture (Figure 5.1): 'large' pores are associated with a more cancellate, 'honeycomb' wall texture (though sometimes not very well developed), while 'small' pores are associated with a '*bulloides*-type' wall texture, with raised spine collars connected by ridges (Hemleben and Olsson, 2006). We note that the ridges in this latter category are sometimes sufficiently high to give a somewhat cancellate appearance, following a similar observation in material from Trinidad (Pearson and Wade, 2009). In our specimens, these higher ridges are typically associated with F-1 and earlier forming chambers, whereas the F chamber has lower ridges, and thus a wall more '*bulloides*-type' in appearance.

5.3.4 Continuous parameters

For automated image analysis, all 396 individuals were mounted onto black-backed glass microscope slides with water-soluble glue, first on their apertural sides, and then later remounted on their spiral sides. For morphometric measurements to be comparable between individuals it is important to produce images in the same orientations for all individuals (Brombacher et al., 2017; MacLeod and Carter, 1984). Slides were thus placed on a universal stage, allowing rotation in any axis (following e.g., Knappertsbusch et al., 2009; Mary and Knappertsbusch, 2013; Pearson and Ezard, 2014). For images of the spiral side, individuals were rotated so that their coiling axis was perpendicular with the image plane (Figure 5.2c). While images of the apertural side would ideally be taken along the same axis as those of the spiral side, the large aperture of *G. bulloides* and morphologically similar forms means that it is difficult to accurately identify the coiling axis from the apertural side. Instead, we chose to make images of the apertural side with the image plane perpendicular to the closest approximation to a flat plane between the final-forming chamber and the remainder of the test (Figure 5.2a). Images were taken with an Infinity 3 Lumenera camera mounted on an Olympus SZX10 light microscope. Image analysis was performed with Image Pro Premier software. For all measurements, 34 individuals were imaged a further two times (by the same worker, RS, but on different occasions) to test the repeatability of the measurements (Figure 5.3).

On the spiral side, automated measurements were made of the test area and major and minor axis lengths for all 396 individuals. From these measurements we then calculated the mean test radius (i.e., the square root of the test area) and test aspect ratio (i.e., ratio of major to minor axis length), respectively, to record test size and elongation. Mean test radius proved extremely repeatable: when the original data are plotted against the first and second repeats, the correlation is very strong in both cases (R^2=0.99,0.99; Figure 5.3a,b). Test aspect ratio was also repeatable (R^2=0.68,0.62; Figure 5.3c,d). Given that both test area and aspect ratio have been demonstrated to be highly

repeatable (Brombacher et al., 2017), it is unclear why aspect ratio is less repeatable than area measurements in our study. We suggest that the globular chamber shape of the individuals considered here means that slight orientation changes during imaging can cause moderate changes in the orientation (and thus length) of the long axis identified by the software during calculation of aspect ratio.

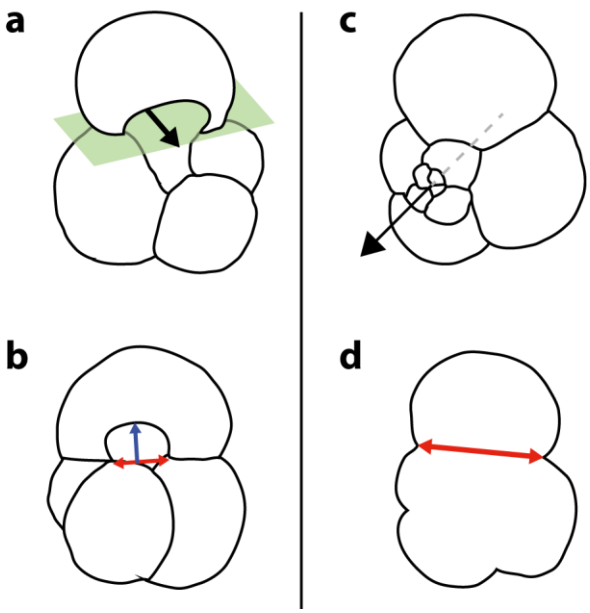

Figure 5.2 Alignment of foraminifera and selected measurements. **a)** Images of the apertural view were taken in with the image plane perpendicular to the closest approximation to a flat plane (in green) between the final-forming chamber and the remainder of the test, i.e., with the black arrow pointing straight up at the camera. **b)** Illustration of measurement of aperture width (red) and height (blue; perpendicular to width measurement). **c)** Images of the spiral view were taken looking directly down the coiling axis, i.e., with the black arrow pointing straight up at the camera. **d)** Measurement of the final-chamber suture separation distance, measured by landmark placement on an automated outline generated by the imaging software.

To determine the symmetry of the aperture (i.e., the extent to which it is umbilical rather than umbilical-extraumbilical) we measured the distance between the points at which the two sutures joining the F chamber to earlier-formed chambers intersect the test outline (Figure 5.2d). The more extraumbilical the aperture, the closer these two points become. This distance was determined by manual placement of landmarks. We size-normalize this measurement by dividing by the mean test radius. This measurement was found to be repeatable (R^2=0.64,0.71; Figure 5.3e,f).

Finally, we measured the shape of the primary aperture. To measure the width of the aperture, we assigned landmarks at the two ends of the arch in the final chamber, at the points where it meets the earlier-formed chambers, and measured the distance between them. The distance perpendicular from this line to the top of the arch, at the point where this distance is greatest (i.e., at the peak of the arch), was then taken as a measure of aperture height (Figure 5.2b). We then divided the aperture height by width to give a measure of the aspect ratio of the aperture, i.e., how arched the aperture is. This measurement is also found to be repeatable (R^2=0.87,0.79; Figure 5.3g,h).

5.3.5 Determination of clusters

We then applied a statistical clustering method to our data, following Ezard et al. (2010) and Pearson and Ezard (2014). Following the methods outlined in these papers (and references therein), we reduced our data to orthogonal components, removed components without substantial explanatory power, and determined a) the statistically most likely number of clusters within this reduced dataset, and b) the cluster to which each individual test is most appropriately classified. This method enables morphological classification of foraminifera with no prior assumptions about species identity, other than the initial coarse classification as having a form loosely similar to that of *G. bulloides*. Statistical analysis was performed in the R environment (v. 3.3.2; R Core Team, 2016) and used the packages "paran" (v. 1.5.1; Dinno, 2009) and "mclust" (v. 5.2.2; Fraley and Raftery, 2002). Default settings were used except for two parameters in the "paran" package (10,000 iterations and a confidence percentile of 99%), which provides a more conservative test of how many components to retain (Peres-Neto et al., 2005).

5.3.6 Stable isotope measurements

Forty-six individual foraminifera were removed from the glass slide used for imaging and washed in water to remove all remaining water-soluble glue. Only individuals of mean radius >212 µm (as determined by the automated measurements) were selected, to provide a sufficient mass of foraminiferal material for the mass spectrometer. After drying, picked individuals were transferred to reaction vials and analysed using a Kiel IV Carbonate Device attached to a Thermo Finnigan MAT 253 dual inlet mass spectrometer at NOCS, University of Southampton. Analytical precision is 0.08‰ for $!^{18}O$ and 0.06‰ for $!^{13}O$. Data were calibrated using a two-point calibration to standard NBS 18 and an internal standard (GS1). Results are reported relative to the Vienna Peedee belemnite (VPDB) standard.

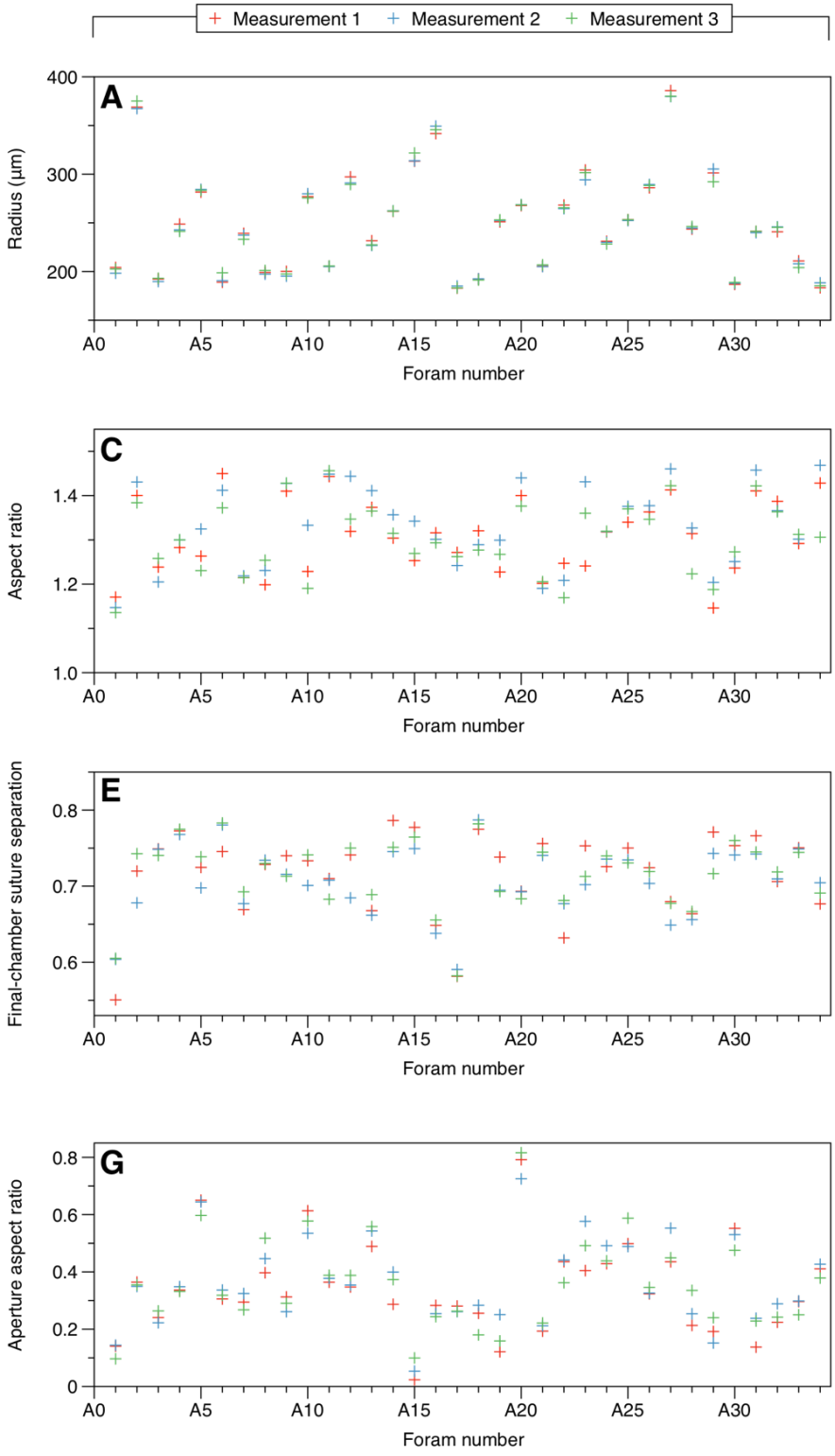

Figure 5.3 (figure spans both pages) Repeatability of measurements. The first 34 foraminifera were each imaged three times on both their spiral and apertural sides, and the measurements on this figure were repeated. Panels on the left show raw data;

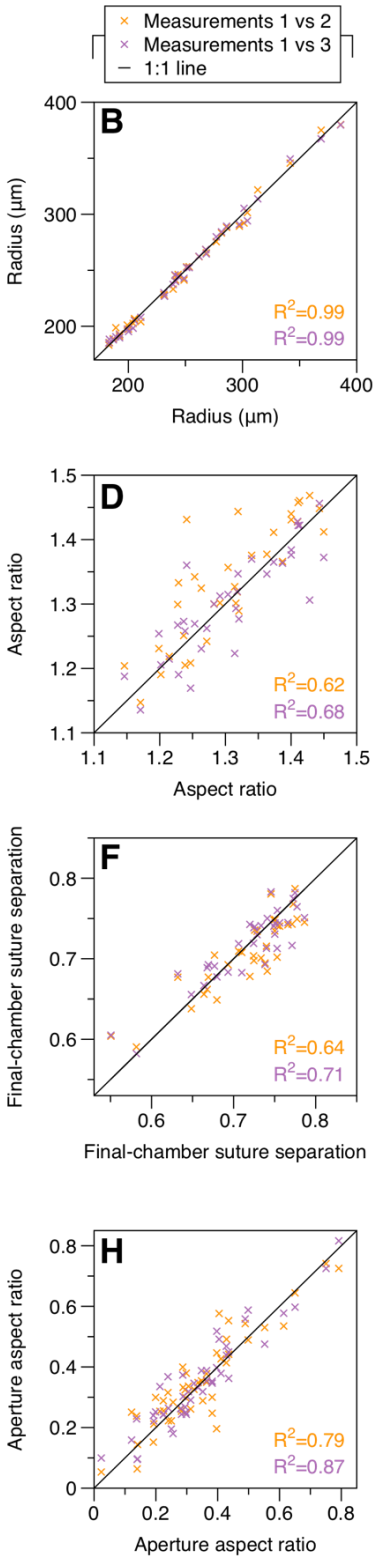

panels on the right show comparison of the second (orange) and third (purple) measurements plotted against the original measurement. The black line represents a 1:1 ratio. R^2 values are calculated using this 1:1 line, not the best-fitting line.

5.4 Results and discussion

5.4.1 Weighting of principal components

One hundred and eighty-six individuals were measured in Sample 1 (23.6 Ma), and 210 in Sample 2 (22.3 Ma). While we did analyse each sample separately (Supplementary Figure 5.2), we chose to combine the samples for our main analysis (Figures 5.5,5.6). This relies on the assumptions that a) no significant morphological changes occurred in the 1.3 Myrs separating the samples; and b) environmental conditions are sufficiently similar between samples that no environmentally driven morphological differences are present between the samples. The similar distributions of properties in each sample (Figure 5.4) suggest that these are reasonable first approximations. We also note the well-mixed distribution of individuals from each sample across the principal components (Figure 5.6), with no region of the principal component axes dominated by one of the two samples. When the samples are analysed independently, the corresponding clusters identified in each sample also have broadly similar properties (Supplementary Figure 5.2). Combining measurements from both samples (Figure 5.6) has the advantage of doubling the number of individuals in the analysis, revealing an additional cluster not identified in the single-sample analyses (Supplementary Figure 5.3.

Three principal components were retained, together reflecting 59.3% (individually 25.9%, 19.2% and 14.2%) of the total variance in the dataset. The average radius, aperture aspect ratio, presence/absence of supplementary aperture, final chamber suture distance and pore size each have similar explanatory power (14.1-15.6%). It is perhaps unsurprising that the presence/absence of a supplementary aperture and pore size have high explanatory power, because traditional foraminiferal taxonomic classification indicates that individuals between which these properties differ must be members of different taxa or genera, respectively. The number of chambers in the final whorl and aspect ratio both have slightly lower explanatory power (12.5% and 10.1%, respectively). We suggest that the lower explanatory power of the number of chambers is a result of the modest abundance (18%) of individuals with >3½ chambers in our analysis. It is unclear why

Figure 5.4 (Opposite) Histograms of raw data**.** Raw data is binned for each parameter to enable comparison of the spread of data in each sample. Data for Sample 1 (Miocene) is displayed in pink; data for Sample 2 (Oligocene) is displayed in blue.

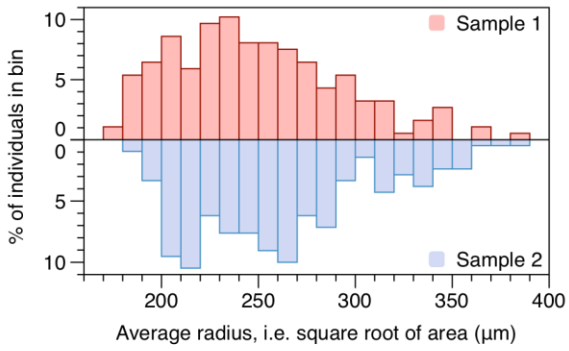
Sample 1
Sample 2
% of individuals in bin
Average radius, i.e. square root of area (µm)

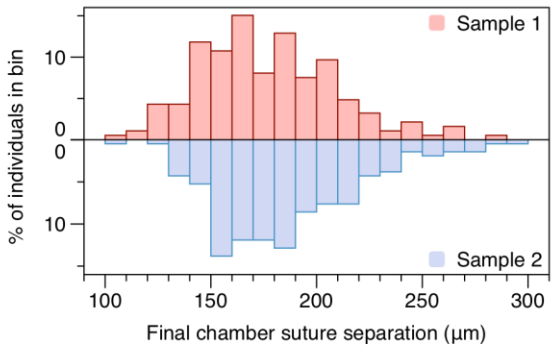
Sample 1
Sample 2
% of individuals in bin
Final chamber suture separation (µm)

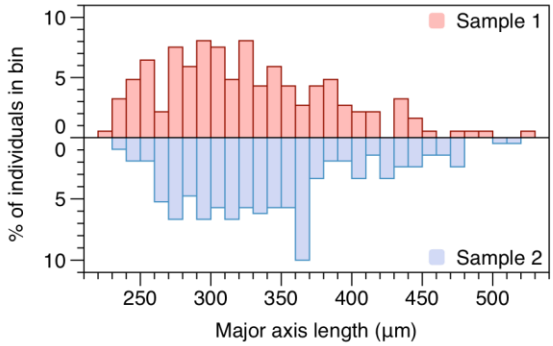
Sample 1
Sample 2
% of individuals in bin
Major axis length (µm)

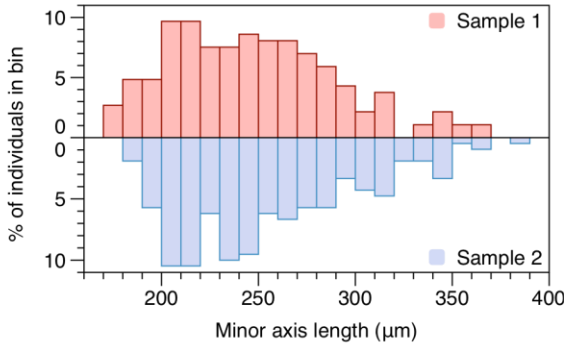
Sample 1
Sample 2
% of individuals in bin
Minor axis length (µm)

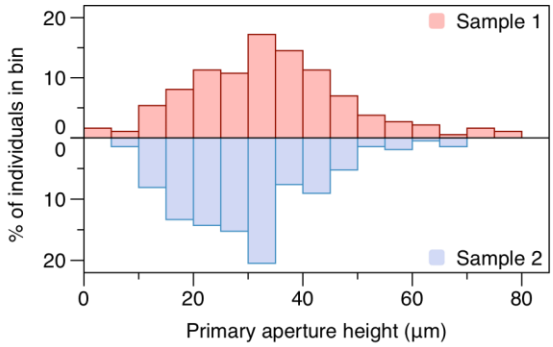
Sample 1
Sample 2
% of individuals in bin
Primary aperture height (µm)

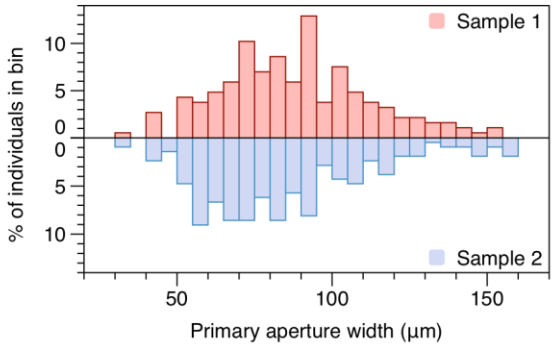
Sample 1
Sample 2
% of individuals in bin
Primary aperture width (µm)

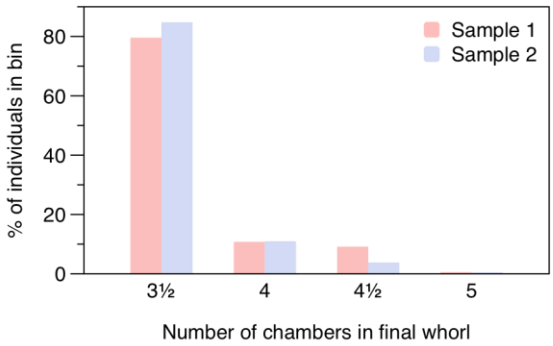
Sample 1
Sample 2
% of individuals in bin
3½
4
4½
5
Number of chambers in final whorl

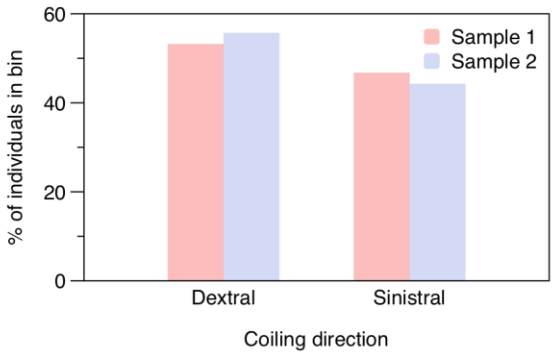
Sample 1
Sample 2
% of individuals in bin
Dextral
Sinistral
Coiling direction

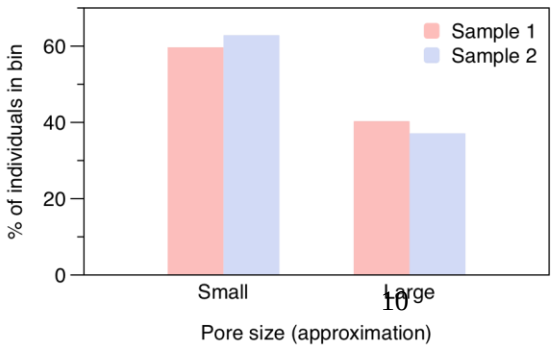
Sample 1
Sample 2
% of individuals in bin
Small
Large
Pore size (approximation)

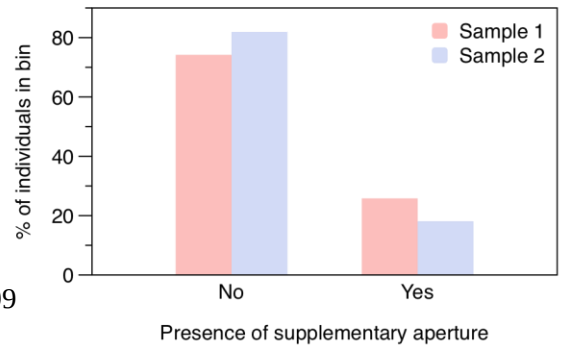
Sample 1
Sample 2
% of individuals in bin
No
Yes
Presence of supplementary aperture

the test aspect ratio has a lower explanatory power than all other parameters except coiling direction. Test shape has long been postulated to be associated with buoyancy, with a flatter shape enabling growth of larger tests without necessitating a change in depth habitat (Fok-Pun, 1981; McNown and Malaika, 1950), though this relationship has recently been called into question (Caromel et al., 2014). If test shape is indeed related to ecology, such a relationship may be obscured in our data because of the lower repeatability of aspect ratio relative to other properties (Figure 5.3b).

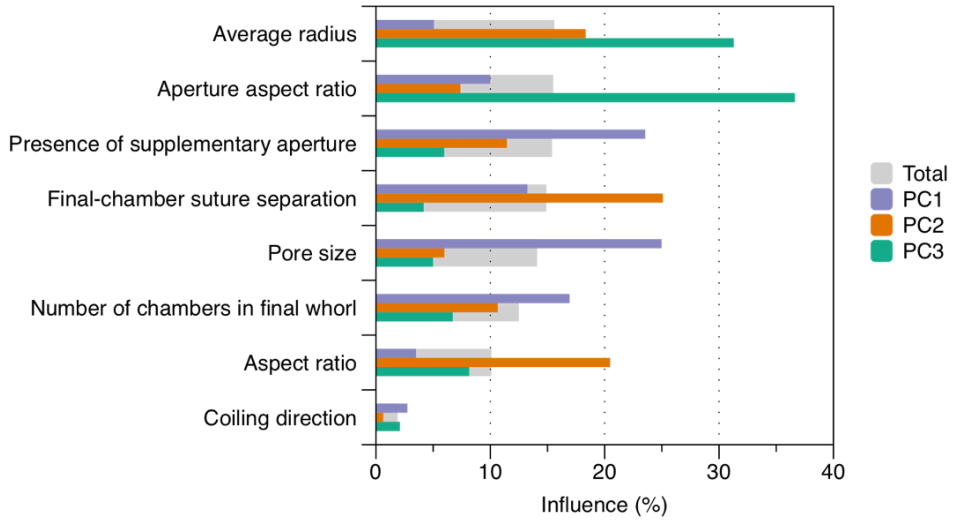

Figure 5.5 Principal components. Weightings of each property on the three retained principal components only in the combined (i.e., samples 1 and 2 together) analysis. The 'total' weighting (grey) incorporates the relative weight of each principal component.

Figure 5.6 (Opposite) Results of clustering analysis. **Top (large) panels:** Each point represents the position of a single foraminifer in principal component space. Unfilled points are individuals from Sample 1; filled points are from Sample 2. The left (principal components 1 and 2) and right (principal components 2 and 3) panels are different views (i.e., different dimensions) of the same dataset. Colours indicate the cluster of which each individual has been determined to statistically most likely be a part. **Bottom (small) panels:** Spread of properties in each cluster. The percentage in the title refers to that property's influence on the three retained principal components. For continuous measurements, each thin horizontal line represents a single foraminifer; thick lines are medians for each cluster.

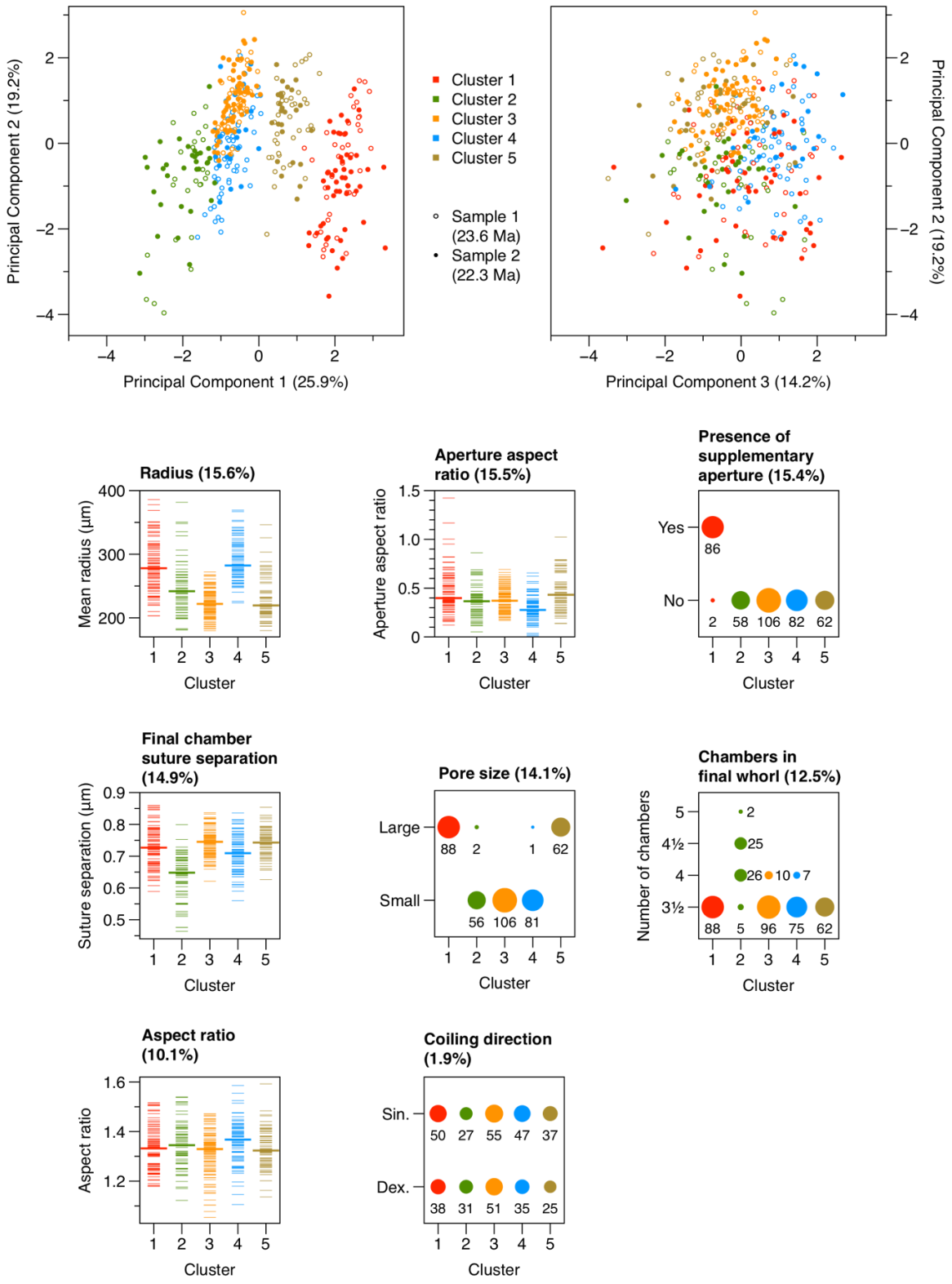
Principal Component 2 (19.2%)
Principal Component 1 (25.9%)
Principal Component 3 (14.2%)
Cluster 1
Cluster 2
Cluster 3
Cluster 4
Cluster 5
Sample 1 (23.6 Ma)
Sample 2 (22.3 Ma)
Radius (15.6%)
Mean radius (µm)
Aperture aspect ratio (15.5%)
Aperture aspect ratio
Presence of supplementary aperture (15.4%)
Yes
No
86
2 58 106 82 62
Final chamber suture separation (14.9%)
Suture separation (µm)
Pore size (14.1%)
Large
Small
88 2 1 62
56 106 81
Chambers in final whorl (12.5%)
Number of chambers
2
25
26 10 7
88 5 96 75 62
Aspect ratio (10.1%)
Aspect ratio
Coiling direction (1.9%)
Sin.
Dex.
50 27 55 47 37
38 31 51 35 25
Cluster

The only property with almost no explanatory power is coiling direction. While modern *G. bulloides* have a coiling preference, with ~63-65% of individuals having sinistral coiling (Brummer and Kroon, 1988; Darling et al., 2003), this coiling preference was reported to be absent in ancestral forms from the Mid-Miocene (Gonera et al., 2003). While we observe a very slight preference for dextral coiling (53% in sample 1, 56% in sample 2), this is not statistically significant (p=0.38, 0.10 in a one-sample t-test with 95% confidence level). An absence of coiling preference in the forms studied here would explain the low explanatory power of coiling direction.

5.4.2 Clusters and species identification

Our analysis determined that the individuals measured are members of one of five distinct clusters. When each sample was analyzed independently, four clusters were identified (Supplementary Figure 5.2): most individuals within clusters 3 and 4 lie together in a single cluster. This is very likely an artefact of the reduced sample size when each sample is analyzed independently. Each of the five clusters resulting from analysis of the combined data represents a group with distinct morphological features, and thus a different morphospecies or morphotype (Figures 5.7, 5.8). We now compare the morphological properties of each cluster with existing species descriptions. For convenience, we refer to both '*G. bulloides*' and '*G. praebulloides*' solely as '*G. bulloides*', except where the distinction is of relevance.

Cluster 1: *Trilobatus primordius*

Ninety-eight percent of individuals in Cluster 1 have a supplementary aperture, a feature unique to this cluster. Taxa with a supplementary aperture are generally placed within the genus *Globigerinoides*, or, as recently suggested, *Trilobatus* (Spezzaferri et al., 2015). They also all have 3½ chambers in their final whorl and 'large' pores; we therefore classify this cluster as *Trilobatus primordius* (see Spezzaferri et al. [2015] for discussion of whether this species instead lies in the genus *Globigerinoides*). The similarity of this form to the other clusters is striking: the range of variability in all properties (except pore size and presence/absence of supplementary aperture) is broad enough to include the median values for all other clusters. Indeed, if the cluster analysis is repeated but with supplementary aperture measurements excluded, almost all individuals from this cluster are found to join the cluster that is otherwise dominated by individuals coming from cluster 5, *G. woodi*, described below (Supplementary Figure 5.3A). This suggests that *T. primordius* may have evolved from *G. woodi*, in contrast to previous suggestions that it evolved from *G. bulloides* (Aze et al., 2011; Kennett and Srinivasan, 1983). We note that individuals resembling *T. primordius* are all placed in a single cluster, in contrast to the multiple "*Globigerinoides*" species identified by Spezzaferri (1994). While this may be a result of our sample size being too small to distinguish between such clusters, a more likely explanation is that mid-latitude Site U1406 lies too far north to record these species, given the low-latitude preferences of early representatives of "*Globigerinoides*" (Spezzaferri, 1994).

The wall texture of this species has been debated. The original description of *T. primordius* (Blow and Banner, 1962) describes it as having a cancellate wall texture, but forms with a primarily *bulloides*-type wall texture have since been identified (Pearson and Wade, 2009). SEM images from our samples (Figure 5.7) indicate a wall texture that is cancellate, but poorly developed in some individuals.

Cluster 2: *Globigerinella obesa*

Cluster 2 has the lowest final-chamber suture separation distance of any cluster, i.e., individuals in Cluster 2 typically have a more umbilical-extra umbilical aperture, compared to the more umbilical apertures typical of other clusters. Individuals in Cluster 2 also almost always (92% of individuals) have more than 3½ chambers in their final whorl, almost always (97% of individuals) have 'small' pores, and never show a supplementary aperture. These individuals therefore essentially resemble *G. bulloides* but have 4-4½ chambers in their final whorl and a more extraumbilical aperture. We therefore identify them as *Globigerinella obesa* Bolli. We suggest that the two individuals with 5 chambers are *Globigerinella praesiphonifera* Blow, generally regarded as having evolved from *G. obesa* around the Oligocene-Miocene boundary (Kennett and Srinivasan, 1983).

Clusters 3 and 4: *Globigerina bulloides*

Specimens in clusters 3 and 4 both lack a supplementary aperture, and have 'small' pores and 3½ (or occasionally 4) chambers in their final whorl. These clusters therefore resemble either/both *G. bulloides/'G. praebulloides'* as described in standard taxonomic works (e.g., Bolli and Saunders, 1985; Kennett and Srinivasan, 1983). The split between these two clusters in our analysis indicates the existence either of Oligo-Miocene forms of *G. bulloides* and *'G. praebulloides'* or morphotypes of the same species. Individuals in Cluster 4 tend to have a slightly less arched aperture and are slightly more elongate than individuals in Cluster 3. Lower arching and elongation are properties typically used to identify *'G. praebulloides'*, and to distinguish it from the higher-arched, less elongate *G. bulloides* (Blow, 1959; Kennett and Srinivasan, 1983; Spezzaferri, 1994). However, individuals in Cluster 4 are consistently larger than those in Cluster 3, at odds with the original description of '*G. praebulloides*', which describes it as being "consistently smaller" than *G. bulloides* (Blow, 1959). As a result, we conclude that a distinction between these species is not supported by our analysis. To verify this interpretation, we consider two other features commonly used to distinguish *'G. praebulloides'* and *G. bulloides*: the rate of chamber expansion and the degree to which chambers are embracing. While we did not measure these features, visual investigation of individuals within clusters 3 and 4 again indicates no consistent difference between the clusters; instead, there is a substantial range of variability within both clusters.

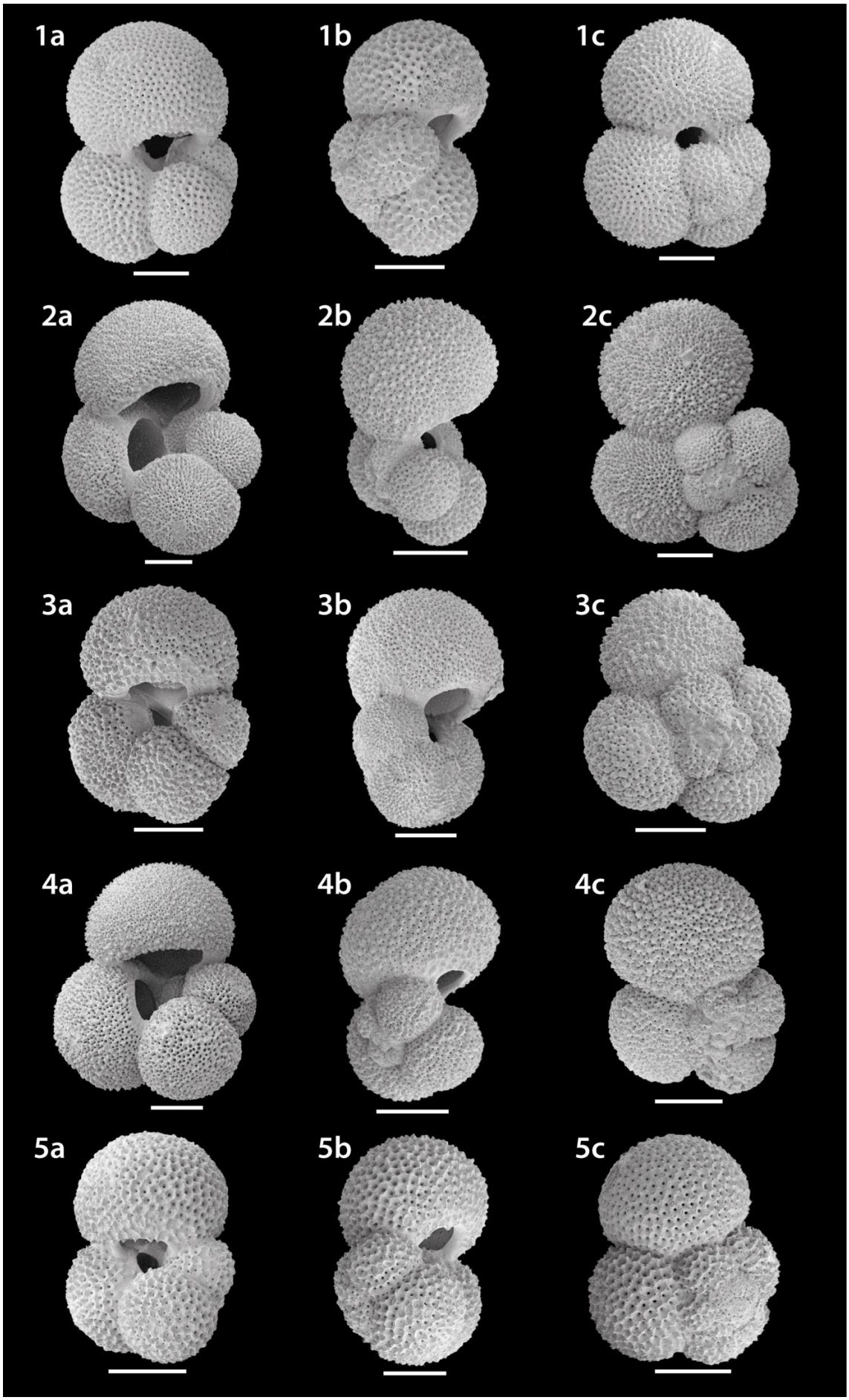
1a
1b
1c
2a
2b
2c
3a
3b
3c
4a
4b
4c
5a
5b
5c

Figure 5.7 (opposite) Representative Scanning Electron Microscope (SEM) images of foraminifera from the five clusters determined using the multivariate statistical clustering method, showing apertural (a), side (b) and spiral (c) views of individuals. 1: *Trilobatus primordius*; 2: *Globigerinella obesa*; 3 and 4: *Globigerina bulloides*; 5: *Globoturborotalita woodi.* For all images, the white scale bar represents 100 µm.

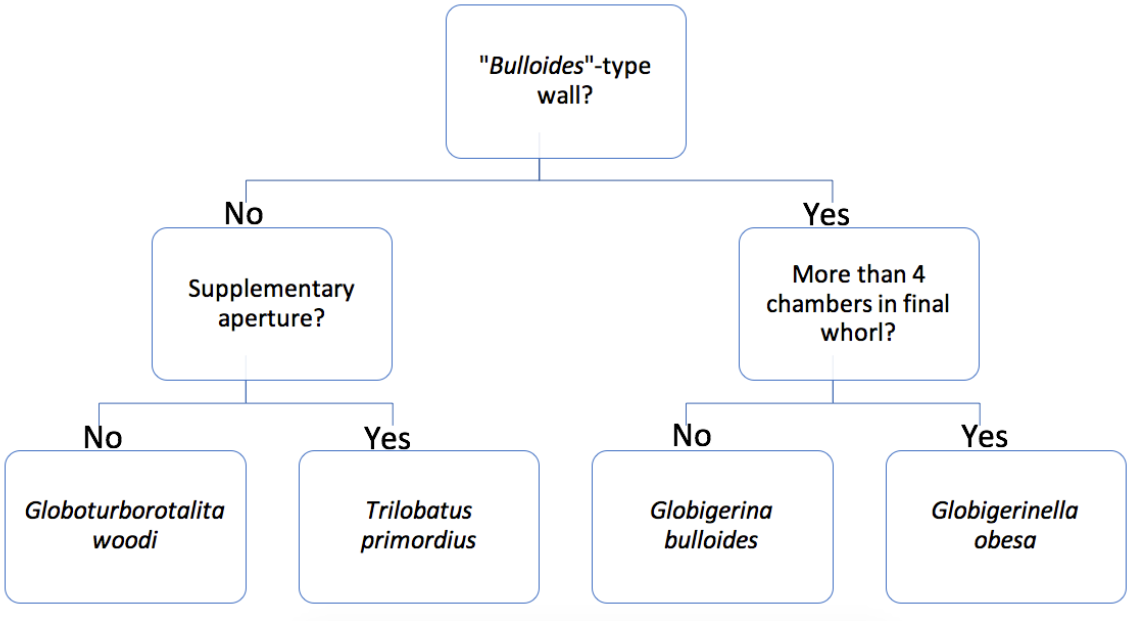

Figure 5.8 Classification tree for late Oligocene/early Miocene foraminifera which fall within the "*bulloides*-like" criteria set out in Section 5.3.2.

While our analysis has identified two distinct morphological groups within *G. bulloides*, it is important to note that the differences in median aperture arching and test elongation are small, and are far exceeded by the range of variability of each property within each cluster. The only property consistently and significantly different between the two groups is the average test size, but alone, this property is not sufficient to divide a group into two species. We therefore suggest that clusters 3 and 4 (which we note were not separated by our method when each sample was considered alone; Supplementary Figure 5.2) are not sufficiently different to justify assignment to two different species. Instead we infer the presence of subtly different morphotypes of a single species.

Following Pearson and Wade (2009), we assign these clusters to the species *G. bulloides*, given their morphological similarity to modern forms.

We now consider the relationship of *G. bulloides* to *G. obesa* in our samples. The inclusion in clusters 3 and 4 of a total of 17 individuals with more than 3½ chambers in their final whorl, and the inclusion in Cluster 2 of 5 individuals with only 3½ chambers in their final chamber whorl, suggests that there is some morphological gradation between these two species. The individuals in Cluster 2 generally have a lower final-chamber suture separation distance (i.e., a more extraumbilical aperture) than those in clusters 3 and 4, but there is some overlap (Supplementary Figure 5.4). Such gradation supports the suggestion that *G. obesa* evolved from *G. bulloides* in the late Oligocene (Kennett and Srinivasan, 1983); this is particularly supported by the '*bulloides*-type' wall texture revealed in SEM images of this cluster (Figure 5.7). We therefore suggest that, for accurate palaeoceanographic geochemical measurements, only individuals with over 4 chambers in their final whorl are identified as *G. obesa*.

Cluster 5: *Globoturborotalita woodi*

Individuals in this cluster never have a supplementary aperture, always have 3½ chambers in their final whorl, and typically have a high final-chamber suture separation, indicating a central (i.e., umbilical) aperture. Individuals in this cluster thus strongly resemble modern *G. bulloides*, except for their 'large' pores and cancellate wall texture similar to that of *T. primordius*. When the cluster analysis is repeated but with pore size excluded, individuals from Cluster 5 join the same clusters as almost all individuals from clusters 3 and 4, identified above to be *G. bulloides* (Supplementary Figure 5.3B).

We note the recent observation of two morphotypes of modern *G. bulloides*, differentiated by the degree of wall encrustation, which gives the appearance of differing pore size when viewed from the exterior wall surface (Osborne et al., 2016). Similar differences in porosity/pore size have been observed between other closely related and morphologically identical species/genotypes (Huber et al., 1997; Osborne et al., 2016; Vargas et al., 1999). However, these examples of 'cryptic speciation' that are differentiated solely by the nature of their wall nevertheless have the same fundamental wall texture (e.g., cancellate or *bulloides*-type). This contrasts with individuals in Cluster 5, which have a fundamentally different wall texture to *G. bulloides* suggesting that, rather than being an example of a cryptic species, individuals in cluster 5 are more appropriately placed in a different genus.

Individuals morphologically resembling '*G. praebulloides*' but with a cancellate wall were previously described in the late mid-Eocene, and named *Globoturborotalita* aff. *praebulloides* (Sexton et al., 2006b). These authors noted that the first appearance of these forms occurred in the same biozone as the first documented appearance of '*G. praebulloides'* (Bolli and Saunders, 1985). Meanwhile, the morphological similarity of '*G. praebulloides'* to early forms of

Globoturborotalita woodi in the Late Oligocene and Early Miocene was discussed by Chaproniere (1988), who noted that the range of morphological variability within both of these species is so large that wall texture is the only way to determine the species identity of many individuals. We therefore assign cluster 5 to *G. woodi*, and note that our results provide quantitative evidence that wall texture is indeed the only way of distinguishing Late Oligocene-Early Miocene forms of *G. woodi* from *G. bulloides*. The morphological similarity of these two species suggests a close evolutionary relationship; while a recent phylogenetic scheme suggested that they had not shared a common ancestor since the Palaeocene (Aze et al., 2011), which would make this a particularly striking example of homeomorphy, we note that the original description of *G. woodi* suggests that this species is in fact a descendant of '*G. praebulloides'* (Jenkins, 1960).

5.4.3 Stable isotope geochemistry

Having determined morphological distinctions among individuals, we next assess the stable isotope characteristics of each cluster (Figure 5.9), and thus the implications of our results for palaeoceanographic studies. Such investigation is complicated by the size-specific stable isotope offsets characteristic of many foraminiferal species (Ezard et al., 2015). While in the following discussion we restrict discussion of differences between clusters to individuals of similar size, we acknowledge that individuals in some clusters (e.g., Cluster 4) are almost always larger than individuals in other clusters (e.g., Cluster 3). Given the size of our dataset we do not attempt to produce inter-species calibrations, but instead use our analysis to highlight where the cluster differentiation we have performed is of most relevance to stable isotope measurements.

For $!^{13}C$, individuals assigned to *T. primordius* and *G. woodi* typically have much higher $!^{13}C$ (2.2‰ and 1.4‰, respectively, taking individuals in the 212-250 µm size fraction) than the two *G. bulloides* morphotypes and *G. obesa* (which together have an average $!^{13}C$ of 0.5‰ in the 212-250 µm size fraction). That *T. primordius* and *G. woodi* have higher $!^{13}C$ values than *G. obesa* is unsurprising, given that the former species were surface dwellers (Keller, 1985; Pearson et al., 2007, 1997; Pearson and Wade, 2009; Poore and Matthews, 1984) and the latter was a thermocline dweller (unpublished data, D. R. M. Stewart; see Aze et al., 2011). Both *G. bulloides* clusters have low $!^{13}C$ values relative to other species, despite this species being a surface dweller (Pearson et al., 1997). This suggests that Oligo-Miocene *G. bulloides* lacked symbionts, like their modern counterparts, contradicting interpretations of results from Trinidad (Pearson and Wade, 2009) that suggest Oligo-Miocene *G. bulloides* hosted symbionts. However, Greenop et al. (submitted) proposed that Oligo-Miocene *G. bulloides* had a number of geographically distinct symbiotic relationships; we thus propose that the North Atlantic was home to non-symbiotic forms of *G. bulloides*. Given that our analysis suggests that there is no morphological difference between *G.*

bulloides and *G. woodi* other than pore size, this isotopic offset highlights the importance of considering pore size when generating a record with either species. We note that there is no significant $\delta^{13}C$ offset between the two morphotypes of *G. bulloides* (clusters 3 and 4).

For $\delta^{18}O$, distinctions between clusters are less clear. The range of isotopic variability within clusters is sufficiently large (e.g., the $\delta^{18}O$ range of 2.5‰ within Cluster 4 in the 250-300 µm size fraction) that it is much greater than the magnitude of offsets between clusters. Again, when only individuals with similar size fractions are considered, there is no marked consistent difference between the two morphotypes of *G. bulloides*.

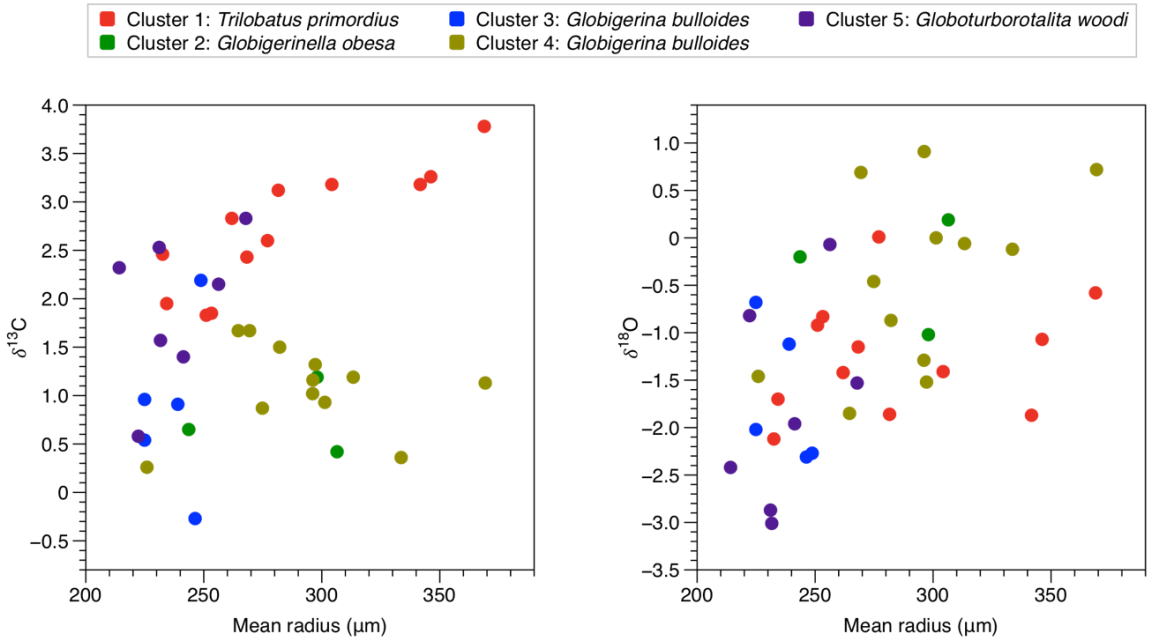

Figure 5.9 Single foraminiferal stable isotope measurements. Mean radius refers to the square root of the test area. Each data point represents a measurement on a single foraminifer. The colour of each data point is determined by the cluster assigned to that individual using the multivariate statistical clustering method.

5.4.4 Species classification of foraminifera: palaeontological vs. genetic approaches

The results in this chapter raise an important point about foraminiferal species classification. It is striking that the morphometric results indicate that species in different genera can only be distinguished from each other by a single feature; for example *Globigerina bulloides* and *Globoturborotalita woodi* are found to be distinguishable only by their differing wall textures (Supplementary Figure 5.3), despite being classified as members of different genera in all previous

literature. This separation is a result of the convention that wall texture is of first-order importance in foraminiferal morphospecies classification; standard morphospecies approaches dictate that while there may be variation in the exact size of pores within a genus (e.g., Bé, 1968), different wall textures necessitate placement of individuals in separate genera. However, paired visual- genetic investigation has revealed markedly different calcification rates (Osborne et al., 2016) and pore distributions (Morard et al., 2009) in foraminifera that are genetically very close, giving the visual impression of markedly different wall textures. We also note that morphometric approaches to taxonomy (Aze et al., 2011) have been found to be greatly at odds with taxonomic trees constructed from genetic information (Strotz and Allen, 2013). Bearing this in mind, that *G. bulloides* and *G. woodi* in this study are morphologically indistinguishable when wall texture is ignored therefore hints at a closer taxonomic relationship than taxonomic conventions would suggest, highlighting the caution that should be taken when treating extinct morphospecies using genetic species concepts used for extant organisms, and demonstrating a potential limitation of the fossil record for taxonomic studies.

5.5 Conclusions

Traditional descriptive approaches to taxonomy result in a subjective approach that is often not consistent between workers. Here, we have used quantitative morphometric measurements and a statistical clustering method to delineate and describe morphospecies in a repeatable, non- subjective way. Our analysis confirms that *G. primordius* and *G. obesa* are best classified as species separate to *G. bulloides*, but that *G. primordius* is so morphologically similar to *G. bulloides* that the presence of a supplementary aperture and cancellate wall texture are the only ways to distinguish it from *G. bulloides*. We suggest that only individuals with over 4 chambers in their final whorl are classified as *G. obesa*. We find that *G. bulloides* in the late Oligocene/early Miocene is best classified as two separate morphological groups, but given the subtleties of these differences in comparison to the range of variability within each group, we choose to assign these as morphotypes within a single *G. bulloides* species, rather than as separate morphospecies. Our analysis confirms that forms morphologically similar to *G. bulloides* but with a cancellate wall texture, as observed in previous studies, are best assigned to *G. woodi*, and are indeed morphologically indistinguishable from *G. bulloides* when wall texture is ignored. These observations highlight the critical importance of wall texture for accurate species identification, and should provoke future research into the extent to which morphospecies and genetic species concepts overlap. Our investigation of the stable isotope properties of individuals within each

cluster suggests that for $!^{18}O$, the range of variability between individuals in the same

cluster/species is so large that it outweighs offsets between clusters. However, for $\delta^{13}C$, this is not the case: we highlight the significant $\delta^{13}C$ offset between *G. bulloides* and *G. woodi*, despite their close morphological similarity, emphasizing the importance of consideration of small morphological differences when constructing stable isotope records.

5.6 Supplementary Figures

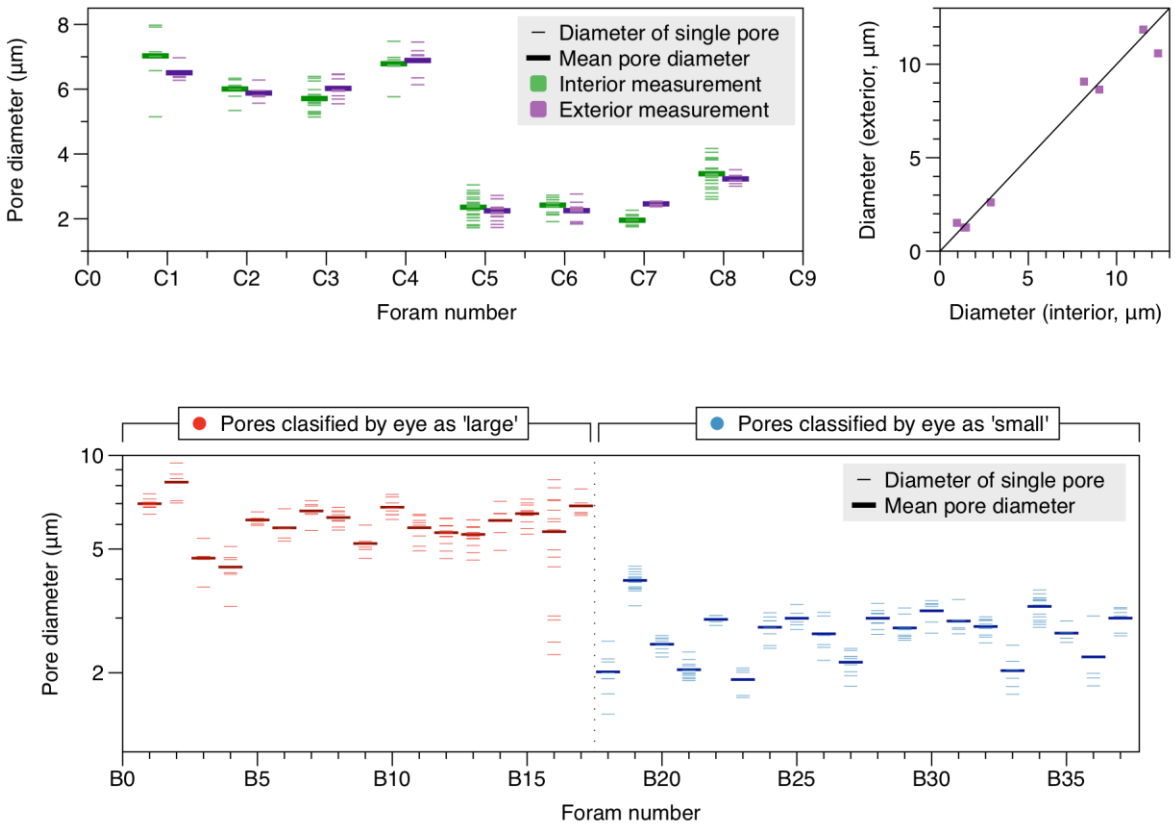

Supplementary Figure 5.1 Pore size measurements. **Top left:** Comparison of measurements made on SEM images of different parts of the same foraminiferal chamber when measurements are made from the interior (green) or exterior (purple) surface of the shell. Thin horizontal lines represent areas of single pores; thick horizontal lines represent the mean area. **Top right:** Cross-plot of mean pore area as measured from the interior and exterior of the shell. **Bottom:** Measurements made on SEM images of the exterior of shells of single foraminifera (each identified by a different 'foram number' on the x-axis). Thin horizontal lines represent areas of single pores; thick horizontal lines represent the mean area. Data presented for individuals estimated by eye with a light microscope to have 'large' (red) and 'small' (blue) pores.

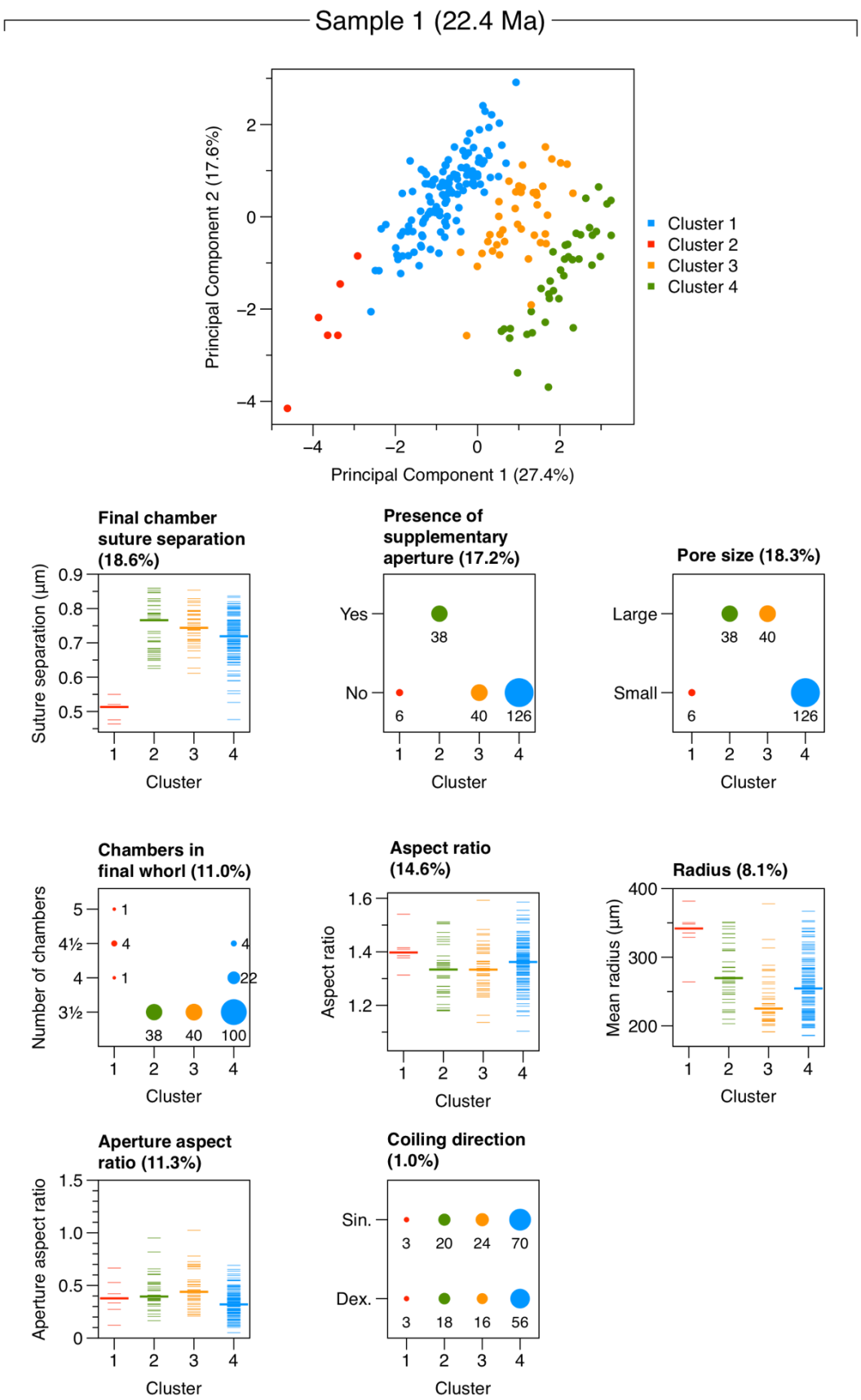

Supplementary Figure 5.2 (figure spans both pages) Results of clustering analysis when samples analyzed independently. See caption for Figure 5.6; the only difference is that here, the two samples are separated and analyzed independently, whereas they are combined and analyzed as a single dataset in Figure 5.6.

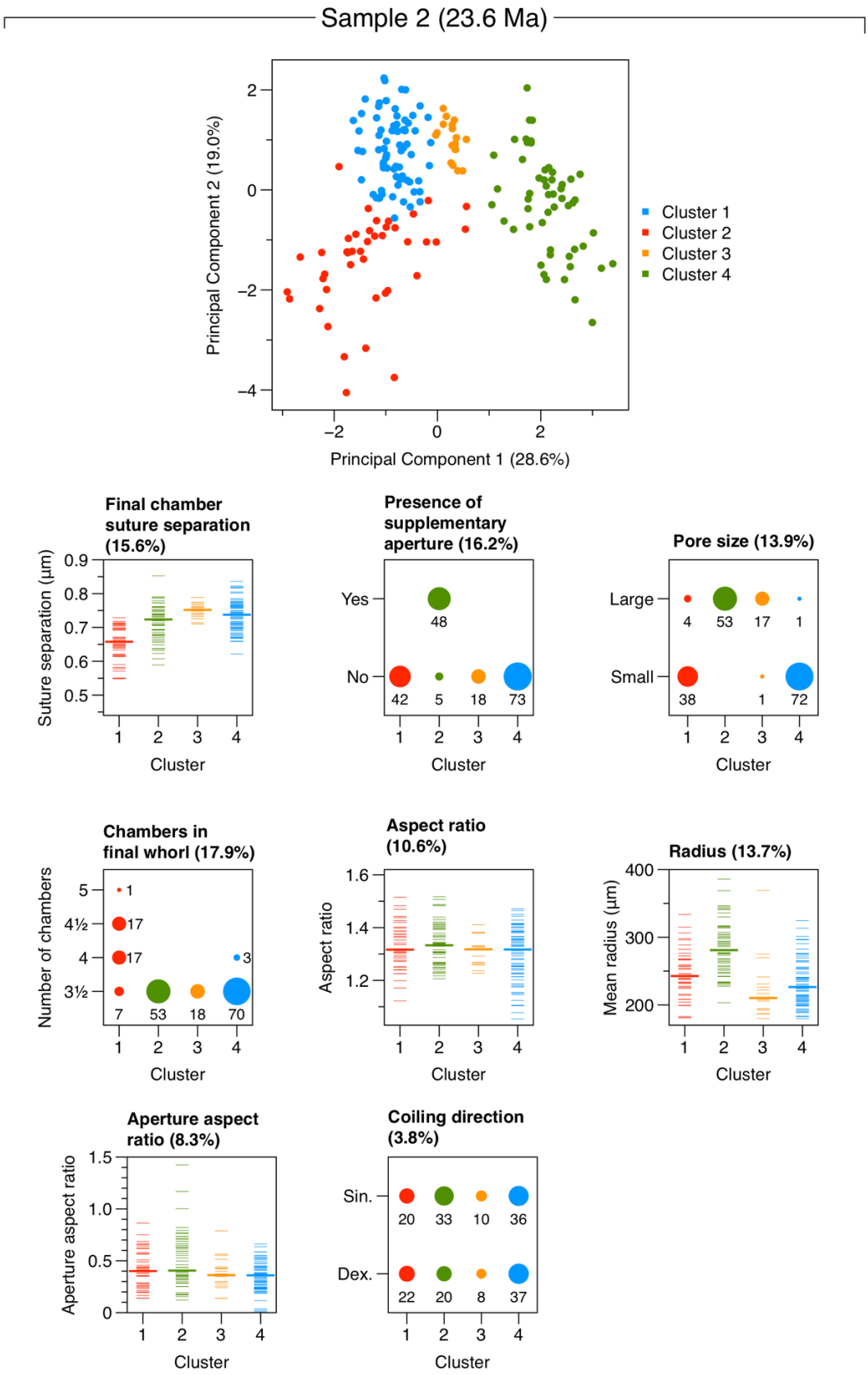
Sample 2 (23.6 Ma)
Principal Component 2 (19.0%)
Principal Component 1 (28.6%)
Cluster 1
Cluster 2
Cluster 3
Cluster 4
Final chamber suture separation (15.6%)
Suture separation (µm)
Presence of supplementary aperture (16.2%)
Yes
No
Pore size (13.9%)
Large
Small
Chambers in final whorl (17.9%)
Number of chambers
Aspect ratio (10.6%)
Aspect ratio
Radius (13.7%)
Mean radius (µm)
Aperture aspect ratio (8.3%)
Aperture aspect ratio
Coiling direction (3.8%)
Sin.
Dex.
Cluster

◐ Cluster number when all parameters included
◑ Cluster number when presence/absence of supplementary aperture removed from cluster analysis
N.B. Position of data points based on principal component analysis with all parameters included

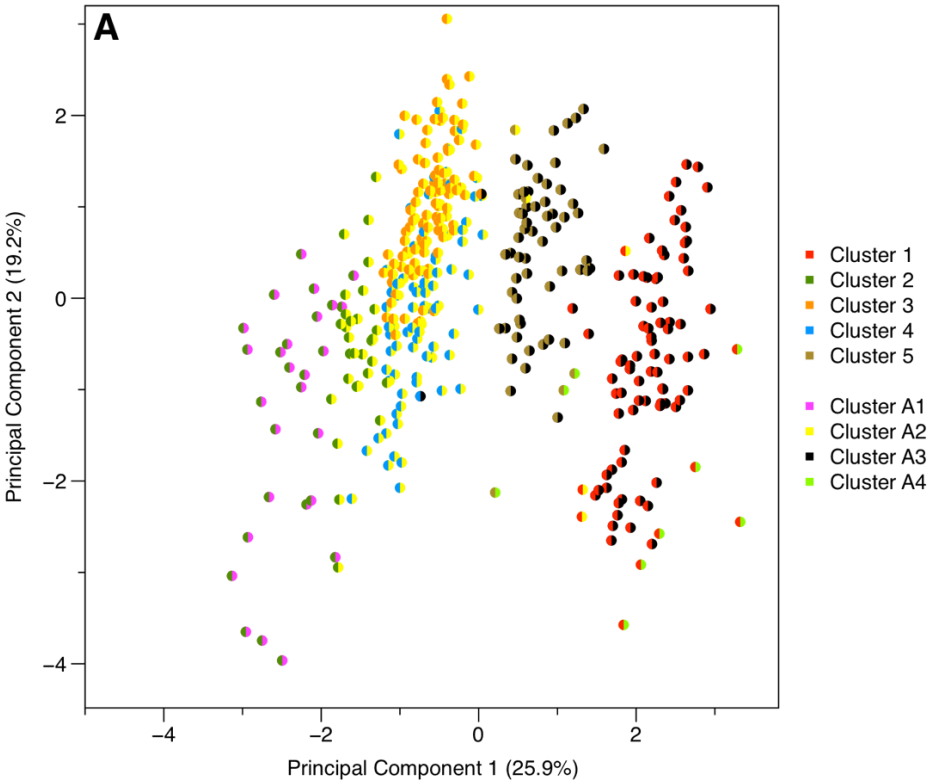

◐ Cluster number when all parameters included
◑ Cluster number when pore size removed from cluster analysis
N.B. Position of data points based on principal component analysis with all parameters included

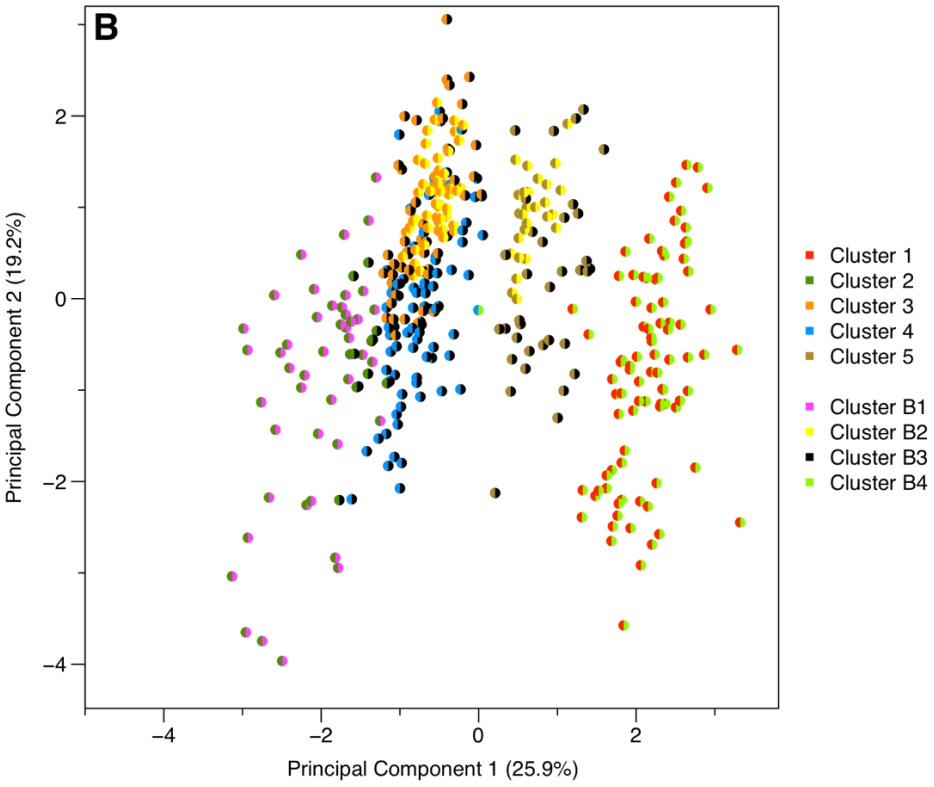

Supplementary Figure 5.3 (opposite) Results of clustering analysis when individual parameters are removed from the analysis. See caption for top panel of Figure 5.6. Each circle represents a single foraminifer. The colour of the left half of the circle indicates the cluster in which the individual is placed when the cluster analysis includes all parameters; the right half of the circle indicates the cluster in which the individual is placed when a single parameter is removed from the cluster analysis. In **A**, the presence or absence of a supplementary aperture has been removed (with new clusters named A1-A4); in **B**, pore size has been removed (with new clusters named B1-B4). The position of each data point is based on a principal component analysis incorporating all measured parameters.

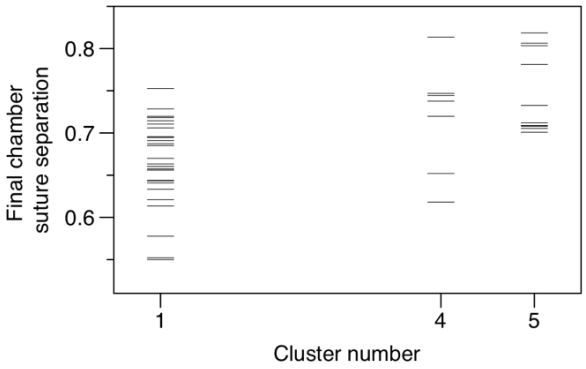

Supplementary Figure 5.4 Final-chamber suture separation distance for individuals with 4 chambers in their final whorl. Each horizontal line represents a single foraminifer.

Chapter 6 Conclusions

6.1 Thesis summary

The research documented in this thesis uses material recently drilled from the Newfoundland Ridge to shed new light on the Oligocene-Miocene Transition (OMT), 23 Ma. The extent of global climatic change over the OMT was staggering, with previous studies estimating that the ~1‰ benthic !^{18}O excursion (Beddow et al., 2016; Billups et al., 2002; Liebrand et al., 2011; Pälike et al., 2006a; Zachos et al., 2001b) was associated with growth and subsequent melting of a volume of ice at least half, or perhaps equal to, that of the modern Antarctic ice sheets (Gasson et al., 2016; Liebrand et al., 2011); associated sea level fall and rise of tens of metres (Liebrand et al., 2011; Pekar et al., 2002; Pekar and DeConto, 2006); and bottom water cooling of ~3°C (Mawbey and Lear, 2013).

Climate records on orbital and sub-orbital timescales have been key to our understanding of many major climatic events spanning the Cenozoic (Coxall et al., 2005; Denton et al., 2010; Zachos et al., 2001b), but previous study of the OMT has been restricted by the low number of seafloor records of this resolution. In particular, there is no previously published record of sea-surface conditions on these timescales, hindering understanding of the relationship between existing deep water records and processes at the sea surface. There is also a complete absence of OMT records of orbital or finer resolution from the North Atlantic, despite this region's critical role in ocean circulation since the Eocene-Oligocene Transition (Abelson and Erez, 2017; Davies et al., 2001). The recovery of material from the Newfoundland Ridge by IODP Expedition 342, which drilled highly expanded sediments containing well-preserved planktic and benthic foraminifera (Expedition 342 scientists, 2012), provides the first opportunity to overcome these gaps in our knowledge of the OMT. Investigation of this material is the focus of this thesis.

In Chapter 3, planktic foraminiferal and XRF core scanning data are used to show that late Oligocene climate underwent cyclical variability on sub-orbital timescales. Despite climate variability on these timescales being one of the key features of Pleistocene climate (Dansgaard et al., 1993; Heinrich, 1988), previously published marine records on sub-orbital timescales extend back only as far as the Pliocene. The results presented in Chapter 3 imply that sub-orbital variability of the Atlantic Meridional Overturning Circulation (AMOC) is a persistent feature of Earth's climate, rather than a recent development. In Chapter 4, an orbital-resolution planktic foraminiferal stable isotope record over the OMT is compared with a benthic foraminiferal record generated from the same samples to show that in the NW Atlantic, temperature changes at the sea surface led changes in benthic temperature and global ice volume by up to tens of kyrs. This study is the first to identify this asynchronous planktic-benthic behaviour over the OMT. Finally, in Chapter 5, the accuracy of planktic foraminiferal proxies commonly used in studies of Oligo-

Miocene climate is assessed and improved by use of a multivariate statistical clustering method. Clustering results of morphological measurements are compared with single-foraminiferal stable isotope measurements, with the aim of assessing the implications of the identified taxonomic differences on palaeoceanographic records. It is shown that several morphospecies with very similar morphologies have markedly different stable isotope behaviour. Together with a variety of other factors, taxonomic error contributes to uncertainty in foraminiferal stable isotope measurements (Fraass and Lowery, 2017); this study provides quantitatively based guidance for future studies of Oligo-Miocene palaeoclimate in which records are generated using planktic foraminifera.

While each of the three chapters in this thesis addresses a different aspect of the OMT, the results also build upon each other. For example, the refinements to foraminiferal taxonomy presented in Chapter 5 provide a robust framework for the foraminiferal picking in chapters 3 and 4, ensuring that the results in these chapters are not affected by bias introduced by incorrect taxonomic identification. As another example, given that high-frequency climate 'noise' has been suggested to supplement astronomical forcing and act as a trigger for major climatic events in the Pleistocene (Vázquez Riveiros et al., 2013), the discovery of climate instability in the run-up to the OMT (Chapter 3) suggests that similar interactions could have taken place over the OMT, providing additional context to the results presented in Chapter 4.

6.2 Future work

The results presented in Chapter 3 demonstrate that AMOC variability on sub-orbital timescales occurs over a wider range of climate states than previously observed. This range could be better constrained by repeating the approach taken in Chapter 3 across additional intervals reflecting different global climate states. Sedimentation rates reach ~10 cm/kyr in other such intervals spanning the OMT at Site U1405 (Expedition 342 scientists, 2012), providing suitable material for future studies. Elucidating whether sub-orbital AMOC variability during peak OMT glacial conditions is weaker or stronger than that pre-OMT may help better establish the cause of this variability. Study of intervals with very high foraminiferal abundance would also enable generation of Mg/Ca temperature proxy records, which would facilitate deconvolution of the $!^{18}O$ signal into temperature and $!^{18}O_{sw}$ components.

IODP Expedition 342 was unusual for an expedition aiming to drill material spanning the Cenozoic in that it targeted drift sediments. While millennial-centennial timescale records from the Plio-Pleistocene are frequently generated on drift sediments, expeditions to recover material from earlier in the Cenozoic instead typically target pelagic sediments because of their often-continuous sedimentary records over millions (or sometimes tens of millions) of years. The results presented in

Chapter 3 demonstrate the value of drilling drift sediments for studies of the pre-Plio-Pleistocene. Drilling of drift sediments at sites elsewhere in the world could help determine to what extent the results presented in Chapter 3 are a local, rather than global, signal, although we note that current dating techniques would preclude cycle-to-cycle matching.

The results presented in Chapter 4 show that cooling in the surface North Atlantic over the OMT preceded global deep water cooling by tens of kyrs; planktic !^{18}O and !^{13}C also responded to orbital forcing several kyrs faster than their benthic counterparts, as revealed by phase analysis. However, it remains unclear whether these planktic leads on kyr and tens-of-kyr timescales had similar causal mechanisms. Some potential mechanisms that explain leads of several kyrs, such as a bipolar seesaw (Broecker, 1998), cannot explain leads of tens of kyrs; meanwhile some potential mechanisms that explain leads of tens of kyrs, for example control of inter-hemispheric heat transport by Antarctic sea ice extent (Ferrari et al., 2014; Pekar and DeConto, 2006), and thus by the extent of Antarctic glacial cover, would be unlikely to explain leads and lags over the shorter orbital timescales outside intervals of major glaciation. Some of the mechanisms proposed in Chapter 4 could be supported or ruled out by determining whether the tens-of-kyr lead is seen only during the OMT, or also during other smaller-magnitude episodes of Antarctic glacial expansion and retreat in the Oligo-Miocene. This could be achieved by extension of the record presented in Chapter 4.

The results presented in Chapter 5 demonstrate the first application of a morphology-based statistical clustering method to the species classification of foraminifera from the Oligo-Miocene, following the previous application of this method to Eocene foraminifera (Pearson and Ezard, 2014). Repetition of the approach presented in Chapter 5 on additional samples from the Oligo- Miocene would help better elucidate the evolutionary relationships between species in *Globigerina* and similar genera, following the approach of the Eocene study. While the automated method employed in Chapter 5 removes most of the subjectivity typically associated with taxonomic studies, the requirement to orient individuals by eye means that the method still retains a small degree of subjectivity. Follow-up work from this study could adopt a three-dimensional imaging technique to overcome this issue, which would also enable rapid measurement of a plethora of additional morphological characteristics to further constrain nuanced morphological differences within and between morphospecies (Hsiang et al., 2016; Speijer et al., 2008).

Appendix

All raw data presented in this thesis are provided in a digital format. This appendix consists of the following files:

- Data files for Chapter 3 (*Sub-orbital climate variability in the Oligocene North Atlantic Ocean*):
    - *"01- Revised splice RS1 U1405"*: The splice table for the revised splice ("RS1") used for this chapter
    - *"02- Age model U1405"*: The precession-tuned age model used in this chapter
    - *"03- XRF 1 mm data U1405"*: The 1 mm resolution XRF dataset used in this chapter; note that this file includes data (for additional elements) not described in the chapter but placed in this file for reference
    - *"04- Coulometry XRF calibration U1405"*: Coulometry %$CaCO_3$ data used to calibrate XRF-measured Ca counts to sediment %$CaCO_3$
    - *"05- Stable isotopes and % bulloides U1405"*: Stable isotope data and % *G. bulloides* (as a proportion of all planktic foraminifera) data
- Data files for Chapter 4 (*Decoupling of surface and deep North Atlantic waters over the Oligocene-Miocene Transition*):
    - *"06- Stable isotope dataset U1406"*: Stable isotope measurements on *G. bulloides* and *G. primordius*; note that this file includes additional data points collected as part of the work in this chapter, but not presented in the chapter results section because of their low resolution
    - "*07- Foraminifera size fraction stable isotope comparison U1406*": stable isotope analyses of different size fractions of G. bulloides
- Data files for Chapter 5 (*Taxonomy of Oligo-Miocene Globigerina bulloides and related forms: refinement using a multivariate statistical clustering method, and investigation of stable isotope variability*):
    - *"08- Morphometric measurement repeatability"*: Data obtained from three repeat measurements of the same foraminifera
    - *"09- Inner vs outer pore size measurement"*: Data comparing measurement of pore size from the interior and exterior of the same foraminifera
    - *"10- Verification of pore size estimation"*: Pore size measurements used to test visual estimation of pore size
    - *"11- Complete morphometric dataset"*: The primary dataset considered in this chapter, including all raw data and clusters assigned to each individual
    - *"12- Single foraminiferal stable isotope analyses"*: Results of single foraminiferal stable isotope analyses of selected individuals

List of References

Abelson, M., Erez, J., 2017. The onset of modern-like Atlantic meridional overturning circulation at the Eocene-Oligocene transition: Evidence, causes, and possible implications for global cooling. Geochem. Geophys. Geosyst. 18, 2177–2199. https://doi.org/10.1002/2017GC006826

Adams, D.C., Rohlf, F.J., Slice, D.E., 2013. A field comes of age: geometric morphometrics in the 21st century. Hystrix, the Italian Journal of Mammalogy 24, 7–14. https://doi.org/10.4404/hystrix-24.1-6283

Anderson, R.Y., 1982. A long geoclimatic record from the Permian. J. Geophys. Res. 87, 7285–7294. https://doi.org/10.1029/JC087iC09p07285

André, A., Weiner, A., Quillévéré, F., Aurahs, R., Morard, R., Douady, C.J., de Garidel-Thoron, T., Escarguel, G., de Vargas, C., Kucera, M., 2012. The cryptic and the apparent reversed: lack of genetic differentiation within the morphologically diverse plexus of the planktonic foraminifer Globigerinoides sacculifer. Paleobiology 39, 21–39. https://doi.org/10.1666/0094-8373-39.1.21

Annan, J.D., Hargreaves, J.C., 2013. A new global reconstruction of temperature changes at the Last Glacial Maximum. Clim. Past 9, 367–376. https://doi.org/10.5194/cp-9-367-2013

Askin, R.A., Raine, J.I., 2000. Oligocene and Early Miocene terrestrial palynology of the Cape Roberts Drillhole CRP-2/2A, Victoria Land Basin, Antarctica. Terra Antartica 7, 493–501.

Aurahs, R., Treis, Y., Darling, K., Kucera, M., 2011. A revised taxonomic and phylogenetic concept for the planktonic foraminifer species Globigerinoides ruber based on molecular and morphometric evidence. Marine Micropaleontology 79, 1–14. https://doi.org/10.1016/j.marmicro.2010.12.001

Aze, T., Ezard, T.H.G., Purvis, A., Coxall, H.K., Stewart, D.R.M., Wade, B.S., Pearson, P.N., 2011. A phylogeny of Cenozoic macroperforate planktonic foraminifera from fossil data. Biological Reviews 86, 900–927. https://doi.org/10.1111/j.1469-185X.2011.00178.x

Bahr, A., Jiménez-Espejo, F.J., Kolasinac, N., Grunert, P., Hernández-Molina, F.J., Röhl, U., Voelker, A.H.L., Escutia, C., Stow, D.A.V., Hodell, D., Alvarez-Zarikian, C.A., 2014. Deciphering bottom current velocity and paleoclimate signals from contourite deposits in the Gulf of Cádiz during the last 140 kyr: An inorganic geochemical approach. Geochem. Geophys. Geosyst. 15, 3145–3160. https://doi.org/10.1002/2014GC005356

Bahr, A., Lamy, F., Arz, H., Kuhlmann, H., Wefer, G., 2005. Late glacial to Holocene climate and sedimentation history in the NW Black Sea. Marine Geology 214, 309–322. https://doi.org/10.1016/j.margeo.2004.11.013

Bailey, I., Hole, G.M., Foster, G.L., Wilson, P.A., Storey, C.D., Trueman, C.N., Raymo, M.E., 2013. An alternative suggestion for the Pliocene onset of major northern hemisphere glaciation based on the geochemical provenance of North Atlantic Ocean ice-rafted debris. Quaternary Science Reviews 75, 181–194. https://doi.org/10.1016/j.quascirev.2013.06.004

Barker, S., Chen, J., Gong, X., Jonkers, L., Knorr, G., Thornalley, D., 2015. Icebergs not the trigger for North Atlantic cold events. Nature 520, 333–336. https://doi.org/10.1038/nature14330

Barron, E.J., Peterson, W.H., 1991. The Cenozoic ocean circulation based on ocean General Circulation Model results. Palaeogeography, Palaeoclimatology, Palaeoecology, The Oceans of the Paleogene 83, 1–28. https://doi.org/10.1016/0031-0182(91)90073-Z

Bartoli, G., Sarnthein, M., Weinelt, M., 2006. Late Pliocene millennial-scale climate variability in the northern North Atlantic prior to and after the onset of Northern Hemisphere glaciation. Paleoceanography 21. https://doi.org/10.1029/2005PA001185

Bé, A.W.H., 1968. Shell Porosity of Recent Planktonic Foraminifera as a Climatic Index. Science 161, 881–884. https://doi.org/10.1126/science.161.3844.881

Bé, A.W.H., Donk, J.V., 1971. Oxygen-18 Studies of Recent Planktonic Foraminifera. Science 173, 167–169. https://doi.org/10.1126/science.173.3992.167

Bé, A.W.H., Hemleben, C., Anderson, O.R., Spindler, M., Hacunda, J., Tuntivate-Choy, S., 1977. Laboratory and Field Observations of Living Planktonic Foraminifera. Micropaleontology 23, 155–179. https://doi.org/10.2307/1485330

Beddow, H., 2016. Orbital forcing and climate response: astronomically-tuned age models and stable isotope records for the Oligocene-Miocene (PhD thesis).

Beddow, H.M., Liebrand, D., Sluijs, A., Wade, B.S., Lourens, L.J., 2016. Global change across the Oligocene-Miocene transition: High-resolution stable isotope records from IODP Site U1334 (equatorial Pacific Ocean). Paleoceanography 31, 2015PA002820. https://doi.org/10.1002/2015PA002820

Beerling, D.J., Royer, D.L., 2011. Convergent Cenozoic CO2 history. Nature Geosci 4, 418–420. https://doi.org/10.1038/ngeo1186

Bemis, B.E., Spero, H.J., Bijma, J., Lea, D.W., 1998. Reevaluation of the oxygen isotopic composition of planktonic foraminifera: Experimental results and revised paleotemperature equations. Paleoceanography 13, 150–160. https://doi.org/10.1029/98PA00070

Bender, M.L., 2013. Paleoclimate. Princeton University Press.

Berger, W., Killingley, J., Vincent, E., 1978. Sable isotopes in deep-sea carbonates-box core erdc-92, west equatorial pacific. Oceanologica Acta 1, 203–216.

Berger, W.H., 1971. Sedimentation of planktonic foraminifera. Marine Geology 11, 325–358. https://doi.org/10.1016/0025-3227(71)90035-1

Bernard, T., Steer, P., Gallagher, K., Szulc, A., Whitham, A., Johnson, C., 2016. Evidence for Eocene–Oligocene glaciation in the landscape of the East Greenland margin. Geology 44, 895–898. https://doi.org/10.1130/G38248.1

Bigg, G.R., Rohling, E.J., 2000. An oxygen isotope data set for marine waters. J. Geophys. Res. 105, 8527–8535. https://doi.org/10.1029/2000JC900005

Billups, K., Channell, J.E.T., Zachos, J., 2002. Late Oligocene to early Miocene geochronology and paleoceanography from the subantarctic South Atlantic. Paleoceanography 17, 4–1–4–11. https://doi.org/10.1029/2000PA000568

Billups, K., Pälike, H., Channell, J.E.T., Zachos, J.C., Shackleton, N.J., 2004. Astronomic calibration of the late Oligocene through early Miocene geomagnetic polarity time scale. Earth and Planetary Science Letters 224, 33–44. https://doi.org/10.1016/j.epsl.2004.05.004

Billups, K., Spero, H.J., 1996. Reconstructing the stable isotope geochemistry and paleotemperatures of the equatorial Atlantic during the last 150,000 years: Results from individual foraminifera. Paleoceanography 11, 217–238. https://doi.org/10.1029/95PA03773

Billups, K., Spero, H.J., 1995. Relationship between shell size, thickness and stable isotopes in individual planktonic foraminifera from two equatorial Atlantic cores. Oceanographic Literature Review 10, 854.

Birch, H., Coxall, H.K., Pearson, P.N., Kroon, D., O'Regan, M., 2013. Planktonic foraminifera stable isotopes and water column structure: Disentangling ecological signals. Marine Micropaleontology 101, 127–145. https://doi.org/10.1016/j.marmicro.2013.02.002

Birner, B., Hodell, D.A., Tzedakis, P.C., Skinner, L.C., 2016. Similar millennial climate variability on the Iberian margin during two early Pleistocene glacials and MIS 3. Paleoceanography 31, 2015PA002868. https://doi.org/10.1002/2015PA002868

Biscaye, P.E., Kolla, V., Turekian, K.K., 1976. Distribution of calcium carbonate in surface sediments of the Atlantic Ocean. J. Geophys. Res. 81, 2595–2603. https://doi.org/10.1029/JC081i015p02595

Bissett, A., Neu, T.R., Beer, D. de, 2011. Dissolution of Calcite in the Twilight Zone: Bacterial Control of Dissolution of Sinking Planktonic Carbonates Is Unlikely. PLOS ONE 6, e26404. https://doi.org/10.1371/journal.pone.0026404

Blow, H., 1959. Age correlation and biostratigraphy of the Upper Tocuyo (San Lorenzo) and Pozon formations, eastern Falcon, Venezuela. Bulletin of American Paleontology 39, 67–252.

Blow, W., 1979. The Cenozoic Globigerina. Leideon, Netherlands 1413.

Blow, W., Banner, F., 1962. The mid-Tertiary (upper Eocene to Aquitanian) globigerinaceae. Cambridge University Press.

Bolli, H., Saunders, J., 1985. Oligocene to Holocene low latitude planktic foraminifera, in: B., 1985. Oligocene to Holocene Low Latitude Planktic Foraminifera. Cambridge University Press, pp. 155–262.

Bolliet, T., Holbourn, A., Kuhnt, W., Laj, C., Kissel, C., Beaufort, L., Kienast, M., Andersen, N., Garbe-Schönberg, D., 2011. Mindanao Dome variability over the last 160 kyr: Episodic

glacial cooling of the West Pacific Warm Pool. Paleoceanography 26, PA1208. https://doi.org/10.1029/2010PA001966

Bolton, C.T., Wilson, P.A., Bailey, I., Friedrich, O., Beer, C.J., Becker, J., Baranwal, S., Schiebel, R., 2010. Millennial-scale climate variability in the subpolar North Atlantic Ocean during the late Pliocene. Paleoceanography 25, PA4218. https://doi.org/10.1029/2010PA001951

Bond, G., Kromer, B., Beer, J., Muscheler, R., Evans, M.N., Showers, W., Hoffmann, S., Lotti-Bond, R., Hajdas, I., Bonani, G., 2001. Persistent Solar Influence on North Atlantic Climate During the Holocene. Science 294, 2130–2136. https://doi.org/10.1126/science.1065680

Bond, G., Showers, W., Cheseby, M., Lotti, R., Almasi, P., deMenocal, P., Priore, P., Cullen, H., Hajdas, I., Bonani, G., 1997. A Pervasive Millennial-Scale Cycle in North Atlantic Holocene and Glacial Climates. Science 278, 1257–1266. https://doi.org/10.1126/science.278.5341.1257

Bout-Roumazeilles, V., Debrabant, P., Labeyrie, L., Chamley, H., Cortijo, E., 1997. Latitudinal control of astronomical forcing parameters on the high-resolution clay Mineral distribution in the 45°–60° N range in the North Atlantic Ocean during the past 300,000 years. Paleoceanography 12, 671–686. https://doi.org/10.1029/97PA00118

Bouvier-Soumagnac, Y., Duplessy, J.-C., 1985. Carbon and oxygen isotopic composition of planktonic foraminifera from laboratory culture, plankton tows and Recent sediment; implications for the reconstruction of paleoclimatic conditions and of the global carbon cycle. Journal of Foraminiferal Research 15, 302–320.

Boyle, E.A., 1988. The role of vertical chemical fractionation in controlling late Quaternary atmospheric carbon dioxide. J. Geophys. Res. 93, 15701–15714. https://doi.org/10.1029/JC093iC12p15701

Boyle, P.R., Romans, B.W., Tucholke, B.E., Norris, R.D., Swift, S.A., Sexton, P.F., 2016. Cenozoic North Atlantic deep circulation history recorded in contourite drifts, offshore Newfoundland, Canada. Marine Geology. https://doi.org/10.1016/j.margeo.2016.12.014

Braun, H., Christl, M., Rahmstorf, S., Ganopolski, A., Mangini, A., Kubatzki, C., Roth, K., Kromer, B., 2005. Possible solar origin of the 1,470-year glacial climate cycle demonstrated in a coupled model. Nature 438, 208–211. https://doi.org/10.1038/nature04121

Brijker, J.M., Jung, S.J.A., Ganssen, G.M., Bickert, T., Kroon, D., 2007. ENSO related decadal scale climate variability from the Indo-Pacific Warm Pool. Earth and Planetary Science Letters 253, 67–82. https://doi.org/10.1016/j.epsl.2006.10.017

Broecker, W.S., 1998. Paleocean circulation during the Last Deglaciation: A bipolar seesaw? Paleoceanography 13, 119–121. https://doi.org/10.1029/97PA03707

Brombacher, A., Wilson, P.A., Ezard, T.H.G., 2017. Calibration of the repeatability of foraminiferal test size and shape measures with recommendations for future use. Marine Micropaleontology. https://doi.org/10.1016/j.marmicro.2017.05.003

Brummer, G., Kroon, D., 1988. Genetically controlled planktonic foraminiferal coiling ratios as tracers of past ocean dynamics, in: Planktonic Foraminifers as Tracers of Ocean-Climate History. Free University Press, Amsterdam, pp. 293–298.

Caromel, A.G.M., Schmidt, D.N., Phillips, J.C., Rayfield, E.J., 2014. Hydrodynamic constraints on the evolution and ecology of planktic foraminifera. Marine Micropaleontology 106, 69–78. https://doi.org/10.1016/j.marmicro.2014.01.002

Chapman, M.R., Shackleton, N.J., 2000. Evidence of 550-year and 1000-year cyclicities in North Atlantic circulation patterns during the Holocene. The Holocene 10, 287–291. https://doi.org/10.1191/095968300671253196

Chaproniere, G.C.H., 1988. Globigerina woodi from the late Oligocene and early Miocene of southeastern Australia. Journal of Foraminiferal Research 18, 124–129. https://doi.org/10.2113/gsjfr.18.2.124

Clark, P.U., Pisias, N.G., Stocker, T.F., Weaver, A.J., 2002. The role of the thermohaline circulation in abrupt climate change. Nature 415, 863–869. https://doi.org/10.1038/415863a

Constandache, M., Yerly, F., Spezzaferri, S., 2013. Internal pore measurements on macroperforate planktonic Foraminifera as an alternative morphometric approach. Swiss J Geosci 106, 179–186. https://doi.org/10.1007/s00015-013-0134-8

Coplen, T.B., 2009. Reporting of stable hydrogen, carbon, and oxygen isotopic abundances (Technical Report). Pure and Applied Chemistry 66, 273–276. https://doi.org/10.1351/pac199466020273

Coxall, H.K., Wilson, P.A., 2011. Early Oligocene glaciation and productivity in the eastern equatorial Pacific: Insights into global carbon cycling. Paleoceanography 26. https://doi.org/10.1029/2010PA002021

Coxall, H.K., Wilson, P.A., Pälike, H., Lear, C.H., Backman, J., 2005. Rapid stepwise onset of Antarctic glaciation and deeper calcite compensation in the Pacific Ocean. Nature 433, 53–57. https://doi.org/10.1038/nature03135

Dansgaard, W., Johnsen, S.J., Clausen, H.B., Dahl-Jensen, D., Gundestrup, N.S., Hammer, C.U., Hvidberg, C.S., Steffensen, J.P., Sveinbjörnsdottir, A.E., Jouzel, J., Bond, G., 1993. Evidence for general instability of past climate from a 250-kyr ice-core record. Nature 364, 218–220. https://doi.org/10.1038/364218a0

Darby, D.A., 2014. Ephemeral formation of perennial sea ice in the Arctic Ocean during the middle Eocene. Nature Geosci 7, 210–213. https://doi.org/10.1038/ngeo2068

Darby, D.A., 2008. Arctic perennial ice cover over the last 14 million years. Paleoceanography 23, PA1S07. https://doi.org/10.1029/2007PA001479

Darby, D.A., Ortiz, J.D., Grosch, C.E., Lund, S.P., 2012. 1,500-year cycle in the Arctic Oscillation identified in Holocene Arctic sea-ice drift. Nature Geosci 5, 897–900. https://doi.org/10.1038/ngeo1629

Darling, K.F., Kucera, M., Kroon, D., Wade, C.M., 2006. A resolution for the coiling direction paradox in Neogloboquadrina pachyderma. Paleoceanography 21, PA2011. https://doi.org/10.1029/2005PA001189

Darling, K.F., Kucera, M., Wade, C.M., von Langen, P., Pak, D., 2003. Seasonal distribution of genetic types of planktonic foraminifer morphospecies in the Santa Barbara Channel and its paleoceanographic implications. Paleoceanography 18, 1032. https://doi.org/10.1029/2001PA000723

Darling, K.F., Wade, C.M., 2008. The genetic diversity of planktic foraminifera and the global distribution of ribosomal RNA genotypes. Marine Micropaleontology 67, 216–238. https://doi.org/10.1016/j.marmicro.2008.01.009

Davies, R., Cartwright, J., Pike, J., Line, C., 2001. Early Oligocene initiation of North Atlantic Deep Water formation. Nature 410, 917–920. https://doi.org/10.1038/35073551

de Villiers, S., 2005. Foraminiferal shell-weight evidence for sedimentary calcite dissolution above the lysocline. Deep Sea Research Part I: Oceanographic Research Papers 52, 671–680. https://doi.org/10.1016/j.dsr.2004.11.014

de Winter, N.J., Zeeden, C., Hilgen, F.J., 2014. Low-latitude climate variability in the Heinrich frequency band of the Late Cretaceous greenhouse world. Clim. Past 10, 1001–1015. https://doi.org/10.5194/cp-10-1001-2014

Debret, M., Bout-Roumazeilles, V., Grousset, F., Desmet, M., McManus, J.F., Massei, N., Sebag, D., Petit, J.-R., Copard, Y., Trentesaux, A., 2007. The origin of the 1500-year climate cycles in Holocene North-Atlantic records. Clim. Past 3, 569–575. https://doi.org/10.5194/cp-3-569-2007

DeConto, R., Pollard, D., Harwood, D., 2007. Sea ice feedback and Cenozoic evolution of Antarctic climate and ice sheets. Paleoceanography 22, PA3214. https://doi.org/10.1029/2006PA001350

DeConto, R.M., Pollard, D., 2003. Rapid Cenozoic glaciation of Antarctica induced by declining atmospheric CO2. Nature 421, 245–249. https://doi.org/10.1038/nature01290

DeConto, R.M., Pollard, D., Wilson, P.A., Pälike, H., Lear, C.H., Pagani, M., 2008. Thresholds for Cenozoic bipolar glaciation. Nature 455, 652–656. https://doi.org/10.1038/nature07337

Denton, G.H., Anderson, R.F., Toggweiler, J.R., Edwards, R.L., Schaefer, J.M., Putnam, A.E., 2010. The Last Glacial Termination. Science 328, 1652–1656. https://doi.org/10.1126/science.1184119

Dickson, R.R., Brown, J., 1994. The production of North Atlantic Deep Water: sources, rates, and pathways. Journal of Geophysical Research: Oceans 99, 12319–12341.

Diester-Haass, L., Billups, K., Emeis, K., 2011. Enhanced paleoproductivity across the Oligocene/Miocene boundary as evidenced by benthic foraminiferal accumulation rates.

Palaeogeography, Palaeoclimatology, Palaeoecology 302, 464–473. https://doi.org/10.1016/j.palaeo.2011.02.006

Dima, M., Lohmann, G., 2009. Conceptual model for millennial climate variability: a possible combined solar-thermohaline circulation origin for the ~1,500-year cycle. Clim Dyn 32, 301–311. https://doi.org/10.1007/s00382-008-0471-x

Dinno, A., 2009. Exploring the Sensitivity of Horn's Parallel Analysis to the Distributional Form of Random Data. Multivariate Behavioral Research 44, 362–388. https://doi.org/10.1080/00273170902938969

Dittert, N., Henrich, R., 2000. Carbonate dissolution in the South Atlantic Ocean: evidence from ultrastructure breakdown in Globigerina bulloides. Deep Sea Research Part I: Oceanographic Research Papers 47, 603–620. https://doi.org/10.1016/S0967-0637(99)00069-2

Dobzhansky, T., Dobzhansky, T.G., 1937. Genetics and the Origin of Species. Columbia University Press.

Draut, A.E., Raymo, M.E., McManus, J.F., Oppo, D.W., 2003. Climate stability during the Pliocene warm period. Paleoceanography 18, 1078. https://doi.org/10.1029/2003PA000889

Duplessy, J.-C., Blanc, P.-L., Bé, A.W.H., 1981. Oxygen-18 Enrichment of Planktonic Foraminifera Due to Gametogenic Calcification Below the Euphotic Zone. Science 213, 1247–1250. https://doi.org/10.1126/science.213.4513.1247

Duplessy, J.-C., Labeyrie, L., Waelbroeck, C., 2002. Constraints on the ocean oxygen isotopic enrichment between the Last Glacial Maximum and the Holocene: Paleoceanographic implications. Quaternary Science Reviews, EPILOG 21, 315–330. https://doi.org/10.1016/S0277-3791(01)00107-X

Ehrmann, W.U., Mackensen, A., 1992. Sedimentological evidence for the formation of an East Antarctic ice sheet in Eocene/Oligocene time. Palaeogeography, Palaeoclimatology, Palaeoecology 93, 85–112. https://doi.org/10.1016/0031-0182(92)90185-8

Elderfield, H., Yu, J., Anand, P., Kiefer, T., Nyland, B., 2006. Calibrations for benthic foraminiferal Mg/Ca paleothermometry and the carbonate ion hypothesis. Earth and Planetary Science Letters 250, 633–649. https://doi.org/10.1016/j.epsl.2006.07.041

Eldrett, J.S., Harding, I.C., Wilson, P.A., Butler, E., Roberts, A.P., 2007. Continental ice in Greenland during the Eocene and Oligocene. Nature 446, 176–179. https://doi.org/10.1038/nature05591

Elliot, M., Labeyrie, L., Duplessy, J.-C., 2002. Changes in North Atlantic deep-water formation associated with the Dansgaard–Oeschger temperature oscillations (60–10 ka). Quaternary Science Reviews, Decadal-to-Millennial-Scale Climate Variability 21, 1153–1165. https://doi.org/10.1016/S0277-3791(01)00137-8

Elrick, M., Hinnov, L.A., 2007. Millennial-scale paleoclimate cycles recorded in widespread Palaeozoic deeper water rhythmites of North America. Palaeogeography, Palaeoclimatology, Palaeoecology 243, 348–372. https://doi.org/10.1016/j.palaeo.2006.08.008

Emerson, S., Hedges, J.I., 1988. Processes controlling the organic carbon content of open ocean sediments. Paleoceanography 3, 621–634. https://doi.org/10.1029/PA003i005p00621

Emiliani, C., 1955. Pleistocene temperatures. The Journal of Geology 63, 538–578.

Emiliani, C., 1954. Temperatures of Pacific bottom waters and polar superficial waters during the Tertiary. Science 119, 853-855.

Epstein, S., Buchsbaum, R., Lowenstam, H.A., Urey, H.C., 1953. Revised Carbonate-Water Isotopic Temperature Scale. Geological Society of America Bulletin 64, 1315–1326. https://doi.org/10.1130/0016-7606(1953)64[1315:RCITS]2.0.CO;2

Erez, J., Luz, B., 1983. Experimental paleotemperature equation for planktonic foraminifera. Geochimica et Cosmochimica Acta 47, 1025–1031. https://doi.org/10.1016/0016-7037(83)90232-6

Expedition 342 scientists, 2012. Paleogene Newfoundland Sediment Drifts (No. 342), IODP Preliminary Reports.

Ezard, T.H., Pearson, P.N., Purvis, A., 2010. Algorithmic approaches to aid species' delimitation in multidimensional morphospace. BMC Evolutionary Biology 10, 175. https://doi.org/10.1186/1471-2148-10-175

Ezard, T.H.G., Edgar, K.M., Hull, P.M., 2015. Environmental and biological controls on size-specific δ13C and δ18O in recent planktonic foraminifera. Paleoceanography 30, 2014PA002735. https://doi.org/10.1002/2014PA002735

Fairbanks, R.G., Sverdlove, M., Free, R., Wiebe, P.H., Bé, A.W.H., 1982. Vertical distribution and isotopic fractionation of living planktonic foraminifera from the Panama Basin. Nature 298, 841–844. https://doi.org/10.1038/298841a0

Fairbanks, R.G., Wiebe, P.H., 1980. Foraminifera and Chlorophyll Maximum: Vertical Distribution, Seasonal Succession, and Paleoceanographic Significance. Science 209, 1524–1526. https://doi.org/10.1126/science.209.4464.1524

Fairbanks, R.G., Wiebe, P.H., Bé, A.W.H., 1980. Vertical Distribution and Isotopic Composition of Living Planktonic Foraminifera in the Western North Atlantic. Science 207, 61–63. https://doi.org/10.1126/science.207.4426.61

Faure, G., 1986. Principles of isotope geology. John Wiley & Sons, New York.

Ferrari, R., Jansen, M.F., Adkins, J.F., Burke, A., Stewart, A.L., Thompson, A.F., 2014. Antarctic sea ice control on ocean circulation in present and glacial climates. PNAS 111, 8753–8758. https://doi.org/10.1073/pnas.1323922111

Fischer, A.G., Herbert, T., Silva, I.P., 1985. Carbonate bedding cycles in Cretaceous pelagic and hemipelagic sequences, in: Fine-Grained Deposits and Biofacies of the Cretaceous Western Interior Seaway: Evidence Od Cyclic Sedimentary Processes. Presented at the SEPM 2nd Annual Midyear Meeting, Golden, Colorado.

Fok-Pun, L., 1981. Settling velocities of planktonic foraminifera: density variations and shape effects. Dissertation, Oregon State University.

Fordham, B.G., 1986. Miocene–Pleistocene planktic foraminifers from D. S. D. P. Sites 208 and 77, and phylogeny and classification of Cenozoic species. University of Chicago.

Forey, P.L., Fortey, R.A., Kenrick, P., Smith, A.B., 2004. Taxonomy and fossils: a critical appraisal. Philosophical Transactions of the Royal Society of London B: Biological Sciences 359, 639–653.

Foster, G.L., Royer, D.L., Lunt, D.J., 2017. Future climate forcing potentially without precedent in the last 420 million years. Nature Communications 8, 14845. https://doi.org/10.1038/ncomms14845

Fox, B.R.S., Wartho, J., Wilson, G.S., Lee, D.E., Nelson, F.E., Kaulfuss, U., 2015. Long-term evolution of an Oligocene/Miocene maar lake from Otago, New Zealand. Geochem. Geophys. Geosyst. 16, 59–76. https://doi.org/10.1002/2014GC005534

Fraass, A.J., Lowery, C.M., 2017. Defining uncertainty and error in planktic foraminiferal oxygen isotope measurements. Paleoceanography 32, 2016PA003035. https://doi.org/10.1002/2016PA003035

Fraile, I., Schulz, M., Mulitza, S., Kucera, M., 2008. Predicting the global distribution of planktonic foraminifera using a dynamic ecosystem model. Biogeosciences 5, 891–911. https://doi.org/10.5194/bg-5-891-2008

Fraley, C., Raftery, A.E., 2002. Model-Based Clustering, Discriminant Analysis, and Density Estimation. Journal of the American Statistical Association 97, 611–631. https://doi.org/10.1198/016214502760047131

Friedrich, O., Schiebel, R., Wilson, P.A., Weldeab, S., Beer, C.J., Cooper, M.J., Fiebig, J., 2012. Influence of test size, water depth, and ecology on Mg/Ca, Sr/Ca, δ18O and δ13C in nine modern species of planktic foraminifers. Earth and Planetary Science Letters 319–320, 133–145. https://doi.org/10.1016/j.epsl.2011.12.002

Friedrich, O., Wilson, P.A., Bolton, C.T., Beer, C.J., Schiebel, R., 2013. Late Pliocene to early Pleistocene changes in the North Atlantic Current and suborbital-scale sea-surface temperature variability. Paleoceanography 28, 274–282. https://doi.org/10.1002/palo.20029 Ganopolski, A., Rahmstorf, S., 2001. Rapid changes of glacial climate simulated in a coupled climate model. Nature 409, 153–158. https://doi.org/10.1038/35051500

Ganssen, G.M., Peeters, F.J.C., Metcalfe, B., Anand, P., Jung, S.J.A., Kroon, D., Brummer, G.-J.A., 2011. Quantifying sea surface temperature ranges of the Arabian Sea for the past 20 000 years. Clim. Past 7, 1337–1349. https://doi.org/10.5194/cp-7-1337-2011

Gasson, E., DeConto, R.M., Pollard, D., Levy, R.H., 2016. Dynamic Antarctic ice sheet during the early to mid-Miocene. PNAS 113, 3459–3464. https://doi.org/10.1073/pnas.1516130113

Ge, L., Lai, W., Lin, Y., 2005. Influence of and correction for moisture in rocks, soils and sediments on in situ XRF analysis. X-Ray Spectrom. 34, 28–34. https://doi.org/10.1002/xrs.782

Gebhardt, H., Sarnthein, M., Grootes, P.M., Kiefer, T., Kuehn, H., Schmieder, F., Röhl, U., 2008. Paleonutrient and productivity records from the subarctic North Pacific for Pleistocene glacial terminations I to V. Paleoceanography 23, PA4212. https://doi.org/10.1029/2007PA001513

Ghil, M., Allen, M.R., Dettinger, M.D., Ide, K., Kondrashov, D., Mann, M.E., Robertson, A.W., Saunders, A., Tian, Y., Varadi, F., Yiou, P., 2002. Advanced Spectral Methods for Climatic Time Series. Rev. Geophys. 40, 1003. https://doi.org/10.1029/2000RG000092

Gonera, M., Peryt, T.M., Durakiewicz, T., 2003. Coiling direction in Globigerina bulloides of Middle Miocene age. Journal of Micropalaeontology 22, 141–146. https://doi.org/10.1144/jm.22.2.141

Gottschalk, J., Skinner, L.C., Misra, S., Waelbroeck, C., Menviel, L., Timmermann, A., 2015. Abrupt changes in the southern extent of North Atlantic Deep Water during Dansgaard-Oeschger events. Nature Geosci 8, 950–954. https://doi.org/10.1038/ngeo2558

Gradstein, F.M., Ogg, J.G., Schmitz, M., Ogg, G., 2012. The Geologic Time Scale 2012. Elsevier.

Grazzini, C.V., 1976. Non-equilibrium isotopic compositions of shells of planktonic foraminifera in the Mediterranean Sea. Palaeogeography, Palaeoclimatology, Palaeoecology 20, 263– 276.

Greenop, R., Wilson, P.A., Foster, G.L., submitted. Morphology and life habit of the planktic foraminifera G. bulloides across the Oligocene-Miocene boundary. Geology.

Grützner, J., Higgins, S.M., 2010. Threshold behavior of millennial scale variability in deep water hydrography inferred from a 1.1 Ma long record of sediment provenance at the southern Gardar Drift. Paleoceanography 25, PA4204. https://doi.org/10.1029/2009PA001873

Han, G., 2007. Satellite Observations of Seasonal and Interannual Changes of Sea Level and Currents over the Scotian Slope. J. Phys. Oceanogr. 37, 1051–1065. https://doi.org/10.1175/JPO3036.1

Haug, G.H., Tiedemann, R., 1998. Effect of the formation of the Isthmus of Panama on Atlantic Ocean thermohaline circulation. Nature 393, 673–676. https://doi.org/10.1038/31447

Hays, J.D., Imbrie, J., Shackleton, N.J., 1976. Variations in the Earth's Orbit: Pacemaker of the Ice Ages. Science 194, 1121–1132. https://doi.org/10.1126/science.194.4270.1121

Healy-Williams, N., 1984. Quantitative image analysys: Application to planktonic foraminiferal paleoecology and evolution. Geobios 17, 425–432. https://doi.org/10.1016/S0016-6995(84)80200-4

Heinrich, H., 1988. Origin and consequences of cyclic ice rafting in the Northeast Atlantic Ocean during the past 130,000 years. Quaternary Research 29, 142–152. https://doi.org/10.1016/0033-5894(88)90057-9

Hemleben, C., Olsson, R.K., 2006. Wall textures of Eocene planktonic foraminifera. Atlas of Eocene Planktonic Foraminifera 47–66.

Hemleben, C., Spindler, M., Anderson, O.R., 1989. Modern Planktonic Foraminifera. Springer Science & Business Media.

Hennekam, R., de Lange, G., 2012. X-ray fluorescence core scanning of wet marine sediments: methods to improve quality and reproducibility of high-resolution paleoenvironmental records. Limnol. Oceanogr. Methods 10, 991–1003. https://doi.org/10.4319/lom.2012.10.991

Hillaire-Marcel, C., Vernal, A. de, 2007. Proxies in Late Cenozoic Paleoceanography. Elsevier.

Hilting, A.K., Kump, L.R., Bralower, T.J., 2008. Variations in the oceanic vertical carbon isotope gradient and their implications for the Paleocene-Eocene biological pump. Paleoceanography 23, PA3222. https://doi.org/10.1029/2007PA001458

Hirahara, S., Ishii, M., Fukuda, Y., 2013. Centennial-Scale Sea Surface Temperature Analysis and Its Uncertainty. J. Climate 27, 57–75. https://doi.org/10.1175/JCLI-D-12-00837.1

Hodell, D.A., Kamenov, G.D., Hathorne, E.C., Zachos, J.C., Röhl, U., Westerhold, T., 2007. Variations in the strontium isotope composition of seawater during the Paleocene and early Eocene from ODP Leg 208 (Walvis Ridge). Geochem. Geophys. Geosyst. 8, Q09001. https://doi.org/10.1029/2007GC001607

Hodell, D.A., Venz, K.A., Charles, C.D., Ninnemann, U.S., 2003. Pleistocene vertical carbon isotope and carbonate gradients in the South Atlantic sector of the Southern Ocean. Geochem.-Geophys.-Geosyst. 4, 1004. https://doi.org/10.1029/2002GC000367

Hsiang, A.Y., Elder, L.E., Hull, P.M., 2016. Towards a morphological metric of assemblage dynamics in the fossil record: a test case using planktonic foraminifera. Phil. Trans. R. Soc. B 371, 20150227. https://doi.org/10.1098/rstb.2015.0227

Huber, B.T., Bijma, J., Darling, K., 1997. Cryptic speciation in the living planktonic foraminifer Globigerinella siphonifera (d'Orbigny). Paleobiology 23, 33–62. https://doi.org/10.1017/S0094837300016638

Huber, C., Leuenberger, M., Spahni, R., Flückiger, J., Schwander, J., Stocker, T.F., Johnsen, S., Landais, A., Jouzel, J., 2006. Isotope calibrated Greenland temperature record over Marine Isotope Stage 3 and its relation to CH4. Earth and Planetary Science Letters 243, 504–519. https://doi.org/10.1016/j.epsl.2006.01.002

Hyeong, K., Lee, J., Seo, I., Lee, M.J., Yoo, C.M., Khim, B.-K., 2014. Southward shift of the Intertropical Convergence Zone due to Northern Hemisphere cooling at the Oligocene-Miocene boundary. Geology G35664.1. https://doi.org/10.1130/G35664.1

Jaccard, S.L., Haug, G.H., Sigman, D.M., Pedersen, T.F., Thierstein, H.R., Röhl, U., 2005. Glacial/Interglacial Changes in Subarctic North Pacific Stratification. Science 308, 1003–1006. https://doi.org/10.1126/science.1108696

Jaffrés, J.B.D., Shields, G.A., Wallmann, K., 2007. The oxygen isotope evolution of seawater: A critical review of a long-standing controversy and an improved geological water cycle model for the past 3.4 billion years. Earth-Science Reviews 83, 83–122. https://doi.org/10.1016/j.earscirev.2007.04.002

Jahnke, R.A., Craven, D.B., McCorkle, D.C., Reimers, C.E., 1997. CaCO3 dissolution in California continental margin sediments: The influence of organic matter remineralization. Geochimica et Cosmochimica Acta 61, 3587–3604. https://doi.org/10.1016/S0016-7037(97)00184-1

Jahnke, R.A., Jahnke, D.B., 2004. Calcium carbonate dissolution in deep sea sediments: reconciling microelectrode, pore water and benthic flux chamber results. Geochimica et Cosmochimica Acta 68, 47–59. https://doi.org/10.1016/S0016-7037(03)00260-6

Jansen, J.H.F., Van der Gaast, S.J., Koster, B., Vaars, A.J., 1998. CORTEX, a shipboard XRF-scanner for element analyses in split sediment cores. Marine Geology 151, 143–153. https://doi.org/10.1016/S0025-3227(98)00074-7

Jenkins, D.G., 1960. Planktonic Foraminifera from the Lakes Entrance Oil Shaft, Victoria, Australia. Micropaleontology 6, 345–371. https://doi.org/10.2307/1484217

Jonkers, L., Kučera, M., 2015. Global analysis of seasonality in the shell flux of extant planktonic Foraminifera. Biogeosciences 12, 2207–2226. https://doi.org/10.5194/bg-12-2207-2015

Joyce, T.M., Zhang, R., 2010. On the Path of the Gulf Stream and the Atlantic Meridional Overturning Circulation. J. Climate 23, 3146–3154. https://doi.org/10.1175/2010JCLI3310.1

Kahn, M., 1979. Non-equilibrium oxygen and carbon isotopic fractionation in tests of living planktonic-foraminifera. Oceanologica Acta 2, 195–208.

Keller, G., 1985. Depth stratification of planktonic foraminifers in the Miocene ocean. Geological Society of America Memoirs 163, 177–196.

Kennett, J.P., Shackleton, N.J., 1976. Oxygen isotopic evidence for the development of the psychrosphere 38 Myr ago. Nature 260, 513–515. https://doi.org/10.1038/260513a0

Kennett, J.P., Srinivasan, M.S., 1983. Neogene planktonic foraminifera: a phylogenetic atlas. Hutchinson Ross.

Killingley, J.S., Johnson, R.F., Berger, W.H., 1981. Oxygen and carbon isotopes of individual shells of planktonic foraminifera from Ontong-Java plateau, equatorial pacific. Palaeogeography, Palaeoclimatology, Palaeoecology, Oxygen and Carbon Isotopes in Foraminifera 33, 193–204. https://doi.org/10.1016/0031-0182(81)90038-9

Kleppin, H., Jochum, M., Otto-Bliesner, B., Shields, C.A., Yeager, S., 2015. Stochastic Atmospheric Forcing as a Cause of Greenland Climate Transitions. J. Climate 28, 7741–7763. https://doi.org/10.1175/JCLI-D-14-00728.1

Knappertsbusch, M., Binggeli, D., Herzig, A., Schmutz, L., Stapfer, S., Schneider, C., Eisenecker, J., Widmer, L., 2009. AMOR-A new system for automated imaging of microfossils for morphometric analyses. Palaeontologia Electronica 12.

Knies, J., Cabedo-Sanz, P., Belt, S.T., Baranwal, S., Fietz, S., Rosell-Melé, A., 2014. The emergence of modern sea ice cover in the Arctic Ocean. Nature Communications 5, 5608. https://doi.org/10.1038/ncomms6608

Koshikawa, T., Kido, Y., Tada, R., 2003. High-Resolution Rapid Elemental Analysis Using an XRF Microscanner. Journal of Sedimentary Research 73, 824–829. https://doi.org/10.1306/020503730824

Kotthoff, U., Greenwood, D.R., McCarthy, F.M.G., Müller-Navarra, K., Prader, S., Hesselbo, S.P., 2014. Late Eocene to middle Miocene (33 to 13 million years ago) vegetation and climate development on the North American Atlantic Coastal Plain (IODP Expedition 313, Site M0027). Clim. Past 10, 1523–1539. https://doi.org/10.5194/cp-10-1523-2014

Koutavas, A., deMenocal, P.B., Olive, G.C., Lynch-Stieglitz, J., 2006. Mid-Holocene El Niño–Southern Oscillation (ENSO) attenuation revealed by individual foraminifera in eastern tropical Pacific sediments. Geology 34, 993–996. https://doi.org/10.1130/G22810A.1

Kozdon, R., Kelly, D.C., Kita, N.T., Fournelle, J.H., Valley, J.W., 2011. Planktonic foraminiferal oxygen isotope analysis by ion microprobe technique suggests warm tropical sea surface temperatures during the Early Paleogene. Paleoceanography 26, PA3206. https://doi.org/10.1029/2010PA002056

Kozdon, R., Kelly, D.C., Kitajima, K., Strickland, A., Fournelle, J.H., Valley, J.W., 2013. In situ δ18O and Mg/Ca analyses of diagenetic and planktic foraminiferal calcite preserved in a deep-sea record of the Paleocene-Eocene thermal maximum. Paleoceanography 28, 517–528. https://doi.org/10.1002/palo.20048

Kozdon, R., Ushikubo, T., Kita, N.T., Spicuzza, M., Valley, J.W., 2009. Intratest oxygen isotope variability in the planktonic foraminifer N. pachyderma: Real vs. apparent vital effects by ion microprobe. Chemical Geology 258, 327–337. https://doi.org/10.1016/j.chemgeo.2008.10.032

Krylov, A.A., Andreeva, I.A., Vogt, C., Backman, J., Krupskaya, V.V., Grikurov, G.E., Moran, K., Shoji, H., 2008. A shift in heavy and clay mineral provenance indicates a middle Miocene onset of a perennial sea ice cover in the Arctic Ocean. Paleoceanography 23, PA1S06. https://doi.org/10.1029/2007PA001497

Kucera, M., 2007. Chapter Six Planktonic Foraminifera as Tracers of Past Oceanic Environments, in: Vernal, C.H. and A.D. (Ed.), Developments in Marine Geology, Proxies in Late Cenozoic Paleoceanography. Elsevier, pp. 213–262. https://doi.org/10.1016/S1572-5480(07)01011-1

Kucera, M., Darling, K.F., 2002. Cryptic species of planktonic foraminifera: their effect on palaeoceanographic reconstructions. Philosophical Transactions of the Royal Society of London A: Mathematical, Physical and Engineering Sciences 360, 695–718. https://doi.org/10.1098/rsta.2001.0962

Kuhlmann, H., Freudenthal, T., Helmke, P., Meggers, H., 2004. Reconstruction of paleoceanography off NW Africa during the last 40,000 years: influence of local and regional factors on sediment accumulation. Marine Geology 207, 209–224. https://doi.org/10.1016/j.margeo.2004.03.017

Lamb, J.L., Beard, J.H., 1972. Late Neogene planktonic foraminifers in the Caribbean, Gulf of Mexico, and Italian stratotypes.

Langer, M.R., 2008. Assessing the Contribution of Foraminiferan Protists to Global Ocean Carbonate Production1. Journal of Eukaryotic Microbiology 55, 163–169. https://doi.org/10.1111/j.1550-7408.2008.00321.x

Laskar, J., Robutel, P., Joutel, F., Gastineau, M., Correia, A.C.M., Levrard, B., 2004. A long-term numerical solution for the insolation quantities of the Earth. A&A 428, 261–285. https://doi.org/10.1051/0004-6361:20041335

Latif, M., Roeckner, E., Botzet, M., Esch, M., Haak, H., Hagemann, S., Jungclaus, J., Legutke, S., Marsland, S., Mikolajewicz, U., Mitchell, J., 2004. Reconstructing, Monitoring, and Predicting Multidecadal-Scale Changes in the North Atlantic Thermohaline Circulation with Sea Surface Temperature. J. Climate 17, 1605–1614. https://doi.org/10.1175/1520-0442(2004)017<1605:RMAPMC>2.0.CO;2

Le, J., Shackleton, N.J., 1992. Carbonate Dissolution Fluctuations in the Western Equatorial Pacific During the Late Quaternary. Paleoceanography 7, 21–42. https://doi.org/10.1029/91PA02854

Lear, C.H., Rosenthal, Y., Coxall, H.K., Wilson, P.A., 2004. Late Eocene to early Miocene ice sheet dynamics and the global carbon cycle. Paleoceanography 19. https://doi.org/10.1029/2004PA001039

Lear, C.H., Rosenthal, Y., Slowey, N., 2002. Benthic foraminiferal Mg/Ca-paleothermometry: a revised core-top calibration. Geochimica et Cosmochimica Acta 66, 3375–3387. https://doi.org/10.1016/S0016-7037(02)00941-9

Leduc, G., Vidal, L., Cartapanis, O., Bard, E., 2009. Modes of eastern equatorial Pacific thermocline variability: Implications for ENSO dynamics over the last glacial period. Paleoceanography 24, PA3202. https://doi.org/10.1029/2008PA001701

LeGrande, A.N., Schmidt, G.A., 2006. Global gridded data set of the oxygen isotopic composition in seawater. Geophys. Res. Lett. 33, L12604. https://doi.org/10.1029/2006GL026011

Liebrand, D. et al., in prep. IODP Site 1406 benthic stable isotope record.

Liebrand, D., Bakker, A.T.M. de, Beddow, H.M., Wilson, P.A., Bohaty, S.M., Ruessink, G., Pälike, H., Batenburg, S.J., Hilgen, F.J., Hodell, D.A., Huck, C.E., Kroon, D., Raffi, I., Saes, M.J.M., Dijk, A.E. van, Lourens, L.J., 2017. Evolution of the early Antarctic ice ages. PNAS 114, 3867–3872. https://doi.org/10.1073/pnas.1615440114

Liebrand, D., Beddow, H.M., Lourens, L.J., Pälike, H., Raffi, I., Bohaty, S.M., Hilgen, F.J., Saes, M.J.M., Wilson, P.A., van Dijk, A.E., Hodell, D.A., Kroon, D., Huck, C.E., Batenburg, S.J., 2016. Cyclostratigraphy and eccentricity tuning of the early Oligocene through early Miocene (30.1–17.1 Ma): Cibicides mundulus stable oxygen and carbon isotope records from Walvis Ridge Site 1264. Earth and Planetary Science Letters 450, 392–405. https://doi.org/10.1016/j.epsl.2016.06.007

Liebrand, D., Lourens, L.J., Hodell, D.A., de Boer, B., van de Wal, R.S.W., Pälike, H., 2011. Antarctic ice sheet and oceanographic response to eccentricity forcing during the early Miocene. Climate of the Past 7. https://doi.org/10.5194/cp-7-869-2011

Lipps, J.H., 1979. Ecology and Paleoecology of Planktic Foraminifera. Special publications of the Society for Sedimentary Geology (SEPM).

Lisiecki, L.E., Raymo, M.E., 2005. A Pliocene-Pleistocene stack of 57 globally distributed benthic δ18O records. Paleoceanography 20, PA1003. https://doi.org/10.1029/2004PA001071

Liu, Z., Pagani, M., Zinniker, D., DeConto, R., Huber, M., Brinkhuis, H., Shah, S.R., Leckie, R.M., Pearson, A., 2009. Global Cooling During the Eocene-Oligocene Climate Transition. Science 323, 1187–1190. https://doi.org/10.1126/science.1166368

Lohmann, G.P., 1995. A model for variation in the chemistry of planktonic foraminifera due to secondary calcification and selective dissolution. Paleoceanography 10, 445–457. https://doi.org/10.1029/95PA00059

Lombard, F., Labeyrie, L., Michel, E., Bopp, L., Cortijo, E., Retailleau, S., Howa, H., Jorissen, F., 2011. Modelling planktic foraminifer growth and distribution using an ecophysiological multi-species approach. Biogeosciences 8, 853–873. https://doi.org/10.5194/bg-8-853-2011

Lyle, M., Olivarez Lyle, A., Gorgas, T., Holbourn, A., Westerhold, T., Hathorne, E., Kimoto, K., Yamamoto, S., 2012. Data report: raw and normalized elemental data along the Site U1338 splice from X-ray fluorescence scanning. Pälike, H., et al., Proceedings of the Integrated Ocean Drilling Program 320, 321.

MacLeod, N., Carter, J.L., 1984. A Method for Obtaining Consistent Specimen Orientations for Use in Microfossil Biometric Studies. Micropaleontology 30, 306–310. https://doi.org/10.2307/1485692

Malmgren, B., Kennett, J.P., 1976. Biometric analysis of phenotypic variation in RecentGlobigerina bulloides d'Orbigny in the southern Indian Ocean. Marine Micropaleontology 1, 3–25. https://doi.org/10.1016/0377-8398(76)90003-7

Malmgren, B.A., Kennett, J.P., 1977. Biometric Differentiation Between Recent Globigerina Bulloides and Globigerina Falconensis in the Southern Indian Ocean. Journal of Foraminiferal Research 7, 131–148. https://doi.org/10.2113/gsjfr.7.2.131

Markle, B.R., Steig, E.J., Buizert, C., Schoenemann, S.W., Bitz, C.M., Fudge, T.J., Pedro, J.B., Ding, Q., Jones, T.R., White, J.W.C., Sowers, T., 2017. Global atmospheric

teleconnections during Dansgaard-Oeschger events. Nature Geosci 10, 36–40. https://doi.org/10.1038/ngeo2848

Mary, Y., Knappertsbusch, M.W., 2013. Morphological variability of menardiform globorotalids in the Atlantic Ocean during Mid-Pliocene. Marine Micropaleontology 101, 180–193. https://doi.org/10.1016/j.marmicro.2012.12.001

Mawbey, E.M., Lear, C.H., 2013. Carbon cycle feedbacks during the Oligocene-Miocene transient glaciation. Geology 41, 963–966. https://doi.org/10.1130/G34422.1

Mayewski, P.A., Rohling, E.E., Curt Stager, J., Karlén, W., Maasch, K.A., David Meeker, L., Meyerson, E.A., Gasse, F., van Kreveld, S., Holmgren, K., Lee-Thorp, J., Rosqvist, G., Rack, F., Staubwasser, M., Schneider, R.R., Steig, E.J., 2004. Holocene climate variability. Quaternary Research 62, 243–255. https://doi.org/10.1016/j.yqres.2004.07.001

Mayr, E., 1963. Animal Species and Evolution (Belknap, Cambridge, MA).

McCrea, J.M., 1950. On the Isotopic Chemistry of Carbonates and a Paleotemperature Scale. The Journal of Chemical Physics 18, 849–857. https://doi.org/10.1063/1.1747785

McDermott, F., Mattey, D.P., Hawkesworth, C., 2001. Centennial-Scale Holocene Climate Variability Revealed by a High-Resolution Speleothem δ18O Record from SW Ireland. Science 294, 1328–1331. https://doi.org/10.1126/science.1063678

McIntyre, A., Molfino, B., 1996. Forcing of Atlantic Equatorial and Subpolar Millennial Cycles by Precession. Science 274, 1867–1870. https://doi.org/10.1126/science.274.5294.1867

McManus, J.F., Oppo, D.W., Cullen, J.L., 1999. A 0.5-Million-Year Record of Millennial-Scale Climate Variability in the North Atlantic. Science 283, 971–975. https://doi.org/10.1126/science.283.5404.971

McNown, J.S., Malaika, J., 1950. Effects of particle shape on settling velocity at low Reynolds numbers. Eos Trans. AGU 31, 74–82. https://doi.org/10.1029/TR031i001p00074

Meinen, C.S., Watts, D.R., 2000. Vertical structure and transport on a transect across the North Atlantic Current near 42°N: Time series and mean. J. Geophys. Res. 105, 21869–21891. https://doi.org/10.1029/2000JC900097

Meyers, S., 2014. Astrochron: An R package for astrochronology.

Miao, Y.-F., Fang, X.-M., Song, C.-H., Yan, X.-L., Xu, L., Chen, C.-F., 2013. Pollen and fossil wood's linkage with Mi-1 Glaciation in northeastern Tibetan Plateau, China. Palaeoworld, Neogene climate and environmental evolution in Eastern Eurasia 22, 101–108. https://doi.org/10.1016/j.palwor.2013.06.001

Milankovitch, M., 1941. Kanon der Erdebestrahlung und seine Anwendung auf das Eiszeitenproblem. Königlich Serbische Akademie.

Miller, K.G., Fairbanks, R.G., 1983. Evidence for Oligocene–Middle Miocene abyssal circulation changes in the western North Atlantic. Nature 306, 250–253. https://doi.org/10.1038/306250a0

Miller, K.G., Tucholke, B.E., 1983. Development of Cenozoic Abyssal Circulation South of the Greenland-Scotland Ridge, in: Bott, M.H.P., Saxov, S., Talwani, M., Thiede, J. (Eds.), Structure and Development of the Greenland-Scotland Ridge, Nato Conference Series. Springer US, pp. 549–589. https://doi.org/10.1007/978-1-4613-3485-9_27

Miller, K.G., Wright, J.D., Fairbanks, R.G., 1991. Unlocking the Ice House: Oligocene-Miocene oxygen isotopes, eustasy, and margin erosion. Journal of Geophysical Research: Solid Earth 96, 6829–6848. https://doi.org/10.1029/90JB02015

Morard, R., Quillévéré, F., Escarguel, G., de Garidel-Thoron, T., de Vargas, C., Kucera, M., 2013. Ecological modeling of the temperature dependence of cryptic species of planktonic Foraminifera in the Southern Hemisphere. Palaeogeography, Palaeoclimatology, Palaeoecology 391, Part A, 13–33. https://doi.org/10.1016/j.palaeo.2013.05.011

Morard, R., Quillévéré, F., Escarguel, G., Ujiie, Y., de Garidel-Thoron, T., Norris, R.D., de Vargas, C., 2009. Morphological recognition of cryptic species in the planktonic foraminifer Orbulina universa. Marine Micropaleontology 71, 148–165. https://doi.org/10.1016/j.marmicro.2009.03.001

Morard, R., Reinelt, M., Chiessi, C.M., Groeneveld, J., Kucera, M., 2016. Tracing shifts of oceanic fronts using the cryptic diversity of the planktonic foraminifera Globorotalia inflata. Paleoceanography 31, 2016PA002977. https://doi.org/10.1002/2016PA002977

Mortyn, P.G., Charles, C.D., 2003. Planktonic foraminiferal depth habitat and δ18O calibrations: Plankton tow results from the Atlantic sector of the Southern Ocean. Paleoceanography 18, 1037. https://doi.org/10.1029/2001PA000637

Moseley, H.G.J.M., 1914. LXXX. The high-frequency spectra of the elements. Part II. Philosophical Magazine Series 6 27, 703–713. https://doi.org/10.1080/14786440408635141

Mulitza, S., Boltovskoy, D., Donner, B., Meggers, H., Paul, A., Wefer, G., 2003. Temperature:δ18O relationships of planktonic foraminifera collected from surface waters. Palaeogeography, Palaeoclimatology, Palaeoecology 202, 143–152. https://doi.org/10.1016/S0031-0182(03)00633-3

Mulitza, S., Prange, M., Stuut, J.-B., Zabel, M., von Dobeneck, T., Itambi, A.C., Nizou, J., Schulz, M., Wefer, G., 2008. Sahel megadroughts triggered by glacial slowdowns of Atlantic meridional overturning. Paleoceanography 23.

Muscheler, R., Beer, J., 2006. Solar forced Dansgaard/Oeschger events? Geophys. Res. Lett. 33, L20706. https://doi.org/10.1029/2006GL026779

Naafs, B.D.A., Stein, R., Hefter, J., Khélifi, N., De Schepper, S., Haug, G.H., 2010. Late Pliocene changes in the North Atlantic Current. Earth and Planetary Science Letters 298, 434–442. https://doi.org/10.1016/j.epsl.2010.08.023

Naish, T.R., Woolfe, K.J., Barrett, P.J., Wilson, G.S., Atkins, C., Bohaty, S.M., Bücker, C.J., Claps, M., Davey, F.J., Dunbar, G.B., Dunn, A.G., Fielding, C.R., Florindo, F., Hannah, M.J., Harwood, D.M., Henrys, S.A., Krissek, L.A., Lavelle, M., van der Meer, J., McIntosh, W.C., Niessen, F., Passchier, S., Powell, R.D., Roberts, A.P., Sagnotti, L., Scherer, R.P., Strong, C.P., Talarico, F., Verosub, K.L., Villa, G., Watkins, D.K., Webb, P.-N., Wonik, T., 2001. Orbitally induced oscillations in the East Antarctic ice sheet at the Oligocene/Miocene boundary. Nature 413, 719–723. https://doi.org/10.1038/35099534

Neff, U., Burns, S.J., Mangini, A., Mudelsee, M., Fleitmann, D., Matter, A., 2001. Strong coherence between solar variability and the monsoon in Oman between 9 and 6 kyr ago. Nature 411, 290–293. https://doi.org/10.1038/35077048

Norris, R.D., 1996. Symbiosis as an evolutionary innovation in the radiation of Paleocene planktic foraminifera. Paleobiology 22, 461–480. https://doi.org/10.1017/S0094837300016468

Norris, R.D. et al., 2014. Paleogene Newfoundland Sediment Drifts and MDHDS Test. Proceedings of the Integrated Ocean Drilling Program 342.

Norris, R.D., Wilson, P.A., 1998. Low-latitude sea-surface temperatures for the mid-Cretaceous and the evolution of planktic foraminifera. Geology 26, 823–826. https://doi.org/10.1130/0091-7613(1998)026<0823:LLSSTF>2.3.CO;2

Obrochta, S.P., Miyahara, H., Yokoyama, Y., Crowley, T.J., 2012. A re-examination of evidence for the North Atlantic "1500-year cycle" at Site 609. Quaternary Science Reviews 55, 23–33. https://doi.org/10.1016/j.quascirev.2012.08.008

Oerlemans, J., 1981. Some basic experiments with a vertically-integrated ice sheet model. Tellus 33, 1–11. https://doi.org/10.1111/j.2153-3490.1981.tb01726.x

Oerlemans, J., Van Der Veen, C.J., 1984. Ice sheets and climate. Springer.

Olsson, R.K., Berggren, W.A., Hemleben, C., Huber, B.T., 1999. Atlas of Paleocene planktonic foraminifera. Smithsonian Institution Press.

Opdyke, B.N., Walker, J.C.G., 1992. Return of the coral reef hypothesis: Basin to shelf partitioning of CaCO3 and its effect on atmospheric CO2. Geology 20, 733–736. https://doi.org/10.1130/0091-7613(1992)020<0733:ROTCRH>2.3.CO;2

Oppo, D.W., Keigwin, L.D., McManus, J.F., Cullen, J.L., 2001. Persistent suborbital climate variability in marine isotope stage 5 and termination II. Paleoceanography 16, 280–292. https://doi.org/10.1029/2000PA000527

Oppo, D.W., McManus, J.F., Cullen, J.L., 2003. Palaeo-oceanography: Deepwater variability in the Holocene epoch. Nature 422, 277–277. https://doi.org/10.1038/422277b

Ortiz, J.D., Mix, A.C., Rugh, W., Watkins, J.M., Collier, R.W., 1996. Deep-dwelling planktonic foraminifera of the northeastern Pacific Ocean reveal environmental control of oxygen and carbon isotopic disequilibria. Geochimica et Cosmochimica Acta 60, 4509–4523. https://doi.org/10.1016/S0016-7037(96)00256-6

Osborne, E.B., Thunell, R.C., Marshall, B.J., Holm, J.A., Tappa, E.J., Benitez-Nelson, C., Cai, W.-J., Chen, B., 2016. Calcification of the planktonic foraminifera Globigerina bulloides and

carbonate ion concentration: Results from the Santa Barbara Basin. Paleoceanography 31, 2016PA002933. https://doi.org/10.1002/2016PA002933

Paillard, D., Labeyrie, L., Yiou, P., 1996. Macintosh Program performs time-series analysis. Eos Trans. AGU 77, 379–379. https://doi.org/10.1029/96EO00259

Pälike, H., Frazier, J., Zachos, J.C., 2006a. Extended orbitally forced palaeoclimatic records from the equatorial Atlantic Ceara Rise. Quaternary Science Reviews 25, 3138–3149. https://doi.org/10.1016/j.quascirev.2006.02.011

Pälike, H., Norris, R.D., Herrle, J.O., Wilson, P.A., Coxall, H.K., Lear, C.H., Shackleton, N.J., Tripati, A.K., Wade, B.S., 2006b. The Heartbeat of the Oligocene Climate System. Science 314, 1894–1898. https://doi.org/10.1126/science.1133822

Palter, J.B., Lozier, M.S., Lavender, K.L., 2008. How Does Labrador Sea Water Enter the Deep Western Boundary Current? J. Phys. Oceanogr. 38, 968–983. https://doi.org/10.1175/2007JPO3807.1

Park, R., Epstein, S., 1960. Carbon isotope fractionation during photosynthesis. Geochimica et Cosmochimica Acta 21, 110–126. https://doi.org/10.1016/S0016-7037(60)80006-3

Passchier, S., Krissek, L.A., 2008. Oligocene–Miocene Antarctic continental weathering record and paleoclimatic implications, Cape Roberts drilling Project, Ross Sea, Antarctica. Palaeogeography, Palaeoclimatology, Palaeoecology 260, 30–40. https://doi.org/10.1016/j.palaeo.2007.08.012

Patara, L., Böning, C.W., 2014. Abyssal ocean warming around Antarctica strengthens the Atlantic overturning circulation. Geophys. Res. Lett. 41, 2014GL059923. https://doi.org/10.1002/2014GL059923

Paul, H.A., Zachos, J.C., Flower, B.P., Tripati, A., 2000. Orbitally induced climate and geochemical variability across the Oligocene/Miocene boundary. Paleoceanography 15, 471–485. https://doi.org/10.1029/1999PA000443

Pearson, P., Olsson, R., Huber, B., Hemleben, C., Berggren, W., Premoli Silva, I., Coxall, H., Premec-Fucek, V., Wade, B., et al., 2006. Atlas of Eocene planktonic foraminifera. Epitome 1, 274–274.

Pearson, P.N., 2012. Oxygen isotopes in foraminifera: Overview and Historical Review, in: Reconstructing Earth's Deep-Time Climate–The State of the Art in 2012. pp. 1–38.

Pearson, P.N., Burgess, C.E., 2008. Foraminifer test preservation and diagenesis: comparison of high latitude Eocene sites. Geological Society, London, Special Publications 303, 59–72. https://doi.org/10.1144/SP303.5

Pearson, P.N., Ditchfield, P.W., Singano, J., Harcourt-Brown, K.G., Nicholas, C.J., Olsson, R.K., Shackleton, N.J., Hall, M.A., 2001. Warm tropical sea surface temperatures in the Late Cretaceous and Eocene epochs. Nature 413, 481–487. https://doi.org/10.1038/35097000

Pearson, P.N., Dongen, B.E. van, Nicholas, C.J., Pancost, R.D., Schouten, S., Singano, J.M., Wade, B.S., 2007. Stable warm tropical climate through the Eocene Epoch. Geology 35, 211–214. https://doi.org/10.1130/G23175A.1

Pearson, P.N., Ezard, T.H.G., 2014. Evolution and speciation in the Eocene planktonic foraminifer Turborotalia. Paleobiology 40, 130–143. https://doi.org/10.1666/13004

Pearson, P.N., Shackleton, N.J., Weedon, G.P., Hall, M.A., 1997. Multispecies planktonic foraminifer stable isotope stratigraphy through Oligocene/Miocene boundary climatic cycles, Site 926. Proc. ODP, Sci. Results 154, 441–449.

Pearson, P.N., Wade, B.S., 2009. Taxonomy and Stable Isotope Paleoecology of Well-Preserved Planktonic Foraminifera from the Uppermost Oligocene of Trinidad. Journal of Foraminiferal Research 39, 191–217. https://doi.org/10.2113/gsjfr.39.3.191

Peeters, F., Ivanova, E., Conan, S., Brummer, G.-J., Ganssen, G., Troelstra, S., van Hinte, J., 1999. A size analysis of planktic foraminifera from the Arabian Sea. Marine Micropaleontology 36, 31–63. https://doi.org/10.1016/S0377-8398(98)00026-7

Pekar, S.F., Christie-Blick, N., Kominz, M.A., Miller, K.G., 2002. Calibration between eustatic estimates from backstripping and oxygen isotopic records for the Oligocene. Geology 30, 903–906. https://doi.org/10.1130/0091-7613(2002)030<0903:CBEEFB>2.0.CO;2

Pekar, S.F., DeConto, R.M., 2006. High-resolution ice-volume estimates for the early Miocene: Evidence for a dynamic ice sheet in Antarctica. Palaeogeography, Palaeoclimatology, Palaeoecology 231, 101–109. https://doi.org/10.1016/j.palaeo.2005.07.027

Peltier, W.R., Vettoretti, G., 2014. Dansgaard-Oeschger oscillations predicted in a comprehensive model of glacial climate: A "kicked" salt oscillator in the Atlantic. Geophys. Res. Lett. 41, 2014GL061413. https://doi.org/10.1002/2014GL061413

Peres-Neto, P.R., Jackson, D.A., Somers, K.M., 2005. How many principal components? stopping rules for determining the number of non-trivial axes revisited. Computational Statistics & Data Analysis 49, 974–997. https://doi.org/10.1016/j.csda.2004.06.015

Peristykh, A.N., Damon, P.E., 2003. Persistence of the Gleissberg 88-year solar cycle over the last −12,000 years: Evidence from cosmogenic isotopes. J. Geophys. Res. 108, 1003. https://doi.org/10.1029/2002JA009390

Petersen, S.V., Schrag, D.P., Clark, P.U., 2013. A new mechanism for Dansgaard-Oeschger cycles. Paleoceanography 28, 24–30. https://doi.org/10.1029/2012PA002364

Peterson, L.C., Prell, W.L., 1985. Carbonate dissolution in Recent sediments of the eastern equatorial Indian Ocean: Preservation patterns and carbonate loss above the lysocline. Marine Geology 64, 259–290. https://doi.org/10.1016/0025-3227(85)90108-2

Pickart, R.S., McKee, T.K., Torres, D.J., Harrington, S.A., 1999. Mean Structure and Interannual Variability of the Slopewater System South of Newfoundland*. J. Phys. Oceanogr. 29, 2541–2558. https://doi.org/10.1175/1520-0485(1999)029<2541:MSAIVO>2.0.CO;2

Pinet, P.R., Popenoe, P., Nelligan, D.F., 1981. Gulf Stream: Reconstruction of Cenozoic flow patterns over the Blake Plateau. Geology 9, 266–270. https://doi.org/10.1130/0091-7613(1981)9<266:GSROCF>2.0.CO;2

Pollard, D., DeConto, R.M., 2005. Hysteresis in Cenozoic Antarctic ice-sheet variations. Global and Planetary Change 45, 9–21. https://doi.org/10.1016/j.gloplacha.2004.09.011

Poore, R., Matthews, R., 1984. Oxygen isotope ranking of late Eocene and Oligocene planktonic foraminifers: implications for Oligocene sea-surface temperatures and global ice-volume. Marine Micropaleontology 9, 111–134.

Prasad, S., Vos, H., Negendank, J.F.W., Waldmann, N., Goldstein, S.L., Stein, M., 2004. Evidence from Lake Lisan of solar influence on decadal- to centennial-scale climate variability during marine oxygen isotope stage 2. Geology 32, 581–584. https://doi.org/10.1130/G20553.1

Quillévéré, F., Morard, R., Escarguel, G., Douady, C.J., Ujiié, Y., de Garidel-Thoron, T., de Vargas, C., 2013. Global scale same-specimen morpho-genetic analysis of Truncorotalia truncatulinoides: A perspective on the morphological species concept in planktonic foraminifera. Palaeogeography, Palaeoclimatology, Palaeoecology, Quantitative analysis of fossil data in the development and application of paleoproxies 391, Part A, 2–12. https://doi.org/10.1016/j.palaeo.2011.03.013

R Core Team, 2016. R: A Language and Environment for Statistical Computing. R Foundation for Statistical Computing, Vienna, Austria.

Rahmstorf, S., 2002. Ocean circulation and climate during the past 120,000 years. Nature 419, 207–214. https://doi.org/10.1038/nature01090

Rahmstorf, S., Box, J.E., Feulner, G., Mann, M.E., Robinson, A., Rutherford, S., Schaffernicht, E.J., 2015. Exceptional twentieth-century slowdown in Atlantic Ocean overturning circulation. Nature Clim. Change 5, 475–480. https://doi.org/10.1038/nclimate2554

Rasmussen, T.L., Thomsen, E., Moros, M., 2016. North Atlantic warming during Dansgaard-Oeschger events synchronous with Antarctic warming and out-of-phase with Greenland climate. Scientific Reports 6, 20535. https://doi.org/10.1038/srep20535

Raspopov, O.M., Dergachev, V.A., Esper, J., Kozyreva, O.V., Frank, D., Ogurtsov, M., Kolström, T., Shao, X., 2008. The influence of the de Vries (− 200-year) solar cycle on climate variations: Results from the Central Asian Mountains and their global link. Palaeogeography, Palaeoclimatology, Palaeoecology 259, 6–16. https://doi.org/10.1016/j.palaeo.2006.12.017

Ravelo, A.C., Claude, H.-M., 2007. Chapter Eighteen The Use of Oxygen and Carbon Isotopes of Foraminifera in Paleoceanography, in: Developments in Marine Geology. pp. 735–764.

Ravelo, A.C., Fairbanks, R.G., 1995. Carbon isotopic fractionation in multiple species of planktonic foraminifera from core-tops in the tropical Atlantic. Oceanographic Literature Review 10, 854.

Ravelo, A.C., Fairbanks, R.G., 1992. Oxygen Isotopic Composition of Multiple Species of Planktonic Foraminifera: Recorders of the Modern Photic Zone Temperature Gradient. Paleoceanography 7, 815–831. https://doi.org/10.1029/92PA02092

Raymo, M.E., Lisiecki, L.E., Nisancioglu, K.H., 2006. Plio-Pleistocene Ice Volume, Antarctic Climate, and the Global δ18O Record. Science 313, 492–495. https://doi.org/10.1126/science.1123296

Reichgelt, T., D'Andrea, W.J., Fox, B.R.S., 2016. Abrupt plant physiological changes in southern New Zealand at the termination of the Mi-1 event reflect shifts in hydroclimate and pCO2. Earth and Planetary Science Letters 455, 115–124. https://doi.org/10.1016/j.epsl.2016.09.026

Richter, T.O., Van der Gaast, S., Koster, B., Vaars, A., Gieles, R., de Stigter, H.C., De Haas, H., van Weering, T.C., 2006. The Avaatech XRF Core Scanner: technical description and applications to NE Atlantic sediments. Geological Society, London, Special Publications 267, 39–50.

Roberts, A., Austin, W., Evans, K., Bird, C., Schweizer, M., Darling, K., 2016. A New Integrated Approach to Taxonomy: The Fusion of Molecular and Morphological Systematics with Type Material in Benthic Foraminifera. PLOS ONE 11, e0158754. https://doi.org/10.1371/journal.pone.0158754

Roberts, C.D., Garry, F.K., Jackson, L.C., 2013. A Multimodel Study of Sea Surface Temperature and Subsurface Density Fingerprints of the Atlantic Meridional Overturning Circulation. J. Climate 26, 9155–9174. https://doi.org/10.1175/JCLI-D-12-00762.1

Röhl, U., Abrams, L.J., 2000. 11. High resolution, downhole, and nondestructive core measurements from sites 999 and 1001 in the Caribbean Sea: Application to the late Paleocene thermal maximum. Proceedings of the Ocean Drilling Program, Scientific Results.

Rohlf, J.F., Marcus, L.F., 1993. A revolution morphometrics. Trends in Ecology & Evolution 8, 129–132. https://doi.org/10.1016/0169-5347(93)90024-J

Rohling, E.J., Cooke, S., 1999. Stable oxygen and carbon isotopes in foraminiferal carbonate shells, in: Modern Foraminifera. Springer Netherlands, pp. 239–258. https://doi.org/10.1007/0-306-48104-9_14

Romanek, C.S., Grossman, E.L., Morse, J.W., 1992. Carbon isotopic fractionation in synthetic aragonite and calcite: Effects of temperature and precipitation rate. Geochimica et Cosmochimica Acta 56, 419–430. https://doi.org/10.1016/0016-7037(92)90142-6

Rosman, K.J.R., Taylor, P.D.P., 2009. Isotopic compositions of the elements 1997 (Technical Report). Pure and Applied Chemistry 70, 217–235. https://doi.org/10.1351/pac199870010217

Rothwell, R.G., Croudace, I. w, 2015. Twenty Years of XRF Core Scanning Marine Sediments: What Do Geochemical Proxies Tell Us?, in: Croudace, I.W., Rothwell, R.G. (Eds.), Micro-XRF Studies of Sediment Cores, Developments in Paleoenvironmental Research. Springer Netherlands, pp. 25–102. https://doi.org/10.1007/978-94-017-9849-5_2

Rousseau, R.M., Willis, J.P., Duncan, A.R., 1996. Practical XRF Calibration Procedures for Major and Trace Elements. X-Ray Spectrom. 25, 179–189. https://doi.org/10.1002/(SICI)1097-4539(199607)25:4<179::AID-XRS162>3.0.CO;2-Y

Sagnotti, L., Florindo, F., Verosub, K.L., Wilson, G.S., Roberts, A.P., 1998. Environmental magnetic record of Antarctic palaeoclimate from Eocene/Oligocene glaciomarine sediments, Victoria Land Basin. Geophys J Int 134, 653–662. https://doi.org/10.1046/j.1365-246x.1998.00559.x

Sanchez-Franks, A., Zhang, R., 2015. Impact of the Atlantic meridional overturning circulation on the decadal variability of the Gulf Stream path and regional chlorophyll and nutrient concentrations. Geophys. Res. Lett. 42, 2015GL066262. https://doi.org/10.1002/2015GL066262

Scher, H.D., Martin, E.E., 2008. Oligocene deep water export from the North Atlantic and the development of the Antarctic Circumpolar Current examined with neodymium isotopes. Paleoceanography 23, PA1205. https://doi.org/10.1029/2006PA001400

Schiebel, R., Hemleben, C., 2005. Modern planktic foraminifera. Paläontol Z 79, 135–148. https://doi.org/10.1007/BF03021758

Schiebel, R., Hiller, B., Hemleben, C., 1995. Impacts of storms on Recent planktic foraminiferal test production and CaCO3 flux in the North Atlantic at 47 °N, 20 °W (JGOFS). Marine Micropaleontology, Selected papers from the Fifth International Symposium of Foraminifera 26, 115–129. https://doi.org/10.1016/0377-8398(95)00035-6

Schiffelbein, P., Hills, S., 1984. Direct assessment of stable isotope variability in planktonic foraminifera populations. Palaeogeography, Palaeoclimatology, Palaeoecology 48, 197–213. https://doi.org/10.1016/0031-0182(84)90044-0

Schmidt, G., Bigg, G., Rohling, E., 1999. Global seawater oxygen-18 database–v1. 21 [WWW Document]. URL https://data.giss.nasa.gov/o18data/

Schrag, D.P., 1999. Effects of diagenesis on the isotopic record of late paleogene tropical sea surface temperatures. Chemical Geology 161, 215–224. https://doi.org/10.1016/S0009-2541(99)00088-1

Schrag, D.P., DePaolo, D.J., Richter, F.M., 1995. Reconstructing past sea surface temperatures: Correcting for diagenesis of bulk marine carbonate. Geochimica et Cosmochimica Acta 59, 2265–2278. https://doi.org/10.1016/0016-7037(95)00105-9

Scott, G.H., 1976. Variation in Globorotalia puncticulata sphericomiozea from New Zealand (Foraminiferida, Neogene). New Zealand Journal of Geology and Geophysics 19, 855–869.

Scott, G.H., 1975. Variation in Globorotalia miozea (Foraminiferida) from the New Zealand neogene. New Zealand Journal of Geology and Geophysics 18, 865–880. https://doi.org/10.1080/00288306.1975.10423532

Seibold, E., Berger, W.H., 2013. The sea floor: an introduction to marine geology. Springer Science & Business Media.

Seidenglanz, A., Prange, M., Varma, V., Schulz, M., 2012. Ocean temperature response to idealized Gleissberg and de Vries solar cycles in a comprehensive climate model. Geophys. Res. Lett. 39, L22602. https://doi.org/10.1029/2012GL053624

Self-Trail, J., Seefelt, E., 2005. Rapid dissolution of calcareous nannofossils: A case study from freshly cored sediments of the South-Eastern Atlantic coastal plain. J. Nannoplankton Res 27, 149–157.

Sexton, P.F., Wilson, P.A., Pearson, P.N., 2006a. Microstructural and geochemical perspectives on planktic foraminiferal preservation: "Glassy" versus "Frosty." Geochemistry, Geophysics, Geosystems 7. https://doi.org/10.1029/2006GC001291

Sexton, P.F., Wilson, P.A., Pearson, P.N., 2006b. Palaeoecology of late middle Eocene planktic foraminifera and evolutionary implications. Marine Micropaleontology 60, 1–16. https://doi.org/10.1016/j.marmicro.2006.02.006

Shackleton, N., Wiseman, J., Buckley, H., 1973. Non-equilibrium isotopic fractionation between seawater and planktonic foraminiferal tests. Nature 242, 177–179.

Shackleton, N.J., Kennett, J.P., others, 1975. Paleotemperature history of the Cenozoic and the initiation of Antarctic glaciation: oxygen and carbon isotope analyses in DSDP Sites 277, 279, and 281. Initial reports of the deep sea drilling project 29, 743–755.

Shrivastav, A., Singh, A.K., Sinha, D.K., Kaushik, T., Singh, V.P., Mallick, K., 2016. Significance of Globigerina Bulloides D'orbigny: A Foraminiferal Proxy for Palaeomonsoon and Past Upwelling Records. Journal of Climate Change 2, 99–110. https://doi.org/10.3233/JCC-160021

Slice, D.E., 2007. Geometric Morphometrics. Annual Review of Anthropology 36, 261–281. https://doi.org/10.1146/annurev.anthro.34.081804.120613

Smith, A., 1994. Systematics and the fossil record. Oxford: Blackwell Scientific.

Smith, R.E., 2017a. Chapter 3 of this thesis.

Smith, R.E., 2017b. Chapter 5 of this thesis.

Smith, R.E., 2017c. Chapter 4 of this thesis.

Speijer, R.P., Loo, D.V., Masschaele, B., Vlassenbroeck, J., Cnudde, V., Jacobs, P., 2008. Quantifying foraminiferal growth with high-resolution X-ray computed tomography: New opportunities in foraminiferal ontogeny, phylogeny, and paleoceanographic applicationsHigh-resolution X-ray CT of foraminifera. Geosphere 4, 760–763. https://doi.org/10.1130/GES00176.1

Spero, H.J., 1992. Do planktic foraminifera accurately record shifts in the carbon isotopic composition of seawater ΣCO2? Marine Micropaleontology 19, 275–285. https://doi.org/10.1016/0377-8398(92)90033-G

Spero, H.J., Bijma, J., Lea, D.W., Bemis, B.E., 1997. Effect of seawater carbonate concentration on foraminiferal carbon and oxygen isotopes. Nature 390, 497–500. https://doi.org/10.1038/37333

Spero, H.J., Lea, D.W., 1993. Intraspecific stable isotope variability in the planktic foraminiferaGlobigerinoides sacculifer: Results from laboratory experiments. Marine Micropaleontology 22, 221–234. https://doi.org/10.1016/0377-8398(93)90045-Y

Spero, H.J., Mielke, K.M., Kalve, E.M., Lea, D.W., Pak, D.K., 2003. Multispecies approach to reconstructing eastern equatorial Pacific thermocline hydrography during the past 360 kyr. Paleoceanography 18, 1022. https://doi.org/10.1029/2002PA000814

Spero, H.J., Williams, D.F., 1989. Opening the carbon isotope "vital effect" black box 1. Seasonal temperatures in the euphotic zone. Paleoceanography 4, 593–601. https://doi.org/10.1029/PA004i006p00593

Spero, H.J., Williams, D.F., 1988. Extracting environmental information from planktonic foraminiferal δ13C data. Nature 335, 717–719. https://doi.org/10.1038/335717a0

Spezzaferri, S., 1994. Planktonic foraminiferal biostratigraphy and taxonomy of the Oligocene and lower Miocene in the oceanic record. An overview. Pacini Editore.

Spezzaferri, S., Kucera, M., Pearson, P.N., Wade, B.S., Rappo, S., Poole, C.R., Morard, R., Stalder, C., 2015. Fossil and Genetic Evidence for the Polyphyletic Nature of the Planktonic Foraminifera "Globigerinoides", and Description of the New Genus Trilobatus. PLOS ONE 10, e0128108. https://doi.org/10.1371/journal.pone.0128108

Stewart, D.R.M., Pearson, P.N., Ditchfield, P.W., Singano, J.M., 2004. Miocene tropical Indian Ocean temperatures: evidence from three exceptionally preserved foraminiferal assemblages from Tanzania. Journal of African Earth Sciences 40, 173–189. https://doi.org/10.1016/j.jafrearsci.2004.09.001

Stewart, J.A., Wilson, P.A., Edgar, K.M., Anand, P., James, R.H., 2012. Geochemical assessment of the palaeoecology, ontogeny, morphotypic variability and palaeoceanographic utility of "Dentoglobigerina" venezuelana. Marine Micropaleontology 84–85, 74–86. https://doi.org/10.1016/j.marmicro.2011.11.003

Stocker, T., 2014. Climate change 2013: the physical science basis: Working Group I contribution to the Fifth assessment report of the Intergovernmental Panel on Climate Change. Cambridge University Press.

Strotz, L.C., Allen, A.P., 2013. Assessing the role of cladogenesis in macroevolution by integrating fossil and molecular evidence. PNAS 110, 2904–2909. https://doi.org/10.1073/pnas.1208302110

Swingedouw, D., Fichefet, T., Huybrechts, P., Goosse, H., Driesschaert, E., Loutre, M.-F., 2008. Antarctic ice-sheet melting provides negative feedbacks on future climate warming. Geophys. Res. Lett. 35, L17705. https://doi.org/10.1029/2008GL034410

Tabachnick, R.E., Bookstein, F.L., 1990. The Structure of Individual Variation in Miocene globorotalia. Evolution 44, 416–434. https://doi.org/10.2307/2409418

Tagliabue, A., Bopp, L., 2008. Towards understanding global variability in ocean carbon-13. Global Biogeochem. Cycles 22, GB1025. https://doi.org/10.1029/2007GB003037

Tang, C.M., Stott, L.D., 1993. Seasonal salinity changes during Mediterranean sapropel deposition 9000 years B.P.: Evidence from isotopic analyses of individual planktonic foraminifera. Paleoceanography 8, 473–493. https://doi.org/10.1029/93PA01319

Taylor, J.R., Ferrari, R., 2011. Ocean fronts trigger high latitude phytoplankton blooms. Geophys. Res. Lett. 38, L23601. https://doi.org/10.1029/2011GL049312

Thornalley, D.J.R., Blaschek, M., Davies, F.J., Praetorius, S., Oppo, D.W., McManus, J.F., Hall, I.R., Kleiven, H., Renssen, H., McCave, I.N., 2013. Long-term variations in Iceland–Scotland overflow strength during the Holocene. Clim. Past 9, 2073–2084. https://doi.org/10.5194/cp-9-2073-2013

Thornalley, D.J.R., Elderfield, H., McCave, I.N., 2009. Holocene oscillations in temperature and salinity of the surface subpolar North Atlantic. Nature 457, 711–714. https://doi.org/10.1038/nature07717

Thunell, R.C., 1976. Optimum indices of calcium carbonate dissolution, in deep-sea sediments. Geology 4, 525–528. https://doi.org/10.1130/0091-7613(1976)4<525:OIOCCD>2.0.CO;2

Tjallingii, R., Röhl, U., Kölling, M., Bickert, T., 2007. Influence of the water content on X-ray fluorescence core-scanning measurements in soft marine sediments. Geochem. Geophys. Geosyst. 8, Q02004. https://doi.org/10.1029/2006GC001393

Toggweiler, J.R., 1999. Variation of atmospheric CO2 by ventilation of the ocean's deepest water. Paleoceanography 14, 571–588. https://doi.org/10.1029/1999PA900033

Turner, J.V., 1982. Kinetic fractionation of carbon-13 during calcium carbonate precipitation. Geochimica et Cosmochimica Acta 46, 1183–1191. https://doi.org/10.1016/0016-7037(82)90004-7

Urey, H.C., 1948. Oxygen isotopes in nature and in the laboratory. Science 108, 489–496.

Urey, H.C., 1947. The thermodynamic properties of isotopic substances. Journal of the Chemical Society (Resumed) 562–581.

van Kreveld, S., Sarnthein, M., Erlenkeuser, H., Grootes, P., Jung, S., Nadeau, M.J., Pflaumann, U., Voelker, A., 2000. Potential links between surging ice sheets, circulation changes, and the Dansgaard-Oeschger Cycles in the Irminger Sea, 60–18 Kyr. Paleoceanography 15, 425–442. https://doi.org/10.1029/1999PA000464

van Peer, T.E. et al., in prep. IODP Site 1406 age model.

Vargas, C. de, Norris, R., Zaninetti, L., Gibb, S.W., Pawlowski, J., 1999. Molecular evidence of cryptic speciation in planktonic foraminifers and their relation to oceanic provinces. PNAS 96, 2864–2868. https://doi.org/10.1073/pnas.96.6.2864

Vautravers, M.J., Shackleton, N.J., Lopez-Martinez, C., Grimalt, J.O., 2004. Gulf Stream variability during marine isotope stage 3. Paleoceanography 19, PA2011. https://doi.org/10.1029/2003PA000966

Vázquez Riveiros, N., Waelbroeck, C., Skinner, L., Duplessy, J.-C., McManus, J.F., Kandiano, E.S., Bauch, H.A., 2013. The "MIS 11 paradox" and ocean circulation: Role of millennial scale events. Earth and Planetary Science Letters 371–372, 258–268. https://doi.org/10.1016/j.epsl.2013.03.036

Veizer, J., Ala, D., Azmy, K., Bruckschen, P., Buhl, D., Bruhn, F., Carden, G.A.F., Diener, A., Ebneth, S., Godderis, Y., Jasper, T., Korte, C., Pawellek, F., Podlaha, O.G., Strauss, H., 1999. 87Sr/86Sr, δ13C and δ18O evolution of Phanerozoic seawater. Chemical Geology 161, 59–88. https://doi.org/10.1016/S0009-2541(99)00081-9

Vernal, A. de, Hillaire-Marcel, C., Turon, J.-L., Matthiessen, J., 2000. Reconstruction of sea-surface temperature, salinity, and sea-ice cover in the northern North Atlantic during the last glacial maximum based on dinocyst assemblages. Canadian Journal of Earth Sciences 37, 725–750. https://doi.org/10.1139/e99-091

Via, R.K., Thomas, D.J., 2006. Evolution of Atlantic thermohaline circulation: Early Oligocene onset of deep-water production in the North Atlantic. Geology 34, 441–444. https://doi.org/10.1130/G22545.1

Villanueva, J., Calvo, E., Pelejero, C., Grimalt, J.O., Boelaert, A., Labeyrie, L., 2001. A latitudinal productivity band in the central North Atlantic over the last 270 kyr: An alkenone perspective. Paleoceanography 16, 617–626. https://doi.org/10.1029/2000PA000543

Vincent, E., Berger, W., 1981. Planktonic foraminifera and their use in paleoceanography. The sea 7, 1025–1119.

von der Heydt, A., Dijkstra, H.A., 2008. The effect of gateways on ocean circulation patterns in the Cenozoic. Global and Planetary Change 62, 132–146. https://doi.org/10.1016/j.gloplacha.2007.11.006

von der Heydt, A., Dijkstra, H.A., 2006. Effect of ocean gateways on the global ocean circulation in the late Oligocene and early Miocene. Paleoceanography 21, PA1011. https://doi.org/10.1029/2005PA001149

Wade, B.S., Houben, A.J.P., Quaijtaal, W., Schouten, S., Rosenthal, Y., Miller, K.G., Katz, M.E., Wright, J.D., Brinkhuis, H., 2012. Multiproxy record of abrupt sea-surface cooling across the Eocene-Oligocene transition in the Gulf of Mexico. Geology 40, 159–162. https://doi.org/10.1130/G32577.1

Wade, B.S., Kroon, D., 2002. Middle Eocene regional climate instability: Evidence from the western North Atlantic. Geology 30, 1011–1014. https://doi.org/10.1130/0091-7613(2002)030<1011:MERCIE>2.0.CO;2

Wade, B.S., Olsson, R.K., 2009. Investigation of pre-extinction dwarfing in Cenozoic planktonic foraminifera. Palaeogeography, Palaeoclimatology, Palaeoecology, Extinction, dwarfing and the Lilliput effect 284, 39–46. https://doi.org/10.1016/j.palaeo.2009.08.026

Wade, B.S., Pälike, H., 2004. Oligocene climate dynamics. Paleoceanography 19. https://doi.org/10.1029/2004PA001042

Wagner, G., Beer, J., Masarik, J., Muscheler, R., Kubik, P.W., Mende, W., Laj, C., Raisbeck, G.M., Yiou, F., 2001. Presence of the Solar de Vries Cycle (−205 years) during the Last Ice Age. Geophys. Res. Lett. 28, 303–306. https://doi.org/10.1029/2000GL006116

Wallmann, K., 2001. The geological water cycle and the evolution of marine δ18O values. Geochimica et Cosmochimica Acta 65, 2469–2485. https://doi.org/10.1016/S0016-7037(01)00603-2

Wang, Y.J., Cheng, H., Edwards, R.L., An, Z.S., Wu, J.Y., Shen, C.-C., Dorale, J.A., 2001. A High-Resolution Absolute-Dated Late Pleistocene Monsoon Record from Hulu Cave, China. Science 294, 2345–2348. https://doi.org/10.1126/science.1064618

Wanner, H., Beer, J., Bütikofer, J., Crowley, T.J., Cubasch, U., Flückiger, J., Goosse, H., Grosjean, M., Joos, F., Kaplan, J.O., Küttel, M., Müller, S.A., Prentice, I.C., Solomina, O., Stocker, T.F., Tarasov, P., Wagner, M., Widmann, M., 2008. Mid- to Late Holocene climate change: an overview. Quaternary Science Reviews 27, 1791–1828. https://doi.org/10.1016/j.quascirev.2008.06.013

Wanner, H., Mercolli, L., Grosjean, M., Ritz, S.P., 2015. Holocene climate variability and change; a data-based review. Journal of the Geological Society 172, 254–263. https://doi.org/10.1144/jgs2013-101

Weber, S.L., Crowley, T.J., Schrier, G. van der, 2004. Solar irradiance forcing of centennial climate variability during the Holocene. Climate Dynamics 22, 539–553. https://doi.org/10.1007/s00382-004-0396-y

Weertman, J., 1961. Stability of ice-age ice sheets. J. Geophys. Res. 66, 3783–3792. https://doi.org/10.1029/JZ066i011p03783

Wefer, G., Berger, W.H., 1991. Isotope paleontology: growth and composition of extant calcareous species. Marine Geology, Anoxic Basins and Sapropel Deposition in the Eastern Mediterranean: Past and Present 100, 207–248. https://doi.org/10.1016/0025-3227(91)90234-U

Wei, K.-Y., 1987. Multivariate morphometric differentiation of chronospecies in the late Neogene planktonic foraminiferal lineageGloboconella. Marine Micropaleontology 12, 183–202. https://doi.org/10.1016/0377-8398(87)90020-X

Weltje, G.J., Tjallingii, R., 2008. Calibration of XRF core scanners for quantitative geochemical logging of sediment cores: Theory and application. Earth and Planetary Science Letters 274, 423–438. https://doi.org/10.1016/j.epsl.2008.07.054

Williams, D.F., Sommer, M.A., Bender, M.L., 1977. Carbon isotopic compositions of Recent planktonic foraminifera of the Indian Ocean. Earth and Planetary Science Letters 36, 391–403. https://doi.org/10.1016/0012-821X(77)90064-4

Williams, M., Haywood, A.M., Taylor, S.P., Valdes, P.J., Sellwood, B.W., Hillenbrand, C.-D., 2005. Evaluating the efficacy of planktonic foraminifer calcite δ18O data for sea surface temperature reconstruction for the Late Miocene. Geobios 38, 843–863. https://doi.org/10.1016/j.geobios.2004.12.001

Wit, J.C., Reichart, G.-J., A Jung, S.J., Kroon, D., 2010. Approaches to unravel seasonality in sea surface temperatures using paired single-specimen foraminiferal δ18O and Mg/Ca analyses. Paleoceanography 25, PA4220. https://doi.org/10.1029/2009PA001857

Woodruff, F., Savin, S.M., 1989. Miocene deepwater oceanography. Paleoceanography 4, 87–140. https://doi.org/10.1029/PA004i001p00087

Zachos, J.C., Flower, B.P., Paul, H., 1997. Orbitally paced climate oscillations across the Oligocene/Miocene boundary. Nature 388, 567–570. https://doi.org/10.1038/41528

Zachos, J.C., Pagani, M., Sloan, L., Thomas, E., Billups, K., 2001a. Trends, Rhythms, and Aberrations in Global Climate 65 Ma to Present. Science 292, 686–693. https://doi.org/10.1126/science.1059412

Zachos, J.C., Shackleton, N.J., Revenaugh, J.S., Pälike, H., Flower, B.P., 2001b. Climate Response to Orbital Forcing Across the Oligocene-Miocene Boundary. Science 292, 274–278. https://doi.org/10.1126/science.1058288

Zeebe, R.E., Ridgwell, A., Zachos, J.C., 2016. Anthropogenic carbon release rate unprecedented during the past 66 million years. Nature Geosci 9, 325–329. https://doi.org/10.1038/ngeo2681

Zelditch, M.L., Swiderski, D.L., Sheets, H.D., 2012. Geometric Morphometrics for Biologists: A Primer. Academic Press.

Zhang, X., Lohmann, G., Knorr, G., Purcell, C., 2014. Abrupt glacial climate shifts controlled by ice sheet changes. Nature 512, 290–294. https://doi.org/10.1038/nature13592

Zhang, Y.G., Pagani, M., Liu, Z., Bohaty, S.M., DeConto, R., 2013. A 40-million-year history of atmospheric CO2. Phil. Trans. R. Soc. A 371, 20130096. https://doi.org/10.1098/rsta.2013.0096